

AVAILABLE TO THE PUBLIC

SD 67-621-3

GPO PRICE \$ _____

CFSTI PRICE(S) \$ _____

Hard copy (HC) 3

Microfiche (MF) 62

ff 653 July 65

FINAL REPORT

TECHNOLOGICAL REQUIREMENTS COMMON TO MANNED PLANETARY MISSIONS

(Contract NAS2-3918)

APPENDIX B

Environments



SPACE DIVISION

NORTH AMERICAN ROCKWELL CORPORATION

FACILITY FORM 602
 (ACCESSION NUMBER) N68-19429
 (THRU) 1
 (PAGES) 207
 (CODE) 30
 (CATEGORY) 1
 (NASA CR OR TAX OR AD NUMBER) NPSP-CR-75190

FACILITY FORM 602

ERRATA

Technological Requirements Common to Manned Planetary Missions

Final Report - Appendix B, SD67-621-3

1. Page 59 - replace " t_1 = mission time" by $t_2 - t_1 = \Delta t$

SD 67-621-3

TECHNOLOGICAL REQUIREMENTS
COMMON TO MANNED PLANETARY MISSIONS
NAS2-3918

Appendix B - Environments

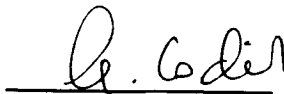
January 1968

Prepared by



R. D. Meston
Project Engineer

Approved by



A. Codik
Project Manager

SPACE DIVISION
NORTH AMERICAN ROCKWELL CORPORATION

PRECEDING PAGE BLANK NOT FILMED.

FOREWORD

This report contains the final results of the studies conducted under Contract NAS2-3918, Technological Requirements Common to Manned Planetary Missions. This report consists of five volumes. The first volume (SD 67-621-1) summarizes the study results. The detailed descriptions of the study are presented in the following volumes:

- | | |
|---|---------------|
| Appendix A - Mission Requirements | (SD 67-621-2) |
| Appendix B - Environments | (SD 67-621-3) |
| Appendix C - Subsystem Synthesis and
Parametric Analysis | (SD 67-621-4) |
| Appendix D - System Synthesis and
Parametric Analysis | (SD 67-621-5) |

PRECEDING PAGE BLANK NOT FILMED.

CONTENTS

	Page
INTRODUCTION	1
METEOROID ENVIRONMENT AND PROTECTION	1
Meteoroid Environment	1
Missions and System Configurations	3
Analysis Methods	8
THERMAL ENVIRONMENT AND PROTECTION	21
Manned Mission Module Heat Balance and Thermal Protection	23
Propellant Storability and Thermal Protection Requirements	32
RADIATION ENVIRONMENT AND PROTECTION	45
Space Radiation Analysis	45
Jupiter Trapped Radiation Analysis	73
REFERENCES	95

ILLUSTRATIONS

Figure		Page
1	Meteoroid Environment Models	2
2	Spacecraft Heliocentric Distance Time History (Venus, Mars, Vesta, and Ceres)	5
3	Spacecraft Heliocentric Distance Time History (Jupiter) .	6
4	System Configurations	7
5	Earth Reentry Module Structure and Allowable Damage .	9
6	Mission Module Structure and Allowable Damage	9
7	Planetary Module Structure and Allowable Damage	10
8	Aerobraker Heatshield Structure and Allowable Damage .	10
9	Propulsion Module Structure and Allowable Damage	11
10	Equilibrium Wall Temperature Versus Distance From Sun	27
11	NRC-2 Superinsulation Integrated Heat Flow Versus Temperature	29
12	Heat Loss From Unexposed Side Versus Insulation Thickness, Including Micrometeoroid Bumper Structure .	30
13	Liquidus Temperature Range of Fuels and Oxidizers	34
14	Comparison of Solar Flare Proton Probabilities for a Four-Week Mission at 1 AU, t = 4 Weeks	47
15	Comparison of Solar Flare Proton Probabilities for a 26- Week Mission at 1 AU, t = 26 Weeks	48
16	Comparison of Solar Flare Proton Probabilities for a 104- Week Mission at 1 AU, t = 104 Weeks	49
17	Relationship Between Flux and Rad Dose for Solar Flare Proton Events	52
18	Comparison of Solar Flare Proton and Alpha Particle Integral Energy Spectra (Summed Over Events for Which Both Spectra Were Available)	54
19	Calculated Multiplicative Correction Factors for Solar Flare Protons to Include Effects of Solar Flare Alpha Particles	55
20	Point Dose Per Solar Flare Proton Above 30 Mev as a Function of Aluminum Shield Thickness	58
21	Point Rad Dose Per High-Thrust Passage Through the Geomagnetically Trapped Radiation Belts	62

Figure		Page
22	Theoretical Probability of Exceeding a Solar Flare Proton Flux of $\int \phi$ ($p/cm^2 > 30$ Mev) on a Mission of Duration t (Weeks)	67
23	Mission Module Space Radiation Shielding	71
24	Electron Flux	82
25	Measured Electron Integral Energy Spectrum at $3.5 R_e$ (Earth Van Allen Belts)	84
26	Electron Dose Rate at Ganymede	85
27	Effect of Shield Thickness	89
28	Added Shielding (1985-1989 Mission)	90
29	Added Shielding (1987-1991 Mission)	91
30	Added Shielding (1990-1994 Mission)	92

TABLES

Table		Page
1	Summary of Constants for Meteoroid Environment	4
2	Penetration Mechanics Constants	13
3	Average Meteoroid Impact Velocity	15
4	Scaling Equation Coefficients - Retrobraker Nominal Environment	17
5	Scaling Equation Coefficients - Retrobraker Maximum Environment	18
6	Scaling Equation Coefficients - Flyby Configuration	19
7	Scaling Equation Coefficients (Aerobraker Spacecraft)	20
8	Summary of Manned Mission Module Multiple Layer Insulation Requirements	22
9	Summary of Internal Heat Generation for the Manned Mission Module	24
10	Propellant Tank Insulation Requirements to Mercury - Rolling Cylinder	41
11	Propellant Tank Insulation Requirements to Mercury - Normal Surface	42
12	Propellant Tank Insulation Requirements to Jupiter (Rolling Cylinder)	43
13	Propellant Tank Insulation Requirements to Jupiter (Normal Surface)	44
14	Range - Energy Constants	72
15	Trapped Electron Populations as a Function of Jovian Equatorial Field, B_0	80
16	Spacecraft Shielding Required Without the Presence of Jupiter Radiation Belts	87

INTRODUCTION

The meteoroid, thermal, and radiation protection requirements have been determined for the missions being considered. The objective of the meteoroid protection studies was to develop meteoroid shield scaling equations. The meteoroid protection requirements are expressed as a set of scaling equation coefficients which define the shield weight as a function of the mission objective, spacecraft configuration, and mission duration. The purpose of the thermal requirements study was to develop weights and weight scaling equations for all systems and structural aspects of long-term space vehicles. The heat balances and requirements on the mission module and the thermal protection required for propellant storage are considered. The radiation protection study developed shielding requirements for the interplanetary legs of the missions, and special consideration was given requirements resulting from the Jupiter trapped radiation belt.

METEOROID ENVIRONMENT AND PROTECTION

The objective of the meteoroid protection study was to develop meteoroid shield scaling equations which would yield optimum shield weight as a function of mission duration and module vulnerable area for each baseline system configuration. The meteoroid environments considered, the structural models adopted for the study, and the resultant scaling equations are discussed in the following sections.

METEOROID ENVIRONMENT

Two meteoroid environment models, provided by the NASA in Reference 1, were considered in the analyses. The meteoroid fluxes are shown in Figure 1 are given by

$$N = \frac{10^{K_1} f(R)}{m^{K_3}}$$

where

$$f(R) = 10^{+K_6 R^2 + K_7 R} \quad \text{for asteroidal particles}$$

$$f(R) = 1.0 \quad \text{for cometary particles}$$

$$N = \text{number of particles/meter}^2 - \text{second}$$

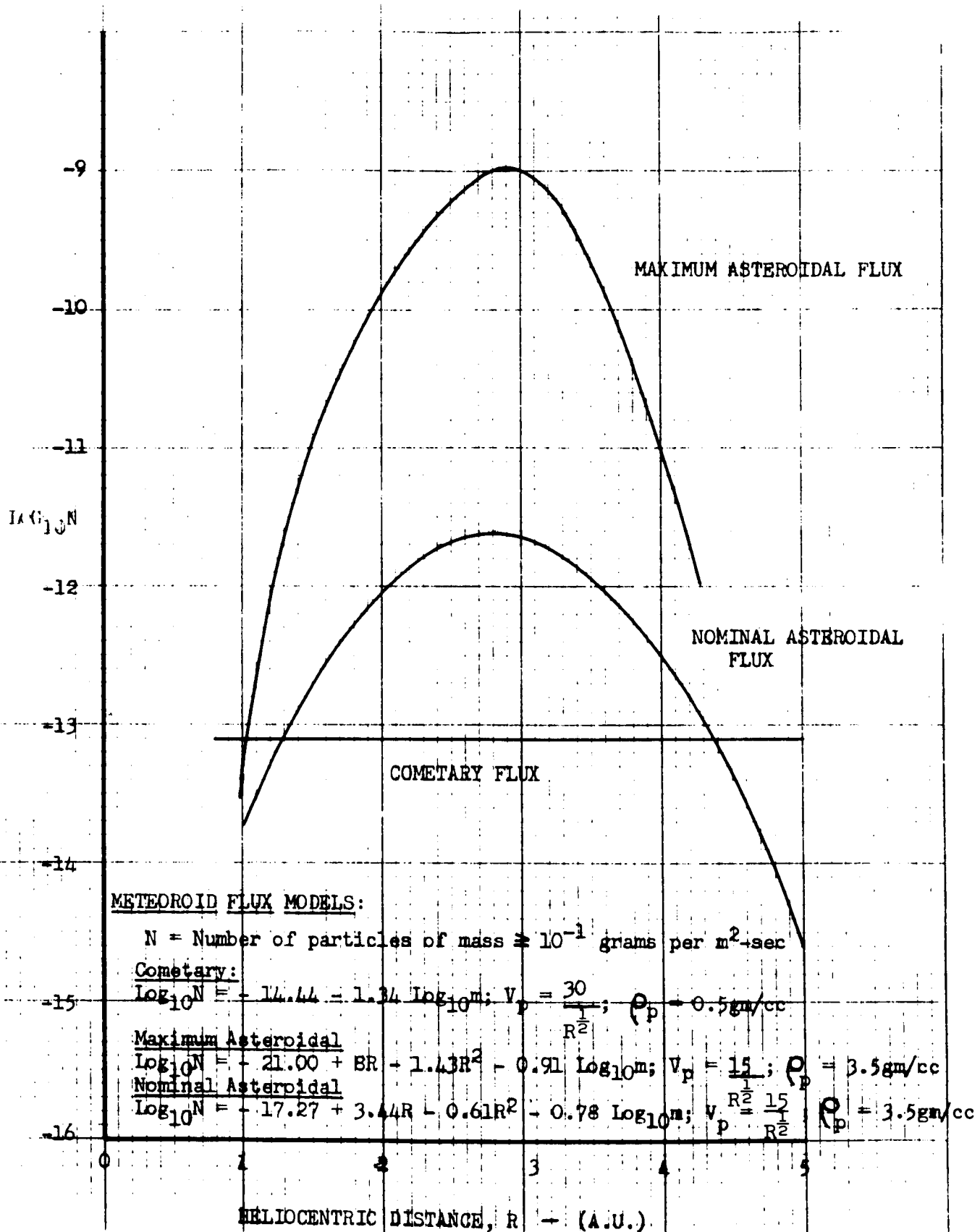


Figure 1. Meteoroid Environment Models

m = particle mass (grams)

R = heliocentric radius (A. U.)

K_i = constants

The values used for the constants (K_i) are given in Table 1. The cometary particles were considered as omnidirectional and the asteroidal particles were considered as unidirectional in direct orbit about the Sun.

The particle densities (ρ_p) and impact velocities (V_p) are given by

$$\begin{aligned}\rho_p &= 0.5 \text{ grams/cubic centimeter for cometary} \\ &= 3.5 \text{ grams/cubic centimeter for asteroidal}\end{aligned}$$

and

$$\begin{aligned}V_p &= 30R^{-1/2} \text{ kilometers/second for cometary} \\ &= 15R^{-1/2} \text{ kilometers/second for asteroidal.}\end{aligned}$$

The nominal cometary environment and maximum asteroidal environment were combined to form a maximum meteoroid environment. The nominal cometary and the nominal asteroidal environments were combined to form a nominal meteoroid environment. Protection requirements were then evaluated relative to the maximum meteoroid environment and the nominal meteoroid environment.

MISSIONS AND SYSTEM CONFIGURATIONS

Representative mission profiles were assumed for each of the mission objectives being considered. The heliocentric radius of the selected missions is shown in Figures 2 and 3 as a function of time since Earth orbit escape. For the purposes of this study, the Vesta mission was assumed to be the same as the Ceres mission.

The baseline system configurations which were assumed for the flyby, orbital, and planetary landing missions are shown in Figure 4. For the flyby and orbital configurations, meteoroid protection must be provided for the Earth reentry module (ERM), mission module (MM), planetary probe module (PPM), and the propulsion module or modules (PM). In addition to the above protection requirements, meteoroid shielding must be provided for the planetary excursion module (PEM) for the lander configurations. The

Table 1. Summary of Constants for Meteoroid Environment

Constant	Cometary	Nominal Asteroidal	Maximum Asteroidal	Reference Environment	
				Cometary, Nominal Asteroidal	Maximum Asteroidal
K_1	-14.44	-17.27	-21.00	-14.33	-11.33
K_2	0	0	0	--	--
K_3	-1.34	-0.78	-0.91	-0.78	-0.91
K_4	30.0	15.0	15.0	30.0, 15.0	15.0
K_5	-0.5	-0.5	-0.5	-0.5	-0.5
K_6	0	-0.61	-1.43	--	--
K_7	0	+3.44	+8.0	--	--
$\log_{10} N = K_1 + K_2 \log_{10} R + K_7 R + K_6 R^2 + K_3 \log_{10} M$ $V_m = K_4 R^{K_5}$					

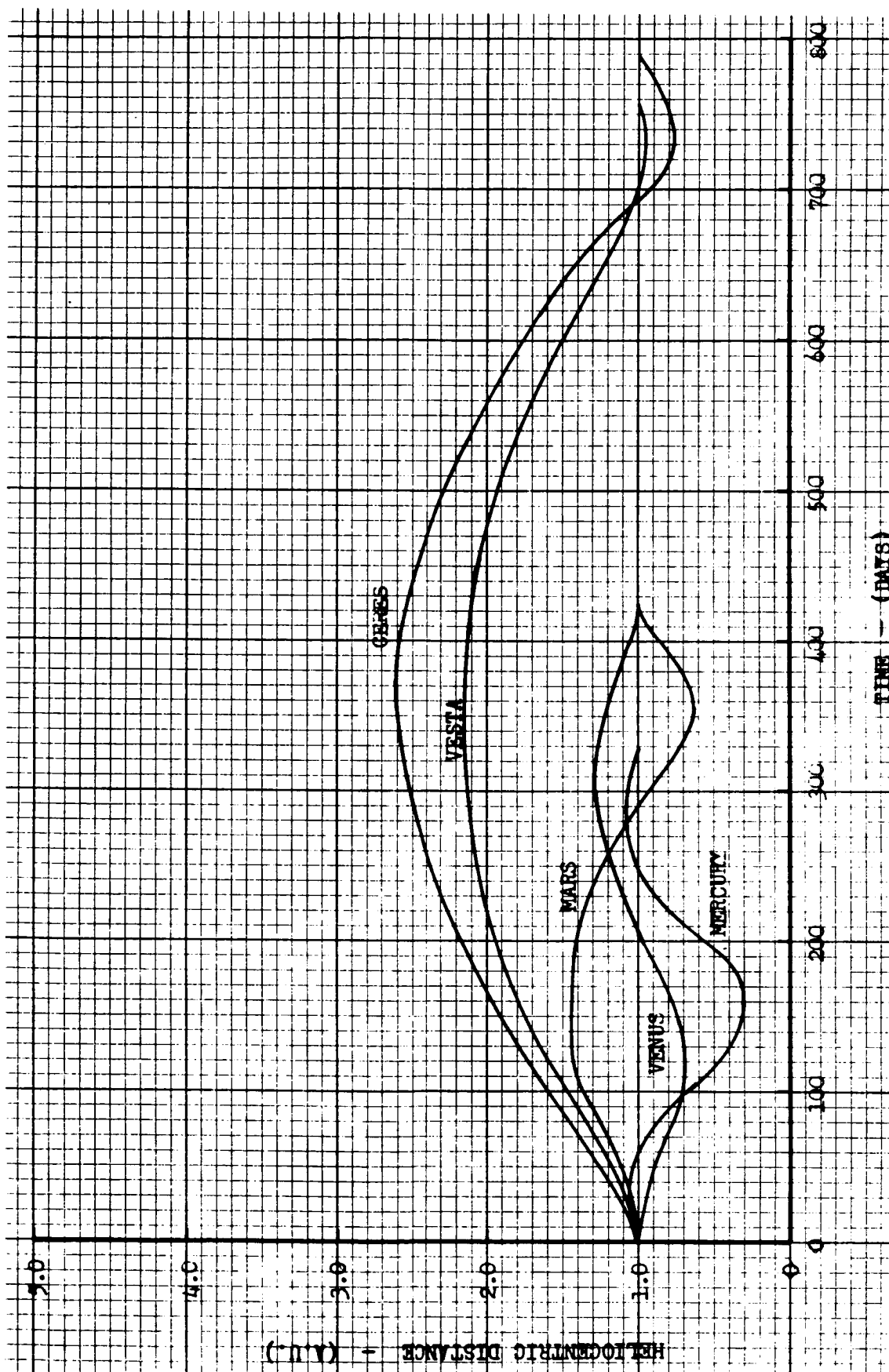


Figure 2. Spacecraft Heliocentric Distance Time History
(Venus, Mars, Vesta, and Ceres)

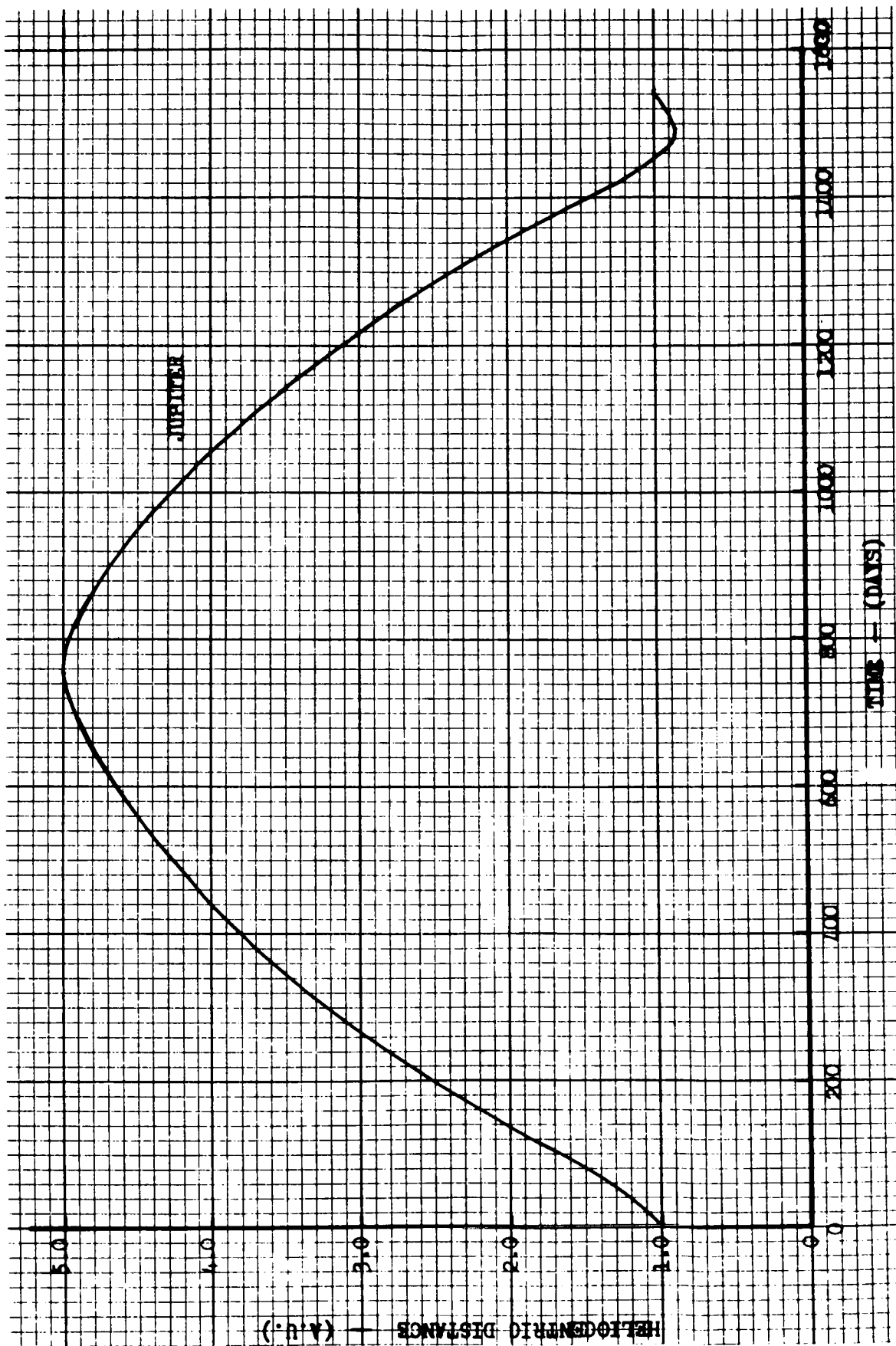


Figure 3. Spacecraft Heliocentric Distance Time History (Jupiter)

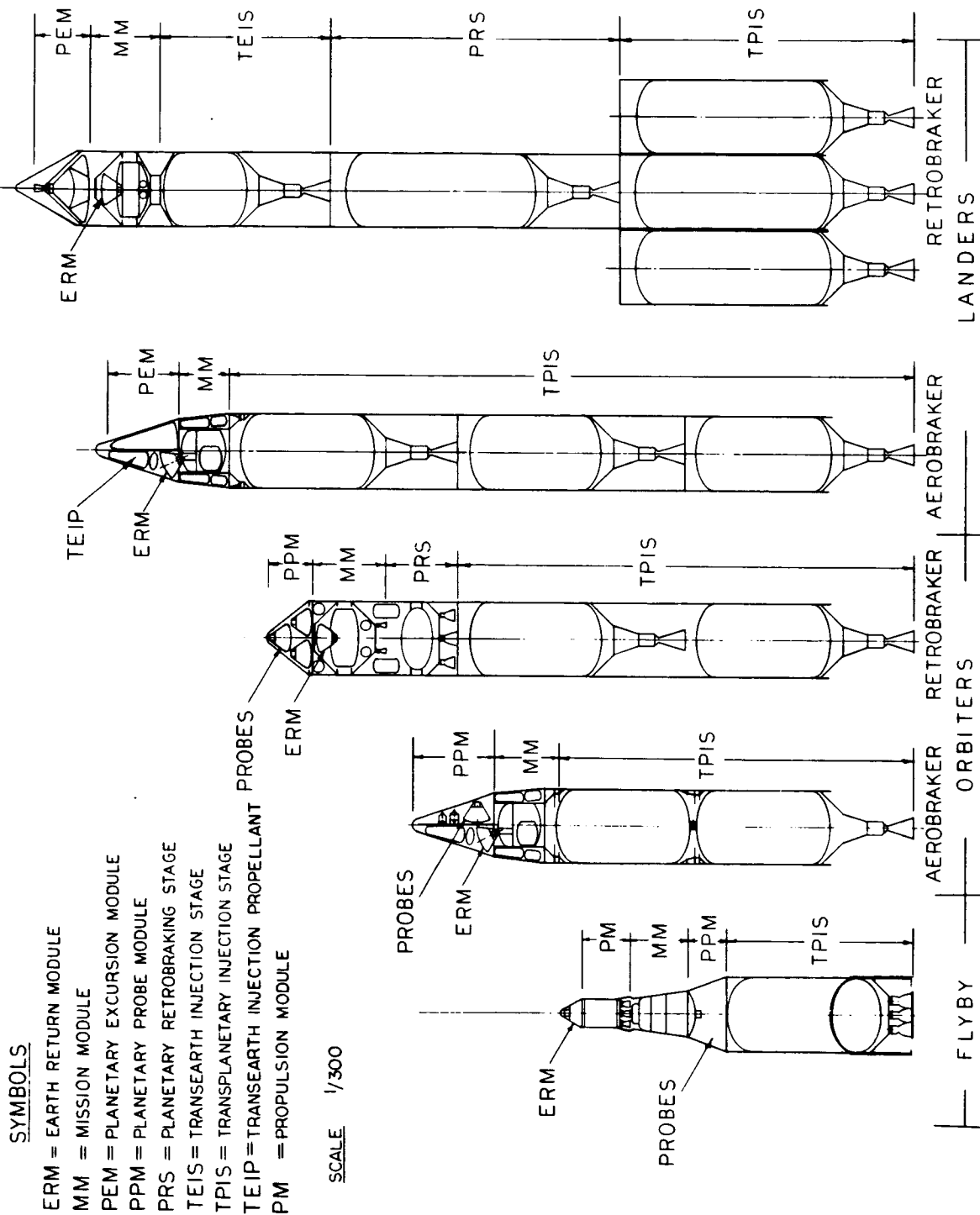


Figure 4. System Configurations

heatshield and the aft bulkhead of the aerobraker must be protected during the transplanet mission phase for the aerobraker configuration, and during the transearth mission phase the ERM and MM must be shielded.

The structural models, damage criteria, and the placement of the meteoroid shielding adopted for each of the modules are shown in Figures 5 through 9. The ERM, Figure 5, is assumed to be within a protective pressurized shroud in order to prevent outgassing from the ablator. The thickness of the load-carrying wall is increased to prevent perforation and loss of internal pressure. Perforation of the mission module wall, Figure 6, is prevented by thickening the load-carrying module wall. The probes and the planetary excursion module are also assumed to be housed within a protective shroud. The additional thickness required to prevent perforation of the housing is added to the load-carrying wall. For cryogenic propulsion modules, the thickness of the load-carrying wall is increased to prevent high-energy impact on the tank wall. The thickness of the aerobraker heat shield is increased, as required to prevent full penetration of the ablator.

ANALYSIS METHODS

As part of the meteoroid shielding analysis of the command and service module (CSM) for project Apollo, the SD initiated hypervelocity impact testing of numerous simulated spacecraft structures. Evaluations that were made of these data indicated that the Summer's penetration equation was too conservative and that the Herrmann and Jones equation was too optimistic. Further evaluations that were made included not only the new Apollo data but all recent high-velocity data available and culminated in the following equation being adopted for the analysis of the Apollo CSM (ablator and windows excepted):

$$p = \frac{1.38 d_p^{1.1} \rho_p^{0.5} V_p^{2/3}}{\rho_t^{1/6} H_t^{1/4}}$$

where

d_p = particle diameter (centimeters)

ρ_p = particle density (grams/centimeter³)

V_p = particle impact velocity (kilometers/second)

ρ_t = target density (grams/centimeter³)

H_t = target Brinell hardness number (kilograms/millimeter²)

ERM

Thicken t_2 as required to prevent perforation of t_2 and loss of internal pressure.

Minimum structure:

t_1 = 0.05 cm aluminum

t_2 = 0.15 cm aluminum

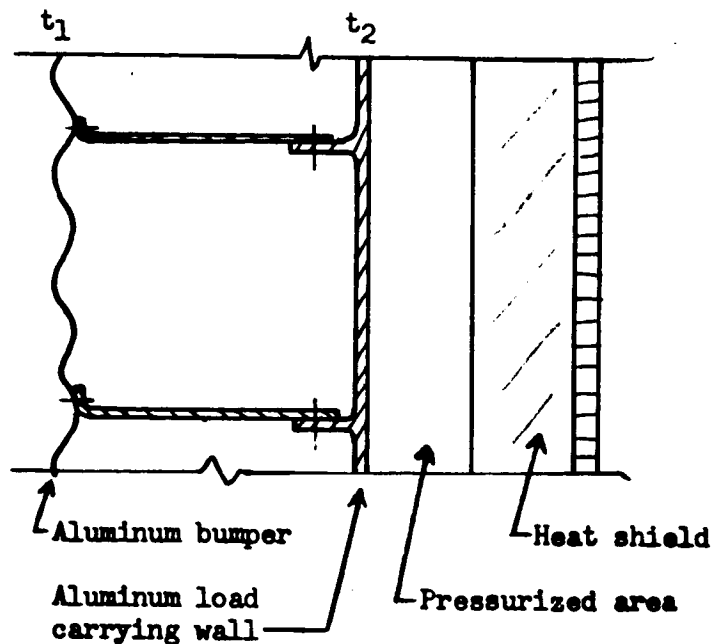


Figure 5. Earth Reentry Module Structure and Allowable Damage

MM

Thicken t_2 as required to prevent perforation of t_2 and loss of cabin pressure

Minimum structure:

t_1 = 0.05 cm aluminum

t_2 = 0.15 cm aluminum

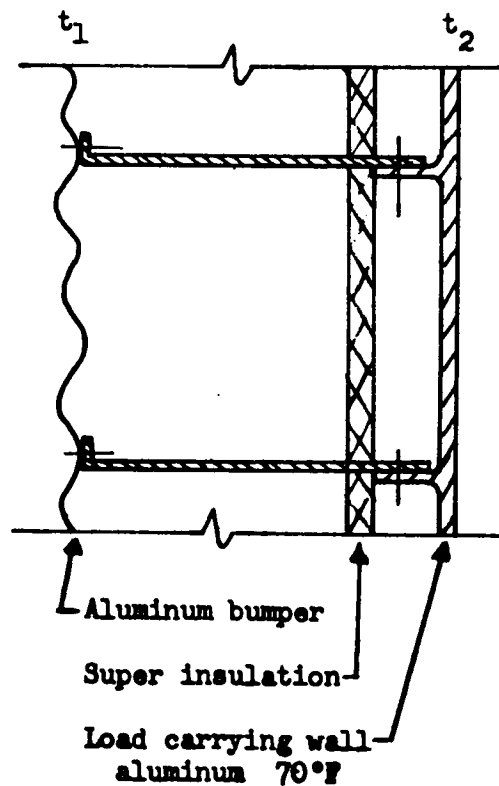


Figure 6. Mission Module Structure and Allowable Damage

PEM

Thicken t_2 as required to prevent perforation of probe housing and damage to probe interior.

Minimum structure:

t_1 = 0.05 cm aluminum

t_2 = 0.15 cm aluminum

t_3 = 0.10 cm aluminum

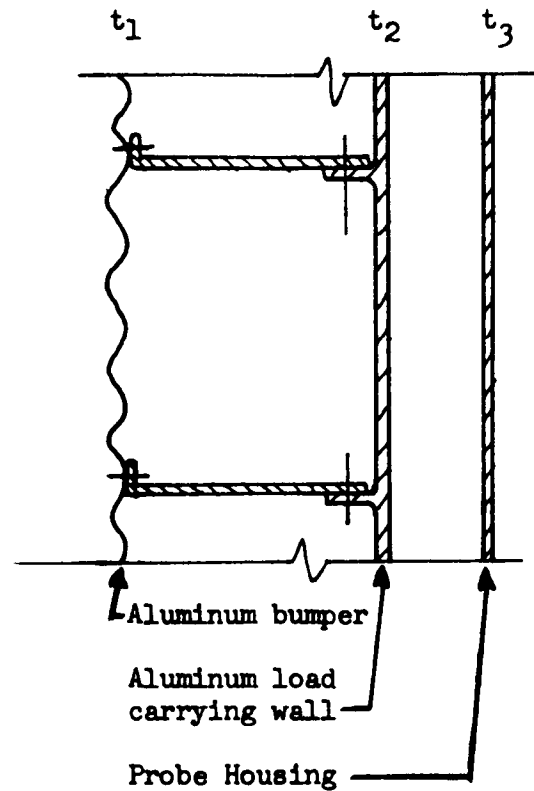


Figure 7. Planetary Module Structure and Allowable Damage

Heatshield (aerobraker)

Thicken t_2 as required to limit penetration into ablator to full depth.

Minimum structure:

t_1 = 0.05 cm aluminum

t_2 = 2.54 cm ablator (AVCO)

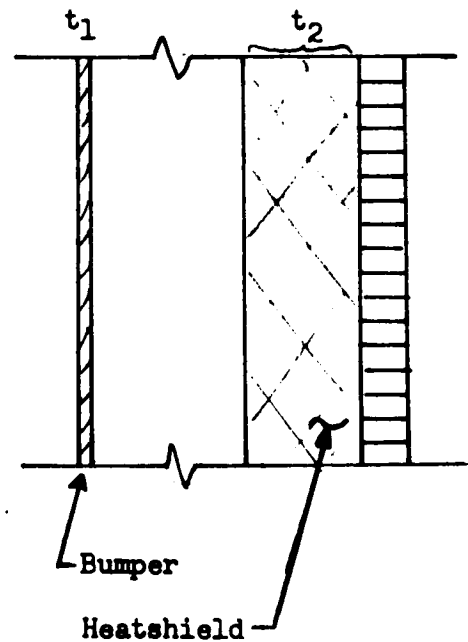


Figure 8. Aerobraker Heatshield Structure and Allowable Damage

PM

Thicken t_2 as required to prevent perforation of t_2 . This prevents high energy impact on cryo tank.

Minimum structure:

- t_1 = 0.05 cm aluminum
 t_2 = 0.32 cm aluminum (Retrobraker Spacecraft)
= 0.15 cm aluminum (Flyby Spacecraft)

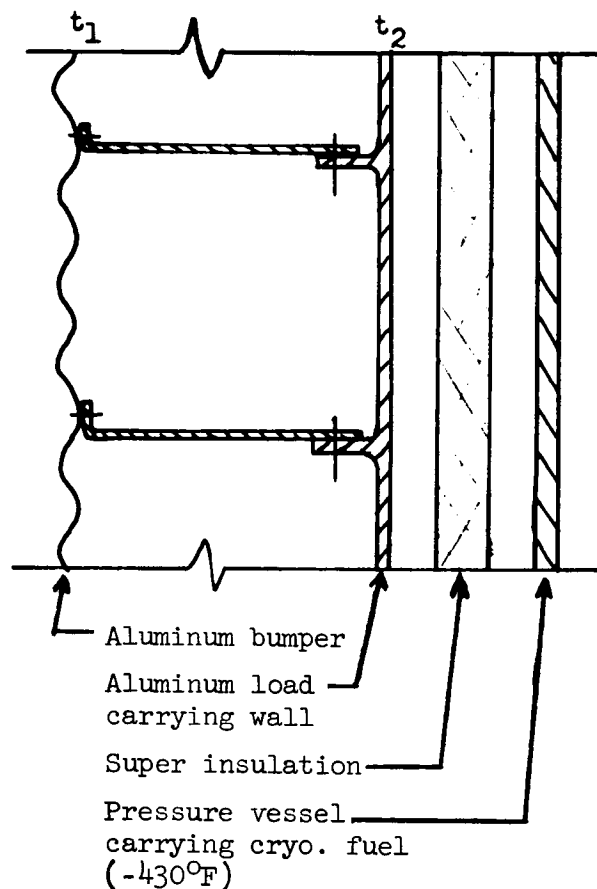


Figure 9. Propulsion Module Structure and Allowable Damage

The above penetration equation was compared with the equation provided by the NASA/MAD and was found to be essentially equivalent when the target material is hard aluminum.

The minimum thickness single sheet or single sheet equivalent thickness, required to resist perforation is given in centimeters, by

$$\bar{t} = 1.8p$$

Considerable testing has also been done at the SD on multisheet structure and the early concept of ballistic limit has been replaced by improved penetration models. The approach adopted for this study was that of the scaled multisheet model that takes account of the relative size of the structure and the particle. For a simplified approach, the equivalent thickness of a multisheet structure may be expressed as

$$\bar{t} = t_1 + \sum_{i=2}^n \frac{t_i}{k_i}$$

where

$$k_i = 1.0 - k' \frac{h_i}{d}, \quad \left(0 \leq \frac{h_i}{d} \leq 10\right)$$

$$k_i = 1.0 - 10k', \quad \left(10 \leq \frac{h_i}{d}\right)$$

$$k' = 0.08 \left(\text{structural efficiency of approximately 5 at } \frac{h_i}{d} = 10 \right)$$

t_i = the i th sheet thickness

k_i = the penetration efficiency of the debris striking the i th sheet

h_i = the spacing of the i th sheet from the sheet which fragments the projectile

d = the particle diameter.

The single sheet equivalent thickness (\bar{t}), target density (ρ_t), target Brinell hardness number (H_t), and the penetration efficiency (k_2) used in the computations of the meteoroid shield requirements are shown in Table 2 for each of the modules considered. The target density and Brinell hardness number for the manned modules are for aluminum. The heatshield density and hardness number are based on Avco ablator (Apollo).

Table 2. Penetration Mechanics Constants

Module	\bar{t}	ρ_t	H_t	k_i
Earth reentry modules	0.811	2.78	120	0.20
Mission modules	0.811	2.78	120	0.20
Planetary excursion modules	1.32	2.78	120	0.20
Propulsion modules	1.635	2.78	120	0.20
Aerobraker Heatshield	2.38	0.552	0.40	0.20
\bar{t} = single sheet equivalent thickness (centimeter) ρ_t = target density (grams/cubic centimeter) H_t = Brinell hardness number (kilograms/millimeter ²) k_i = penetration efficiency				

The penetration efficiency assumes spacing between the bumper and the meteoroid shield such that the ratio of spacing to particle diameter (h_2/d) is greater than ten, resulting in a second sheet structural efficiency of five.

Treatment of the time dependent flux by effective exposure time is given by:

$$T_r = 10^{K_{1a} - K_{1r}} \int_0^{T_a} f(R) dT$$

where

T_r = the effective exposure time (days)

K_{1a} = a constant of the actual flux

K_{1r} = a constant of the reference flux (flux that is inherent to the meteoroid protection computer program)

$f(R)$ = the variable time parameter of the flux

T_a = the actual mission duration (days)

An average meteoroid impact velocity (\bar{V}_p) was used for each mission and was determined from

$$\bar{V}_p = \frac{1}{T_a} \int_0^{T_a} V_p(R) dT$$

where $V_p(R)$ equals the previously defined particle velocities. The resultant average meteoroid impact velocities are shown in Table 3 for the six mission objectives.

Allocation of shielding to the modules for minimum total spacecraft shielding mass is determined by use of Lagrange's method of the undetermined multiplier,

$$\frac{\partial W_T}{\partial P_{oi}} + \lambda \frac{\partial (P_{ot} - P_{o1} P_{o2} P_{o3} \dots P_{on})}{\partial P_{oi}} = 0$$

where W_T is the spacecraft total shielding mass, P_{oi} is the probability of no failure of the i^{th} module, P_{ot} is the spacecraft probability of no failure, n is the number of modules, and λ is the undetermined multiplier that

Table 3. Average Meteoroid Impact Velocity

Mission	Average Impact Velocity (kilometers/second)	
	Cometary	Asteroidal
Jupiter	19.0	9.5
Ceres Vesta	22.7	11.35
Mars	29.4	14.7
Venus	30.7	*
Mercury	38.3	*
*Asteroidal environment considered negligible to cometary.		

ensures W_T to be a minimum. The SD Minimum Weight Shielding computer program developed for the Apollo spacecraft was utilized to determine the optimum shielding mass required for the various missions. The program determines the additional mass (W_{si}) and the additional thickness of material (t_{si}) required for shielding. For the present study, an overall probability (P_{ot}) of no failure of 0.99 was assumed.

The total structural unit weight of the i^{th} module (W_{ti}) required for meteoroid protection is given by

$$W_{ti} = W_{mi} + W_{si}$$

where W_{mi} is the minimum module structural unit weight required for loads and thermal protection and W_{si} is the additional structural unit weight required for meteoroid protection. For a constant minimum structural unit weight

$$W_{ti} = C_1 + W_{si}$$

It can be shown that for a given reliability goal, the shielding unit weight needed as a function of the module exposure time and vulnerable area is of the form

$$W_{si} = C_b(A_{vi}T_{ai} - C_a)^a; (A_{vi}T_{ai} \geq C_a)$$

where

A_{vi} = vulnerable area of the i^{th} module and

T_{ai} = time the i^{th} module is exposed to the meteoroid environment.

The total structural unit weight is then

$$W_{ti} = C_1 + C_b(A_{vi}T_{ai} - C_a)^a$$

which can be approximated by the following meteoroid protection weight scaling equation

$$W_{ti} \approx C_1 + C_2(A_{vi}T_{ai})^a$$

For the omnidirectional cometary flux, the vulnerable area (A_{vi}) is equal to the surface area. For the unidirectional asteroidal flux, the vulnerable area is equal to the projected area which was assumed to be equal to one-third the surface area. The required incremental structural unit weight for meteoroid protection $[C_2(A_{vi}T_{ai})^a]$ is, in both cases, applied to the entire module surface area which permits flexibility in the spacecraft attitude time history.

The scaling equation coefficients (C_1 , C_2 , and a) which were determined are given in Tables 4 through 7 for the various modules considered in the study for a probability of no failure (P_{ot}) of 0.99. The vulnerable area (A_{vi}) is in square feet and the exposure time (T_{ai}) is the length in days that each module is exposed to the meteoroid environment. The coefficients defined in these tables were used during the system synthesis analyses (Appendix D) to define the meteoroid protection requirements for each of the modules. During the weight synthesis analyses, it was assumed that the incremental weight required for protection of the propulsion modules was jettisoned prior to ignition.

Scaling equation coefficients are not shown for the Earth orbit escape propulsion module since the characteristics of such a meteoroid protection bumper are essentially independent of the mission. To provide protection for Earth orbit stay times in excess of 100 days the additional structural unit weight, which is jettisoned prior to the Earth orbit escape maneuver, is approximately 2 kg/m^2 (0.4 lb/ft^2). This value is based on a bumper thickness of 0.05 cm (0.02 in) plus an additional 50 percent for the stand-off support structure.

Table 4. Scaling Equation Coefficients - Retrobraker Nominal Environment

$$W_{ti} = C_1 (A_{vi} T_{ai})^\alpha + C_2, \text{ Pounds/Feet}^2$$

Module	Values of C_1				α	C_1	α	C_2
	Mercury	Venus	Mars	Ceres Vesta		Jupiter		
Earth reentry	0.0880	0.0668	0.0645	0.0903	0.273	0.0303	0.403	1.44
Mission	0.0563	0.0428	0.0412	0.0600	0.273	0.0156	0.403	1.44
Planetary excursion	0.0338	0.0241	0.0229	0.0512	0.273	0.0188	0.403	1.44
Insertion propulsion	0.0148	0.00523	0.00536	0.0217	0.273	0.00647	0.403	2.38
Escape propulsion	0.0179	0.00635	0.00650	0.0263	0.273	0.00860	0.403	2.38

Table 5. Scaling Equation Coefficients - Retrobraker Maximum Environment

$$W_{ti} = C_1 (A_{vi} T_{ai})^\alpha + C_2, \text{ Pounds/Feet}^2$$

Module	Values of C_1		α Mercury and Venus	Values of C_1			α Mars, Ceres/ Vesta and Jupiter	C_2
	Mercury	Venus		Mars	Ceres Vesta	Jupiter		
Earth reentry module	0.0880	0.0668	0.273	0.0283	0.376	0.307	0.403	1.44
Mission module	0.0563	0.0428	0.273	0.0147	0.195	0.160	0.403	1.44
Planetary excursion module	0.0338	0.0241	0.273	0.00955	0.169	0.138	0.403	1.44
Insertion propulsion module	0.0148	0.00523	0.273	0.00415	0.112	0.0915	0.403	2.38
Escape propulsion module	0.0179	0.00635	0.273	0.00555	0.148	0.122	0.403	2.38

Table 6. Scaling Equation Coefficients - Flyby Configuration

$$W_{ti} = C_1 (A_{vi} T_{ai})^\alpha + C_2, \text{ Pounds/Feet}^2$$

Module	Nominal Environment			Maximum Environment			C ₂
	Values of C ₁		α	Values of C ₁		α	
	Ceres Vesta	Jupiter		Ceres Vesta	Jupiter		
Earth reentry module	0.0435	0.0333	0.273	0.222	0.182	0.403	1.44
Mission module	0.0278	0.0295	0.273	0.115	0.0942	0.403	1.44
Probe module	0.0124	0.0173	0.273	0.136	0.111	0.403	1.44
Propulsion module	0.0390	0.0295	0.273	0.188	0.153	0.403	1.44

Table 7. Scaling Equation Coefficients (Aerobraker Spacecraft)

$$W_{ti} = C_1 \left[A_{vi} T_{ai} \right]^\alpha + C_2, \text{ Pounds/Feet}^2$$

Module	Nominal Environment		Maximum Environment			C ₂
	Values of C ₁		Values of C ₁		α	
	Mars	Venus	Mars	Venus		
Earth reentry module	0.0335	0.0335	0.273	0.0335	0.273	1.44
Mission module	0.0214	0.0214	0.273	0.0214	0.273	1.44
Heatshield	0	0	0.273	0	0.273	5.76
Aft bulkhead	0.0183	0.0215	0.273	0.0183	0.273	1.44

THERMAL ENVIRONMENT AND PROTECTION

The primary objective of the thermal analysis was to establish the overall heat balances as well as heat rejection and thermal protection systems requirements for the manned mission module. The second objective was to determine the required insulation systems for the storage of the propellants in space. This investigation does not consider the need of active refrigeration in the case of cryogenic propellants, but aims primarily at the passive storage or thermal insulation requirements involved. The section will be presented in two parts, the first dealing with the heat balances and requirements on the mission module and the second dealing with thermal protection required for propellant storage.

A summary of the essential results of the thermal protection studies is shown on Table 8. An insulation weight of approximately 0.1 pounds/foot² is adequate for the closed ecological system encompassing a range of 3 to 20 men in the mission module. It is important to note that because of the extreme heating near Mercury, either solar orientation control or a shadow shield will be required to keep direct solar radiation away from the environmental control subsystem (ECS) radiators. If solar radiation impinges on the radiators even cyclically, as in a rolling mode, it will be impossible to maintain life-zone temperatures in the mission module. The alternative to orientation control or shadow shielding involves the use of active refrigeration systems. Such systems may be of value in achieving greater mission flexibility, but development of reliable space designed units for long-duration missions was considered to be only speculative at this time. Such systems were eliminated from consideration in this study.

A heavier insulation requirement is evident for the open ecological system on missions to Jupiter. This results from the reduced heat generation within the module and an assumed criteria which limits the heat lost from the external surfaces to 10 percent of the internal heat generation. In all probability it is satisfactory to fix the insulation requirement at the 0.1 pound/foot² value and modify the ECS radiator flow control to reduce the heat rejection to about 80 percent of the design internal heat dissipation. As an alternative to this, it is possible to supply additional electrical power for heating purposes in the Jupiter mission case.

Each pound of radiator, including its glycol coolant within the tubes, is capable of rejecting 50 Btu/hour of internally generated heat. By allowing a 10 percent greater weight for the Mercury mission, a common radiator requirement is established consistent with the thermal protection. It is

Table 8. Summary of Manned Mission Module Multiple Layer Insulation Requirements

Mission	Open System		Closed System	
	3 Men	20 Men	3 Men	20 Men
Mercury	0.10 lb/ft ² * (0.49 kg/m ²)	0.10 lb/ft ² * (0.49 kg/m ²)	0.10 lb/ft ² ** (0.49 kg/m ²)	0.10 lb/ft ² ** (0.49 kg/m ²)
Jupiter	0.26 lb/ft ² ** (1.27 kg/m ²)	0.21 lb/ft ² ** (1.03 kg/m ²)	0.14 lb/ft ² ** (0.69 kg/m ²)	0.11 lb/ft ² (0.54 kg/m ²)
<p>Notes:</p> <p>*Either a solar orientation control or a solar shield is required in order to keep direct solar radiation off the ECS radiator.</p> <p>**The larger insulation thickness results from lower heat dissipation within the volume and the criteria of a maximum of 10 percent of internal generation allowed to be lost through surfaces.</p> <p>It is recommended that to control temperature, 0.10 lb/ft² be used for all cases. Then (1) additional electrical heating may be supplied at Jupiter, or (2) the radiator heat rejection may be reduced by 20 percent.</p>				

emphasized that no considerations of redundant radiator area for mission reliability purposes are included in this analysis.

Weight scaling equations are developed for the optimization of the propulsion module insulation thickness and boil-off propellant requirements, and representative thermal protection requirements are presented. The insulation heat-flow rates were integrated for missions to Mercury and Jupiter for each propellant to give a net integrated heat transfer, which was balanced against the net heat capacity in the fluid to yield insulation thickness requirements. For the mission to Mercury, only the hydrogen tank insulation thicknesses tend to exceed one inch on practical tankage area-to-volume ratios; however, the effect of a shadow shield or selective orientation control would lead to somewhat reduced requirements. The analysis has allowed an additional 50 percent¹ of the insulation heat transfer to account for support heat transfer (and other penetrations). Results are expressed as a function of the area-to-volume ratio since many tank configurations are involved in the task of vehicle design.

For a no-loss propellant storage technique, the tank volume must be sized for the lowest density or highest usable saturation temperature. For hydrogen, this would mean almost a 20-percent volume increase, thus making the case of 20-percent boil-off (evaporative storage) at 14.7 psia comparable to the equivalent no-loss storage tank in volume. For the other fluids, the volumetric coefficient of thermal expansion is less severe but may amount to 10 percent or more. A no-loss propellant storage technique also requires an increased wall thickness due to the high vapor pressure.

MANNED MISSION MODULE HEAT BALANCE AND THERMAL PROTECTION

The required weight for insulation and heat-rejection systems for a spectrum of missions and crew sizes were determined. The missions range from earth to Mercury and Jupiter on the extremes. The crew sizes include 3 to 20 men for each target body, and body heating is studied for two orientations. The orientations involve a rolling mode (where the external surface is exposed to a cyclically varying heat flux from the sun), and an end-oriented mode (where the end of the mission module is exposed directly to solar radiation). The internal heat sources considered in the heat balances included crew metabolic heating, life support and environment control systems, and other electrical loads. The electrical generating system was considered to be independent of the mission module and was not involved in the heat balances on that module aside from the energy dissipation within it. The assumed internally generated heat is shown in Table 9 for crew sizes of 3, 9, and 20 men for an open and closed system.

¹ This is an arbitrary allowance. Some heat input in excess of that which is conducted through the insulation will occur but the actual value must await experimental effort on particular configurations.

Table 9. Summary of Internal Heat Generation for the
Manned Mission Module

System	3 Men	9 Men	20 Men
Open	1.4 kw	2.9 kw	5.8 kw
Closed	2.1 kw	5.0 kw	10 kw
Note: This heat generation includes metabolic, electrical power, life support system and environmental control system sources.			

The only external heat load considered was that of direct radiation from the sun. Thus, this study requires the reservation that the spacecraft is assumed to be a minimum of 2 to 3 planetary radii from the planets at all times, so that heat received by albedo and planetary emission can be ignored in the heat balances for ECS and thermal-protection-requirement considerations.

Assumptions and Method

The study of heat balances was divided into two subtasks; first, a determination of the heating influence of surface coatings and second, the insulation and heat rejection radiator requirements. Conceivably, a totally passive system could be constructed so that the delicate balance between insulation and internal heat generation could be used to maintain life zone temperatures at any given point in the trajectories. However, for any practical mission, since a wide range of conditions are encountered and since these are continuously changing during the mission, it was mandatory that a system be defined using a glycol circulation heat rejection means. In this way it was possible to identify one coating system which was consistent with all missions and one insulation system which would also be usable for all missions. In order to accomplish this ideal approach, it was initially estimated that the insulation system would be designed so that not more than 10 percent of the internal heat generation on a given vehicle would be either lost or gained from the external surfaces of the mission module. That means that the ECS radiator would be used to accomplish the predominant heat rejection from the module. In this manner it is possible to minimize the effect of heliocentric radius on the internal temperatures. It was further estimated that for the purpose of this study the mission module sizes would be approximately 15 feet in diameter by 15 feet long for a three-man crew size (representing the minimum mission module), and 30 feet in diameter by 30 feet long for a 20-man crew (representing a maximum mission module size). A glycol circulation system was considered for heat rejection because it is the simplest system available and is typical of existing systems. No active refrigeration system such as a vapor compression cycle is included in this study although it appears that such a system might be necessary in the case of a mission to Mercury if solar orientation control or shadow shielding were not utilized. An active system could also be required for Mercury (and possibly Venus) missions if a low parking orbit altitude were used throughout the planetary stay.

The effect of the optical-thermal properties of surface coatings on the surface temperatures of the mission module and propulsion module was examined as a function of the heliocentric position, with the result that a

preferred choice is expressed for the lowest practical absorptivity to emissivity ratio. In this manner it is possible to isolate the effects of internal and external heat sources and minimize the interaction of orientation control. The philosophy applied here is expected to provide the most direct approach to thermal control and protection systems design and serves to clarify where reliability considerations of redundancy and increased design margin will be most valuably applied to achieve mission success.

Orientation and Surface Coatings

Equilibrium temperature results for rotating spheres and surfaces normal to the sun's rays which radiate from the front only are shown in Figure 10. These limits bound the equilibrium temperatures which will be achieved for all module attitude time histories. The figure shows the equilibrium temperature as a function of heliocentric distance, over the range from Mercury to Jupiter, including absorptivity to emissivity values of 0.2, 1 and 5. The equilibrium temperature range varies between 1100 K and 83 K and, since the life zone is at approximately 290 K, it is evident that a simple, completely static environmental control system is not achievable. This wide range of values partially substantiates the design approach to use the glycol ECS radiator for primary heat rejection, and insulation to isolate the module from solar heating. It should be noted that to achieve an α/ϵ of 0.2, it is necessary to use a white surface coating such as zinc oxide which is highly reflective to incident solar radiation wavelengths and highly emissive for long wavelength surface radiation. To approach an α/ϵ of 5, a very specular surface is required; that is, one which is capable of reflecting a great deal of the incident solar radiation but is not capable of emitting at low temperatures even as much energy as it reflects. Similarly, for a α/ϵ of 1, it is necessary to have surfaces such as black lacquers, deposited carbon black, or other materials which emit and absorb all wavelengths equally.

Since temperature is a prime consideration in the availability of the structural materials, either for the insulation or for the primary structure of the modules, it is evident that the lowest temperatures would generally allow the widest range of material selection and therefore the least cost in development, design, and fabrication. The high effectiveness of the super-insulation makes it qualitatively evident that a rather low weight penalty is involved in the use of insulation to isolate the ECS from the influence of the solar heat source which further supports adopting this approach.

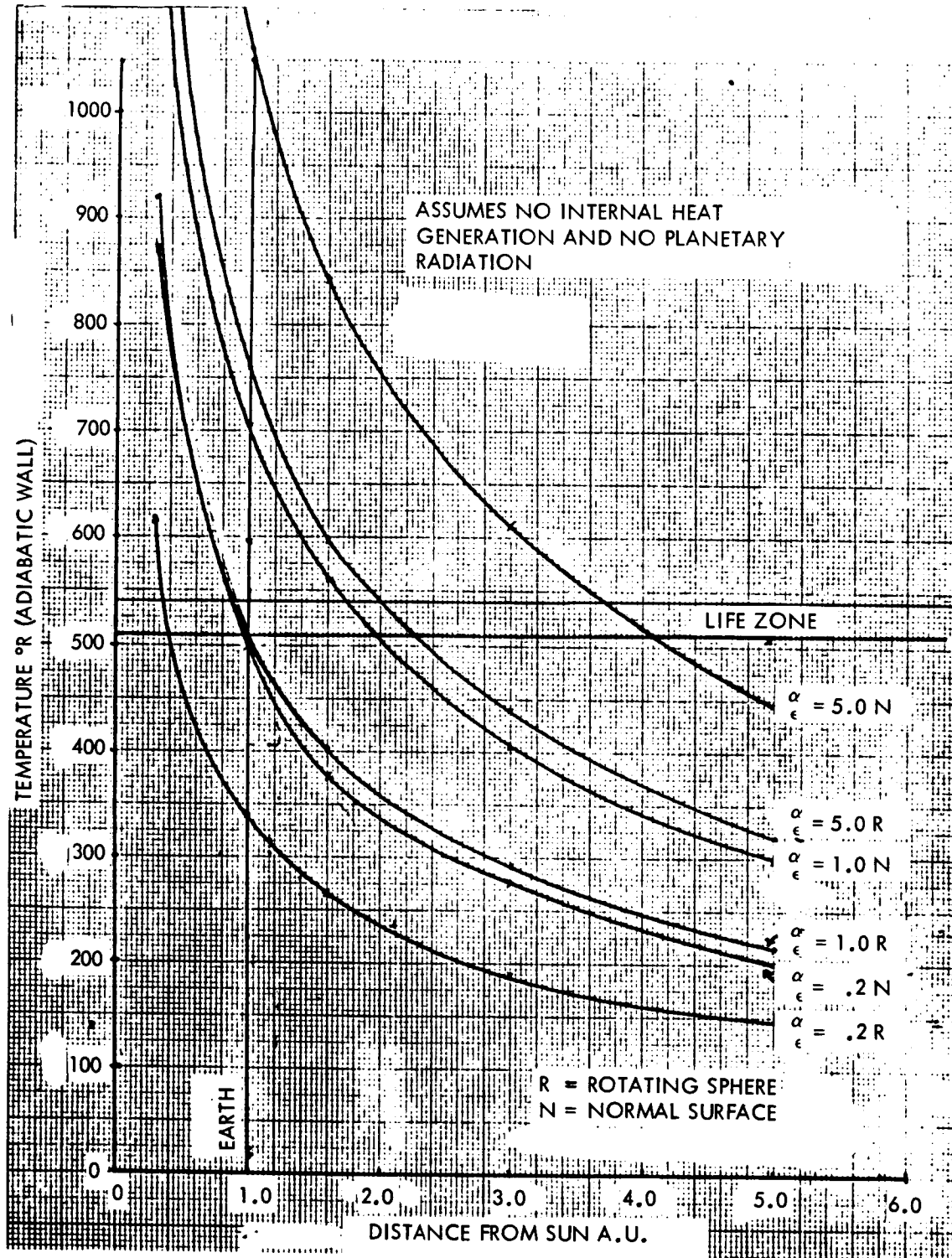


Figure 10. Equilibrium Wall Temperature Versus Distance From Sun

An absorptivity to emissivity ratio of 0.2 is considered representative of the lowest practically obtainable ratios available in the current technology and it is currently being approached on slab-sided spacecraft. With improvements in the state of the art it may be possible to reduce this ratio to a smaller value and work has been going on for many years in this direction. Concepts involving diffraction gratings and very selective materials have been the subject of much research in the aerospace industry, but to the present there has been no significant breakthrough in the achieving of very low α/ϵ . Therefore, a value of $\alpha/\epsilon = 0.2$ has been selected for this entire study. From Figure 10, it is evident that 0.2 leads to a much lower surface temperature than a ratio of 5 and is well below the life zone for the more distant planetary bodies. If it were desired to achieve a higher temperature, a black coating could be used, but the amount of insulation required to protect a vehicle would be only slightly influenced in this study. The micrometeoroid penetration barrier support structure (Figure 6) was studied in terms of the heat transfer which bypasses the insulation. The results show the current recommended design is adequate for thermal purposes on the mission modules.

Superinsulation Types

The types of superinsulation available for the current application are quite wide and encompass ranges of densities from 55 to over 120 kg/m³ (3.5 to 7.5 lb/ft³). The Linde type of superinsulation such as the SI-61 is the most dense and is constructed of aluminum foil of about 1/4 mil thickness with glass fiber separators between each of the aluminum foil reflector layers. Other types of insulation applicable to this study include NRC-2, the Quality Electric "Dimplar" and a design developed by Goodyear Company. The NRC-2 type of insulation, which was the insulation assumed during this study, is composed of 1/4 mil aluminized mylar which has a random crinkle built into the surface so that no separators are necessary. This insulation has a density of 55 kg/m³ (3.5 lb/ft³) but a value of 80 kg/m³ (5 lb/ft³) was used during this study to account for attachments and supports.

The results of tests performed at SD on NRC-2 type of insulation are presented on Figure 11 in the form from which data was reduced. The superinsulation integrated heat flow versus temperature is based on tests taken over a range of approximately 78 K to 390 K. The analytical representation of the curve is shown in Figure 11. Figure 12 is a derived analytical curve which is based on an assumed design of the micrometeoroid bumper structure which has low conductivity, 2 inch thick, fiber glass standoffs which have been structurally designed to minimize heat transfer. Figure 12 shows

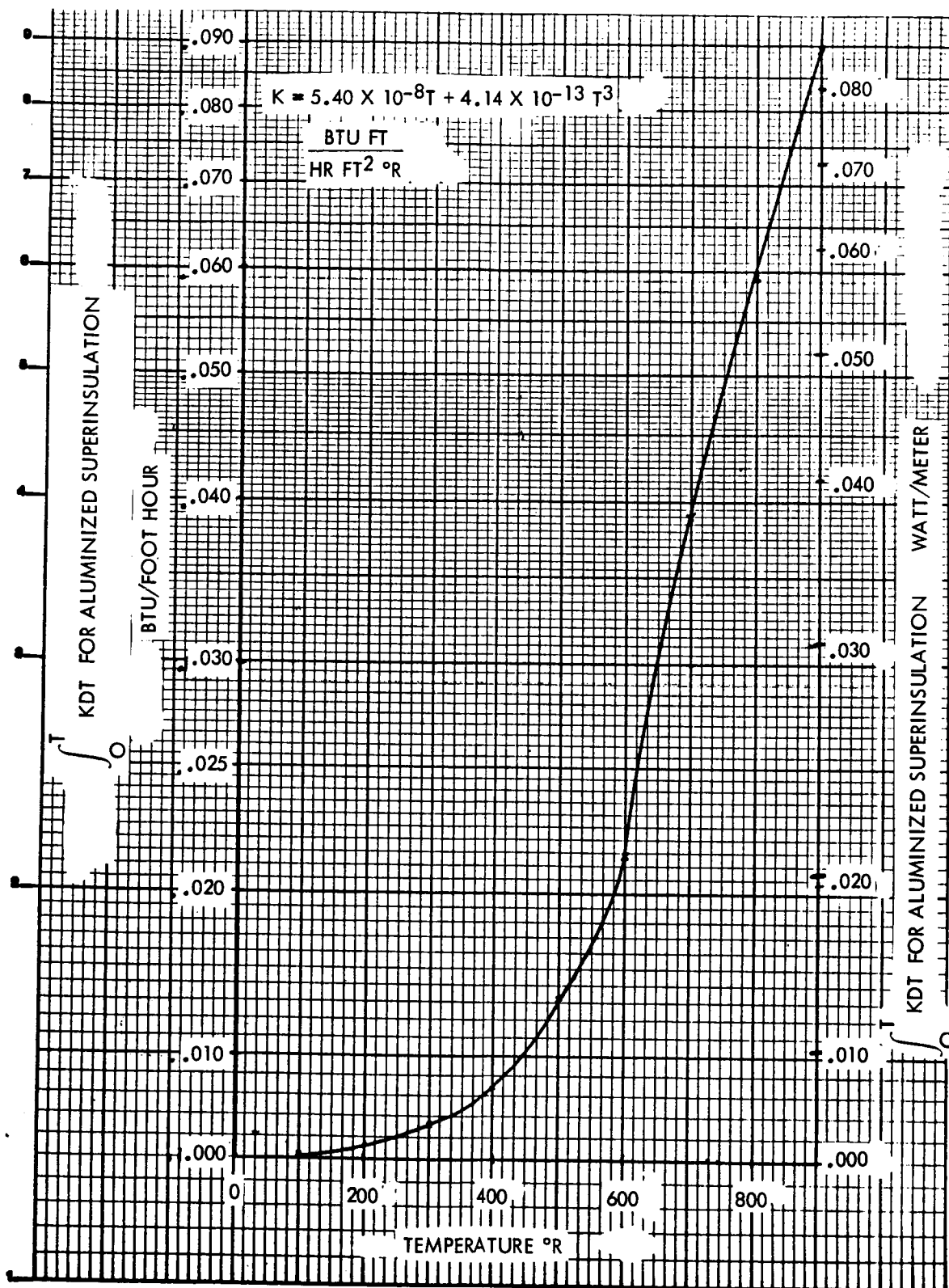


Figure 11. NRC-2 Superinsulation Integrated Heat Flow Versus Temperature

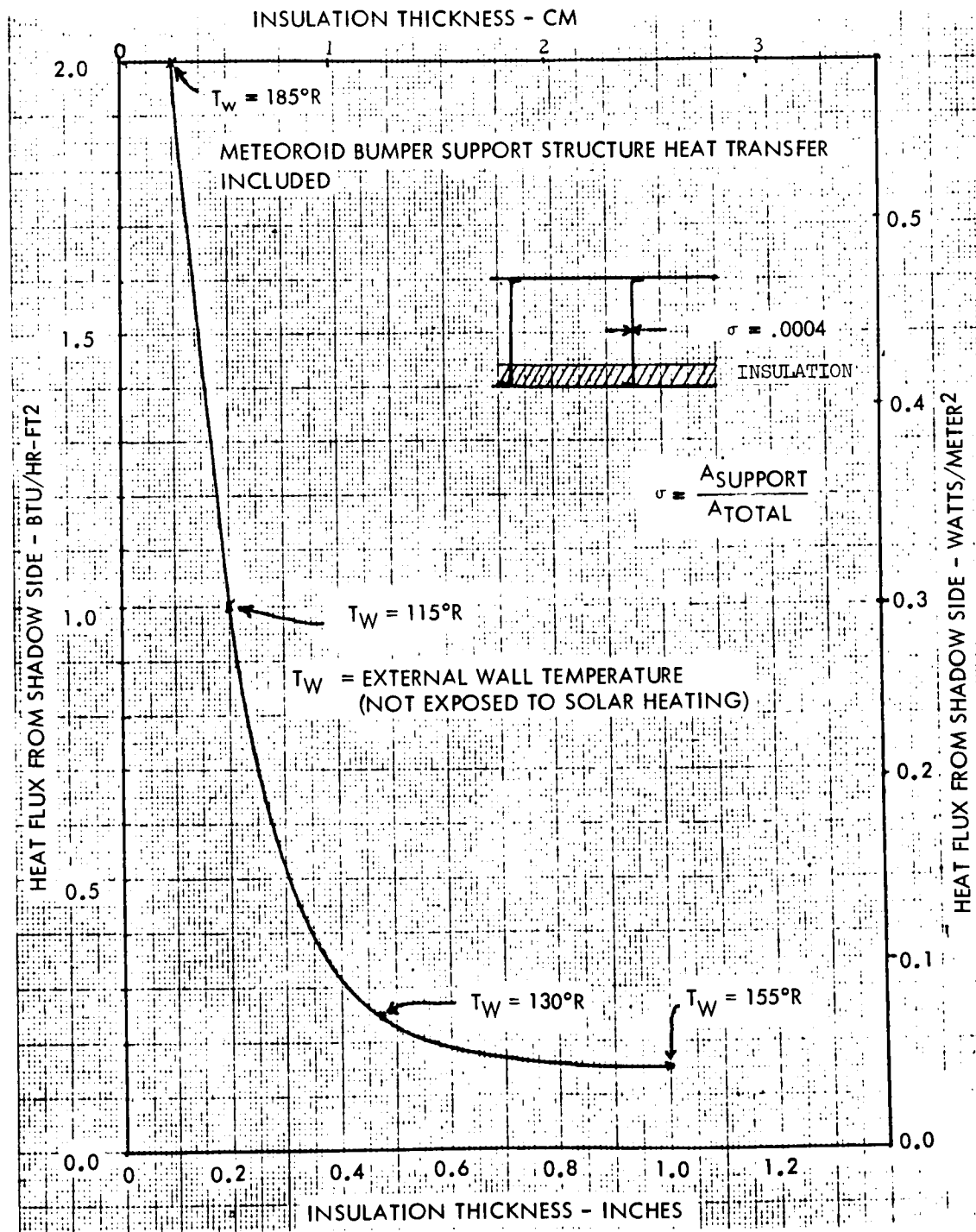


Figure 12. Heat Loss From Unexposed Side Versus Insulation Thickness, Including Micrometeoroid Bumper Structure

clearly that its impossible to get much below 0.1 of a Btu/hour square foot just because the structure of the micrometeoroid bumper achieves this minimum value in the case of unexposed surfaces rejecting heat to space ("unexposed" means not directly exposed to solar radiation).¹

Space Radiator Sizing

The design of space radiators, while fairly simple in principle, requires some consideration of the structure of the radiator itself. It is possible to use heat exchange tubes built into a sheet, such as the "panel-coil" design of Dean Products Corp., or designs such as the roll-bonded structures which are actually heat exchanger surfaces permitting transfer of the fluid through tubes that are embedded and embossed within the surface of the heat exchanger. The available patterns and weights are widely varying but it is possible to achieve a radiator weight of approximately 2 pounds/square foot including the fluids which are occupying the space inside the heat exchanger tubes.

While the best stainless steel heat exchangers today have a weight of approximately 2.1 pounds/square foot, it is clear that with little additional development a value 2 pounds/square foot, including fluids, can be achieved practically in the space vehicles. Since a square foot of radiator which is operating at approximately 300 K can reject approximately 100 Btu/hour in a water-glycol circulation system, (allowing its temperature to drop down to approximately 290 K in circulation) the design weight factor for a radiator should be about 50 Btu/hour/pound/radiator. This figure can be used for rough radiator sizing and while, perhaps, it can be somewhat reduced by very careful radiator design, the sensitivity of this small factor should not be significant in the overall system design. For example, 1 kilowatt is 3,412 Btu/hour; therefore in the case of the 20-man mission module for which approximately 10 kW are rejected if the partially closed life support subsystem is employed, the radiator area would be about 340 square feet, and the radiator weight including fluids in the radiator would amount to approximately 680 pounds as a representative value. To place this value in further perspective, the area represents about 15 percent of the mission module area; the weight represents about 1 percent of the total mission module weight.

¹ A problem of some note which has been evident on recent space vehicle flights is that of preventing liquefaction (condensation) of water vapor inside the occupied compartment. The condensation may take place on any surfaces which are below the dew point of the water vapor. It appears that by keeping heat transfer rate through the compartment walls to a value of approximately 1.0 Btu/hour square foot or below, it is easy to prevent this condensation from occurring with the forced convection available from the environmental control subsystem (ECS) conditioning and circulating system.

Conclusions

A minimum amount of thermal protection will be required on all missions being considered. Ideally about 10 layers of multilayer superinsulation will be sufficient and this corresponds to a weight of approximately 0.1 pounds/square foot on the entire external surface of the mission module. It is also concluded that in a mission to Jupiter actual orientation is not very important. Results show that heat loss is the major consideration and, while slightly more than 0.1 of a pound/square foot of insulation is needed to stay within the 10 percent of the system heat rejection internally, it is clear that there is sufficient adjustability in the heat rejection capability of the ECS Radiator that the recommended 0.1/pound square foot of insulation will be sufficient for all purposes.

A further conclusion is that for trips to Mercury, either solar orientation will be an absolute requirement or it will be necessary for a shadow shield to be erected which prevents the direct solar heating from impingement upon the radiator areas of the mission module. The primary limitation is not the insulation in this case but rather the heat rejection from the radiators which, if directly exposed to solar heating or cyclically exposed to solar heating, would cause the internal temperature of the mission module to become excessive. The result of the analysis shows that with a solar oriented system, the net heat gain stays below 10 percent of the system radiator rejection as long as insulation of approximately 0.1 pounds/square foot is maintained on all surfaces.

The final conclusion regards the design of radiators for environmental control purposes. These radiators should be painted white to maintain a high emissivity, and for the purpose of commonality analysis it should be assumed that 50 Btu/hour can be rejected from each pound of radiator surface.

PROPELLANT STORABILITY AND THERMAL PROTECTION REQUIREMENTS

The purpose of this portion of the study was to develop propellant boil-off and insulation thickness weight scaling equations and to examine typical insulation mass requirements for long-term propellant storage. Both the factors of heat transfer into the tank and heat storage within the propellant were examined. The examination includes both no-loss type of storage and evaporative storage techniques. For the no-loss storage of cryogenics, pressure rises of 14.7 to 90 psia and 50 percent slush to 90 psia were used to establish the allowable heat budget. In addition, the insulation requirements for total evaporation of 5, 10, and 20 percent of the total propellant were examined.

A comparison of the liquidus ranges of all of the propellants of importance in this study is shown in Figure 13. The liquids range includes the freezing point at the bottom, the normal boiling point at 14.7 psia, the 90 psia limiting pressure point for storability of propellants, and the critical point, which is the upper liquid limit for any of the propellants involved. Figure 13 will allow an estimate of where potential boiling and freezing problems will occur. For example, at Jupiter monomethylhydrazine (MMH) is well below its freezing condition. Insulation must be added to prevent heat from being lost or it may be necessary to add heat to the system. The diborane and methane may possibly freeze if left at Jupiter for a long time, so insulation will be required. Oxygen, FLOX, and oxygendifluorine are all storable propellants, and liquid hydrogen will boil off, but it has a small differential temperature. At 3 A. U., or approximately the asteroid belt, oxygen difluoride and methane are storable, LOX and FLOX are slightly above the 90 psia limit, liquid hydrogen is only slightly changed from Jupiter, and diborane is near its freezing point. For diborane this is approximately the limit of storability, and monomethylhydrazine is still likely to freeze. At Mars all of the oxidizers and methane are well above their boiling points at 90 psia; therefore, insulation is always required for closer approach to the sun. The diborane is storable in this region and somewhat beyond, but MMH still requires insulation to prevent freezing. At Earth, all of the oxidizers, methane and hydrogen are cryogenics, while diborane is storable. MMH is essentially storable between Earth and Mercury; however, at Mercury all of the fuels and oxidizers may be considered to be cryogenics with the exception of MMH which is storable at pressure slightly above the normal boiling point and below 90 psia.

The calculation of the heat input to the tanks (or in some cases the heat extracted) is based on a time-trajectory integration of the heat rate. The heat flow into the propellant is given by

$$H = \frac{A}{d} \int_{T_1}^{T_2} K dT; \text{ cal/sec} \quad (1)$$

where

A = the total surface area; m²

d = the insulation thickness; m

K = the thermal conductivity; cal m/sec m² °K

T = temperature; °K

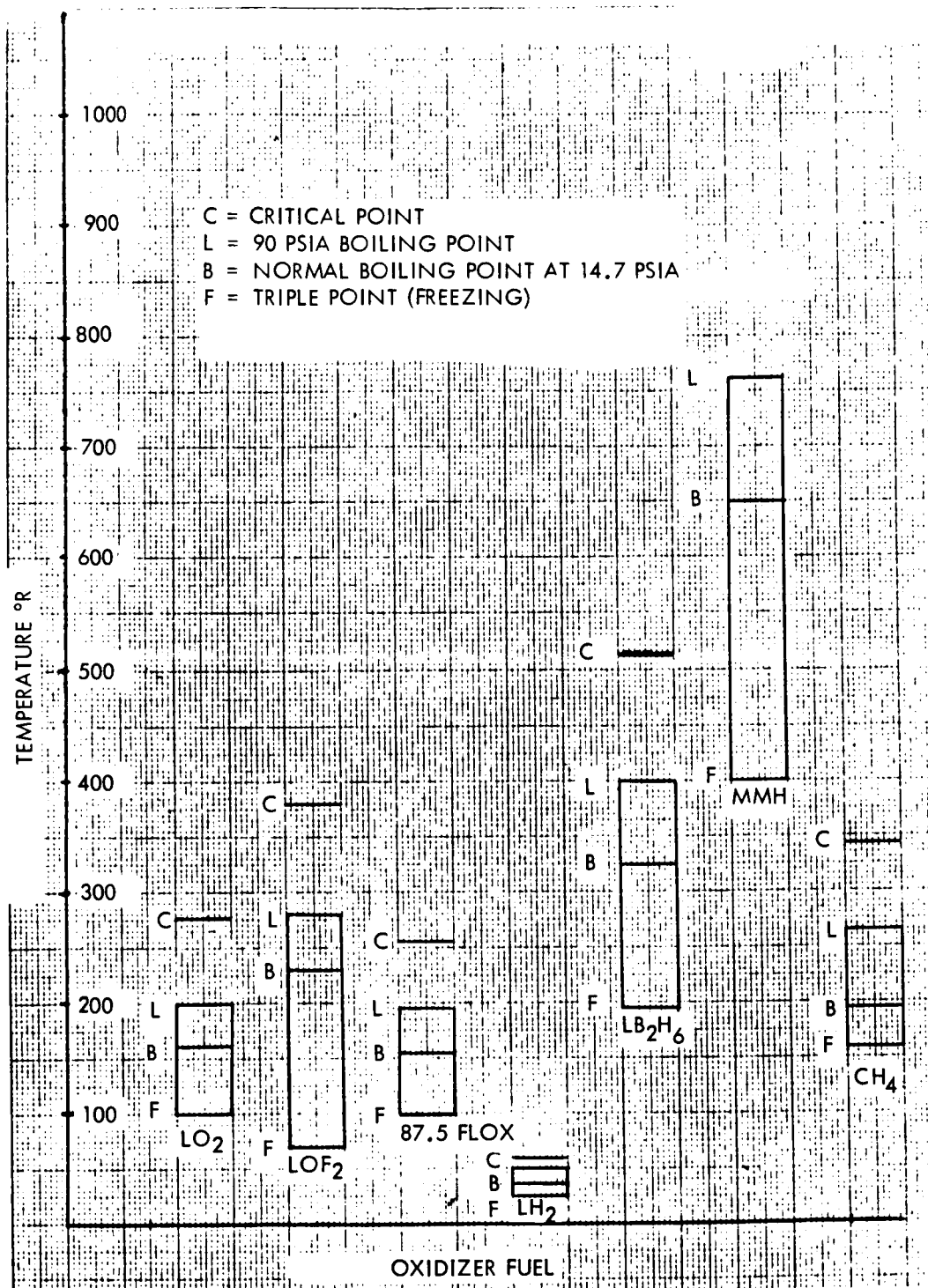


Figure 13. Liquidus Temperature Range of Fuels and Oxidizers

For the case of evaporative storage, the interior surface temperature (T_1) of the propellant tanks is assumed to be equal to the fuel or oxidizer at the boil-off (constant saturation) temperature. The surface temperature (T_2) is assumed to be equal to the equilibrium wall temperature, which is given by

$$T_2 = \left[\left(\frac{\alpha_s}{\epsilon} \right) \left(\frac{A_A}{A_E} \right) \left(\frac{S}{\sigma} \right) \right]^{\frac{1}{4}}; \text{ } ^\circ\text{K} \quad (2)$$

where

α_s = the surface coating absorptivity

ϵ = the surface coating emissivity

A_A = the effective absorbing area; m^2

A_E = the effective emitting area; m^2

S = the solar constant; cal/sec m^2

σ = the Stefan-Boltzmann constant

The solar constant is given by

$$S = \frac{S_\odot}{R^2} \quad (3)$$

where R is the distance of the spacecraft from the sun. As shown previously, the thermal conductivity (K) is given by

$$K = 0.383 \times 10^{-8}T + 0.89984 \times 10^{-13}T^3; \text{ cal/m sec } ^\circ\text{K} \quad (4)$$

Therefore,

$$\int_{T_1}^{T_2} KdT = 0.1915 \times 10^{-8} \left(T_2^2 - T_1^2 \right) + 0.22496 \times 10^{-14} \left(T_2^4 - T_1^4 \right); \text{ cal/m sec. } (5)$$

For a given fuel or oxidizer,

$$\int_{T_1}^{T_2} KdT = 0.1915 \times 10^{-8} T_2^2 + 0.22496 \times 10^{-14} T_2^4 - C_3; \text{ cal/m sec. } (6)$$

where

$$C_3 = 0.1915 \times 10^{-8} T_1^2 + 0.22496 \times 10^{-14} T_1^4 ;$$

Substituting Equations (2) and (3) into (6), the heat flow into the propellant is then

$$\int_{T_1}^{T_2} KdT = \frac{C_1}{R} + \frac{C_2}{R^2} - C_3 \quad (7)$$

where

$$C_1 = 0.1915 \times 10^{-8} \left[\left(\frac{\alpha_s}{\epsilon} \right) \left(\frac{A_A}{A_E} \right) \left(\frac{S_{\oplus}}{\sigma} \right) \right]^{\frac{1}{2}} ;$$

and

$$C_2 = 0.22496 \times 10^{-14} \left[\left(\frac{\alpha_s}{\epsilon} \right) \left(\frac{A_A}{A_E} \right) \left(\frac{S_{\oplus}}{\sigma} \right) \right] ;$$

The total heat input (Q_{IN}) is

$$Q_{IN} = \frac{A}{d} \int_{t_1}^{t_2} \int_{T_1}^{T_2} KdTdt; \quad (8)$$

or, from Equation (7)

$$Q_{IN} = \frac{A}{d} \int_{t_1}^{t_2} \left(\frac{C_1}{R} + \frac{C_2}{R^2} - C_3 \right) dt; \quad (9)$$

where $t_2 - t_1$ is the exposure time of the propellant module under consideration. Integration of Equation (9) results in

$$Q_{IN} = \frac{A}{d} \left[\frac{C_1 a \sqrt{1-e^2} (\Delta E) + C_2 (\Delta v)}{h} - C_3 (\Delta t) \right] \quad (10)$$

where

a = semimajor axis of the heliocentric conic

e = eccentricity

ΔE = change in eccentric anomaly

Δv = change in true anomaly

Δt = exposure time

h = angular momentum

The heat absorbed by the propellant for the evaporative storage case is given by

$$Q = mL; \text{ cal} \quad (11)$$

where m is the fuel or oxidizer allowed to boil off and L is the heat of vaporization.

Equating the heat input [Equation (10)] and the heat absorbed [Equation (11)] results in the following expression for the propellant boil-off mass as a function of the insulated area, the insulation thickness, and the heliocentric trajectory characteristics:

$$W_{\text{BOIL-OFF}} = \frac{A}{dL} \left[\frac{C_1 a \sqrt{1-e^2} (\Delta E) + C_2 (\Delta v)}{h} - C_3 (\Delta t) \right] \quad (12)$$

The optimum relationship between the boil-off propellant and the insulation thickness is obtained by minimizing the total spacecraft mass. The mass ratios for a two-stage vehicle are given by

$$\mu_1 = \frac{W_{PL} + W_{S1} + W_{S2} + W_{\text{INS1}} + W_{\text{INS2}} + W_{P1} + W_{P2} + W'_{B1}}{W_{PL} + W_{S1} + W_{S2} + W_{\text{INS1}} + W_{\text{INS2}} + W_{P2} + W'_{B1}} \quad (13)$$

and

$$\mu_2 = \frac{W_{PL} + W_{S2} + W_{\text{INS2}} + W_{P2}}{W_{PL} + W_{S2} + W_{\text{INS2}}} \quad (14)$$

where

W_{PL} = payload mass

W_S = stage mass

W_{INS} = insulation mass

W_P = propellant mass

W'_{B1} = boil-off propellant mass between the use of the first and second stages.

The initial spacecraft mass is given by

$$W_O = W_{PL} + W_{S1} + W_{S2} + W_{INS1} + W_{INS2} + W_{P1} + W_{P2} + W_{B1} + W_{B2} \quad (15)$$

where, in addition to the previously defined variables,

W_B = total boil-off propellant mass.

Combining Equations (13), (14), and (15),

$$W_O = \mu_1 \left[W_{B2} + W_{S1} + W_{INS1} + \mu_2 (W_{PL} + W_{S2} + W_{INS2}) \right] + W_{B1} + W_{B2} \quad (16)$$

For a monopropellant (nuclear) stage, let

$$W_{B1} = \frac{A_1 K_1}{d_1 L}, \quad (17)$$

$$W_{B2} = \frac{A_2 K_2}{d_2 L} \quad (18)$$

where K_1 and K_2 are determined from Equation (12). The insulation mass is given by

$$W_{INS1} = A_1 d_1 \rho_{INS} \quad (19)$$

$$W_{INS2} = A_2 d_2 \rho_{INS} \quad (20)$$

where ρ_{INS} is the insulation density.

Therefore,

$$W_o = \mu_1 \left[\frac{A_2 K_2}{d_2 L} + W_{S1} + A_1 d_1 \rho_{INS} + \mu_2 (W_{PL} + W_{S2} + A_2 d_2 \rho_{INS}) \right] \quad (21)$$

$$+ \frac{A_1 K_1}{d_1 L} + \frac{A_2 K_2}{d_2 L}$$

The optimum insulation thicknesses are then

$$d_{1opt} = \sqrt{\frac{K_1}{\mu_1 \rho_{INS} L}} \quad (22)$$

and

$$d_{2opt} = \sqrt{\frac{K_1 + \mu_1 K_2}{\mu_1 \mu_2 \rho_{INS} L}} \quad (23)$$

The optimum boil-off propellant requirements for the two stages are then

$$W_{B1opt} = A_1 \sqrt{\frac{\mu_1 K_1 \rho_{INS}}{L}} \quad (24)$$

and

$$W_{B2opt} = W'_{B2} + W''_{B2} = A_2 (K_1 + K_2) \sqrt{\frac{\mu_1 \mu_2 \rho_{INS}}{(K_1 + \mu_1 K_2) L}} \quad (25)$$

where W_{B2}'' is the boil-off propellant of the second stage prior to the use of the first stage. The above method can be extended for any number of stages and to include the case of bipropellant propulsion stages. The extension of the above equations were incorporated in the SD-developed Weight Synthesis digital computer program for computing the insulation thickness and propellant boil-off requirements during the mission/system analyses (Appendix D).

Tables 10 through 13 were prepared to illustrate the propellant tank insulation requirements for missions to Mercury and Jupiter. The results include an additional 50 percent heat transfer to cover the effects of structural supports attaching the insulation to the module structure. As noted previously, the heat transfer is arbitrary but was included to account for some heat leaks through the insulation. As in the previous part of the study to determine the external skin temperature, an absorptivity-to-emissivity ratio of 0.2 was assumed. In general, the insulation requirement is no greater than 2.54 cm (1 inch) even for the most cryogenic application of superinsulations. It is significant that similar amounts of insulation on a weight-per-square-meter basis are required to keep the monomethylhydrazine from freezing during transfers to Jupiter (Ganymede PEM) as are required for keeping liquid hydrogen from boiling on a mission to Mercury.

Table 10. Propellant Tank Insulation Requirements to Mercury - Rolling Cylinder

Propellant	Condition											
	Boiloff						No Loss					
	5 Percent			10 Percent			20 Percent			14.7 → 90 psia		
	A/V Ratio			A/V Ratio			A/V Ratio			A/V Ratio		
	0.633	0.844	1.266	0.633	0.844	1.266	0.633	0.844	1.266	0.633	0.844	1.266
LO ₂	0.019 (1.49)	0.025 (1.98)	0.037 (2.98)	0.009 (0.708)	0.012 (0.952)	0.018 (1.416)	0.004 (0.317)	0.005 (0.415)	0.008 (0.635)	0.005 (0.440)	0.007 (0.586)	0.011 (0.879)
LH ₂ (A)	0.073 (5.81)	0.096 (7.72)	0.015 (11.62)	0.034 (2.71)	0.045 (3.59)	0.067 (5.40)	0.015 (1.22)	0.020 (1.61)	0.031 (2.44)	0.015 (1.22)	0.020 (1.64)	0.031 (2.44)
FLOX	0.016 (1.29)	0.022 (1.73)	0.032 (2.59)	0.008 (0.610)	0.010 (0.806)	0.015 (1.22)	0.003 (0.269)	0.005 (0.366)	0.007 (0.537)	0.005 (0.391)	0.006 (0.513)	0.010 (0.757)
LOF ₂	0.015 (1.20)	0.020 (1.59)	0.030 (2.37)	0.007 (0.562)	0.010 (0.757)	0.014 (1.12)	0.003 (0.244)	0.004 (0.342)	0.006 (0.488)	0.004 (0.342)	0.006 (0.464)	0.009 (0.684)
B ₂ H ₆	0.013 (1.07)	0.018 (1.44)	0.027 (2.15)	0.006 (0.513)	0.009 (0.684)	0.013 (1.03)	0.003 (0.220)	0.004 (0.293)	0.006 (0.439)	0.003 (0.244)	0.004 (0.317)	0.006 (0.488)
MMH (B)	0.000 (0.000)	0.000 (0.000)	0.000 (0.000)	0.000 (0.000)	0.000 (0.000)	0.000 (0.000)	0.000 (0.000)	0.000 (0.000)	0.000 (0.000)	0.000 (0.000)	0.000 (0.000)	0.000 (0.000)

Notes: Insulation thickness requirements are given in meters. Figures in parentheses give mass-per-square-meter requirements in kilograms.

Mass per area based on assuming an insulation volume density = 24.4 kilograms per cubic meter.

A. Different A/V ratios have been used for LH₂
They are: 0.299, 0.399, and 0.598

B. MMH tanked at 525

Table 11. Propellant Tank Insulation Requirements to Mercury - Normal Surface

Propellant	Condition														
	Boiloff										No Loss				
	5 Percent					10 Percent					20 Percent				
	A/V Ratio					A/V Ratio					A/V Ratio				
	0.633	0.844	1.266	0.633	0.844	1.266	0.633	0.844	1.266	0.633	0.844	1.266	0.633	0.844	1.266
LO ₂	0.052 (4.15)	0.069 (5.52)	0.104 (8.30)	0.025 (1.98)	0.033 (2.64)	0.049 (3.96)	0.011 (0.855)	0.014 (1.15)	0.021 (1.71)	0.016 (1.29)	0.021 (1.71)	0.032 (2.56)	0.006 (0.464)	0.008 (0.610)	0.016 (0.928)
LH ₂ (A)	0.173 (13.8)	0.230 (48.4)	0.346 (27.7)	0.084 (6.69)	0.111 (8.89)	0.167 (13.4)	0.037 (2.98)	0.049 (3.96)	0.074 (5.96)	0.037 (2.98)	0.049 (3.96)	0.074 (5.96)	0.020 (1.59)	0.027 (2.15)	0.040 (3.17)
Flox	0.045 (3.59)	0.060 (4.79)	0.090 (7.18)	0.021 (1.71)	0.028 (2.27)	0.043 (3.42)	0.010 (0.757)	0.013 (1.00)	0.019 (1.51)	0.013 (1.05)	0.017 (1.39)	0.026 (2.10)	0.005 (0.415)	0.007 (0.562)	0.010 (0.830)
LOF ₂	0.040 (3.17)	0.053 (4.22)	0.079 (6.35)	0.019 (1.49)	0.025 (1.98)	0.037 (2.98)	0.008 (0.659)	0.011 (0.879)	0.017 (1.34)	0.011 (0.903)	0.015 (1.20)	0.022 (1.78)	0.004 (0.317)	0.005 (0.415)	0.008 (0.635)
B ₂ H ₆	0.052 (4.99)	0.070 (5.57)	0.105 (8.40)	0.025 (2.00)	0.033 (2.66)	0.500 (4.00)	0.011 (0.879)	0.015 (1.17)	0.022 (1.76)	0.012 (0.952)	0.016 (1.27)	0.024 (1.90)			
MMH (B)	0.009 (0.684)	0.011 (0.903)	0.017 (1.37)	0.004 (3.17)	0.005 (0.415)	0.008 (0.635)	0.002 (0.147)	0.002 (0.195)	0.004 (0.293)	0.002 (0.122)	0.002 (0.171)	0.003 (0.244)			

Notes: Insulation thickness requirements are given in meters. Figures in parentheses give mass-per-square-meter requirements in kilograms.

Mass per area based on assuming an insulation volume density = 24.4 kilograms.

A. Different A/V ratios have been used for LH₂
They are: 0.299, 0.399, and 0.598

B. MMH tanked at 525 R.

Table 12. Propellant Tank Insulation Requirements to Jupiter (Rolling Cylinder)

Propellant	Condition											
	Boiloff						No Loss					
	5 Percent			10 Percent			20 Percent			14.7 → 90 psia		
	A/V Ratio			A/V Ratio			A/V Ratio			A/V Ratio		
LO ₂ (A)	0.633 (0.220)	0.844 (0.293)	1.266 (0.440)	0.633 (0.098)	0.844 (0.147)	1.266 (0.195)	0.633 (0.049)	0.844 (0.073)	1.266 (0.098)	0.633 (0.073)	0.844 (0.098)	1.266 (0.147)
LH ₂ (B)	0.024 (1.93)	0.032 (2.56)	0.048 (3.81)	0.012 (0.928)	0.015 (1.22)	0.023 (1.86)	0.005 (0.415)	0.007 (0.562)	0.010 (0.830)	0.005 (0.415)	0.007 (0.537)	0.010 (0.806)
FLOX (C)	0.002 (0.195)	0.003 (0.269)	0.005 (0.391)	0.001 (0.098)	0.002 (0.122)	0.002 (0.195)	0.001 (0.049)	0.001 (0.049)	0.001 (0.098)	0.001 (0.049)	0.001 (0.073)	0.001 (0.098)
LOF ₂ (D)	0.001 (0.073)	0.001 (0.098)	0.002 (0.147)	0.001 (0.049)	0.001 (0.049)	0.001 (0.098)	0.000 (0.024)	0.000 (0.024)	0.001 (0.049)	0.000 (0.024)	0.000 (0.024)	0.001 (0.049)
B ₂ H ₆ (E)	0.000 ---	0.000 ---	0.000 ---	0.000 ---	0.000 ---	0.000 ---	0.000 ---	0.000 ---	0.000 ---	0.002 (0.171)	0.003 (0.244)	0.004 (0.342)
MMH (F) (G)	---	---	---	---	---	---	---	---	---	0.013 (1.03)	0.017 (1.32)	0.026 (0.205)

Notes: Insulation thickness requirements are given in meters. Figures in parentheses give mass-per-square-meter requirements in kilograms. Mass per area based on assuming an insulation volume density = 24.4 kilograms per cubic meter.

- (A) LO₂ boils till tank is 3.8 A. U. from sun. For no loss, pressure builds to 90² psia until tank is 2.4 A. U. from sun. LO₂ is storable at Jupiter.
- (B) Different A/V ratios have been used for LH₂. They are: 0.299, 0.399, and 0.598.
- (C) FLOX boils till it reaches 4.2 A. U. For no loss, pressure will build to 90 psia until it reaches 2.8 A. U. FLOX is storable at Jupiter.
- (D) LOF₂ boils till it reaches 2.0 A. U. For no loss, pressure builds to 90 psia till it reaches 1.4 A. U. LOF₂ is storable at Jupiter.
- (E) B₂H₆ will not boil significantly at 1.0 A. U. and farther from sun. Insulation will be necessary to keep from freezing and has been listed under no loss, 14.7 → 90 psia.
- (F) MMH always in danger of freezing. The necessary insulation has been listed under no loss, 14.7 → 90 psia.
- (G) MMH tanked at 525 R.

Table 13. Propellant Tank Insulation Requirements to Jupiter (Normal Surface)

Propellant	Condition													
	Boiloff							No Loss						
	5 Percent			10 Percent				20 Percent				14.7 → 90 psia		
	A/V Ratio			A/V Ratio				A/V Ratio				A/V Ratio		
LO ₂ (A)	0.633 (0.733)	0.844 (0.806)	1.266 (1.47)	0.633 (0.342)	0.844 (0.391)	1.266 (0.684)	0.009 (0.146)	0.633 (0.293)	0.844 (0.195)	1.266 (0.440)	0.006 (0.098)	0.633 (0.098)	0.844 (0.147)	1.266 (0.220)
LH ₂ (B)	0.057 (4.42)	0.076 (5.97)	0.114 (4.22)	0.027 (2.13)	0.035 (2.74)	0.053 (4.22)	0.012 (0.952)	0.024 (1.92)	0.016 (1.22)	0.024 (1.92)	0.006 (0.513)	0.008 (0.635)	0.013 (1.02)	0.013 (1.02)
FLOX (C)	0.008 (0.610)	0.010 (0.806)	0.015 (1.22)	0.004 (0.293)	0.005 (0.391)	0.007 (0.586)	0.002 (0.122)	0.003 (0.244)	0.002 (0.171)	0.004 (0.342)	0.001 (0.098)	0.002 (0.122)	0.002 (0.195)	0.002 (0.195)
LOF ₂ (D)	0.005 (0.366)	0.006 (0.488)	0.009 (0.733)	0.002 (0.171)	0.003 (0.220)	0.004 (0.342)	0.001 (0.098)	0.003 (0.220)	0.002 (0.147)	0.002 (0.122)	0.006 (0.513)	0.009 (0.684)	0.013 (1.03)	0.013 (1.03)
B ₂ H ₆ (E)	0.001 (0.073)	0.001 (0.098)	0.002 (0.146)	0.000 (0.024)	0.000 (0.024)	0.001 (0.049)	0.000 (0.024)	0.001 (0.049)	0.000 (0.024)	0.002 (0.171)	0.003 (0.244)	0.003 (0.244)	0.003 (0.244)	0.003 (0.244)
MMH (F) (G)	---	---	---	---	---	---	---	---	---	---	---	---	---	---

Notes: Insulation thickness requirements are given in meters. Figures in parentheses give mass-per-square-meter requirements in kilograms. Mass per area based on assuming an insulation volume density = 24.4 kilograms per cubic meter.

- (A) LO₂ boils till tank is 3.8 A. U. from sun. For no loss, pressure builds to 90 psia until tank is 2.4 A. U. from sun. LO₂ is storable at Jupiter.
- (B) Different A/V's have been used for LH₂. They are: 0.299, 0.399, and 0.598
- (C) FLOX boils till it reaches 4.2 A. U. For no loss, pressure will build to 90 psia until it reaches 2.8 A. U. FLOX is storable at Jupiter.
- (D) LOF₂ boils till it reaches 2.0 A. U. For no loss, pressure builds to 90 psia till it reaches 1.4 A. U. LOF₂ is storable at Jupiter.
- (E) B₂H₆ will not boil significantly at 1.0 A. U. and farther from sun. Insulation will be necessary to keep from freezing and has been listed under no loss, 14.7 → 90 psia.
- (F) MMH always in danger of freezing. The necessary insulation has been listed under no loss, 14.7 → 90 psia.
- (G) MMH tanked at 525 R.

RADIATION ENVIRONMENT AND PROTECTION

An analysis has been performed to determine the effects of the space-radiation and the Jupiter trapped radiation environment on spacecraft design. The analysis of the space-radiation environment can be carried out by two different methods. One is to calculate the expected solar environment for the mission being considered from statistical correlations obtained from past solar events. This technique provides the most accurate expected particle fluxes and doses possible from the available data. The other method is to obtain analytical representations between solar and mission parameters which can be combined to yield mission fluxes and/or doses. While this second technique is somewhat less accurate, it has the advantage of easy and rapid computation and is thus desirable when many mission and vehicle combinations are being considered.

The work described in the following sections is concerned with the development of an analytical representation of the space radiation dose expected on a deep space mission. The development of the analytical representation incorporates those factors known to have major effects upon the mission dose while neglecting factors considered less important.

A short bibliography dealing with solar, Van Allen, and galactic sources of nuclear radiation is listed in References 2 through 15.

SPACE RADIATION ANALYSIS

The development of an analytical representation for mission-dose calculation is composed of several parts. These parts are discussed separately in this section, then incorporated into the final equation in the next section.

Solar Radiation

Solar flare radiation is usually treated statistically, since our knowledge of the physical mechanisms involved does not currently permit a deterministic treatment. There have been several studies (References 2, 3, 16, and 17) of the probabilities of solar flare radiation, most of which were averaged over the years since 1956. Two of the most-referenced studies are those of Webber (References 2 and 3) and of Modisette, Vinson, and Hardy (Reference 16). Webber obtained his probabilities by "flying" a series of hypothetical missions, starting a new one each day. Modisette,

Vinson, and Hardy used a Poisson-distribution function which was extrapolated to low probabilities after being normalized at high probabilities. These two probability functions are shown in Figures 14 through 16 for mission durations of 4, 26, and 104 weeks.

These probability functions agree fairly well for probabilities ≥ 10 percent. Each method has limitations in the low-probability region. The overlapping hypothetical missions of Webber are not independent, and cannot be treated as statistically isolated. On the other hand, the extrapolations of Modisette, Vinson, and Hardy are (for the longer missions) based on only a few points which fit a curve better than a straight line. The direction of the curve is toward a decrease of the proton fluxes at low probabilities, thus decreasing the disagreement between the two analyses.

It is possible to approximately fit the proton flux probability curves by a function of the following form (Reference 18):

$$P(t) = e^{-\beta \left(\frac{\int \phi}{t} \right)^\eta} \quad (1)$$

where

$\int \phi$ is the mission flux (protons/centimeter²) > 30 Mev

t = the mission duration (weeks),

$\beta = 2.5 \times 10^{-4}$

and

$\eta = 0.5$

The comparisons of Equation 1 with the analyses of Webber and of Modisette, Vinson, and Hardy are also shown in Figures 14 through 16. The agreement with these analyses is better for long duration missions ($t = 26$, and $t = 104$ weeks). For short missions ($t = 4$ weeks), the comparison is poor. However, planetary mission durations of less than 26 weeks will not take place based on current technology projected into the foreseeable future.

For low probabilities (less than 10 percent) Equation 1 lies between the analysis of Webber and that of Modisette, Vinson, and Hardy. As discussed previously, this represents a compromise in the probability region where each analysis has limitations.

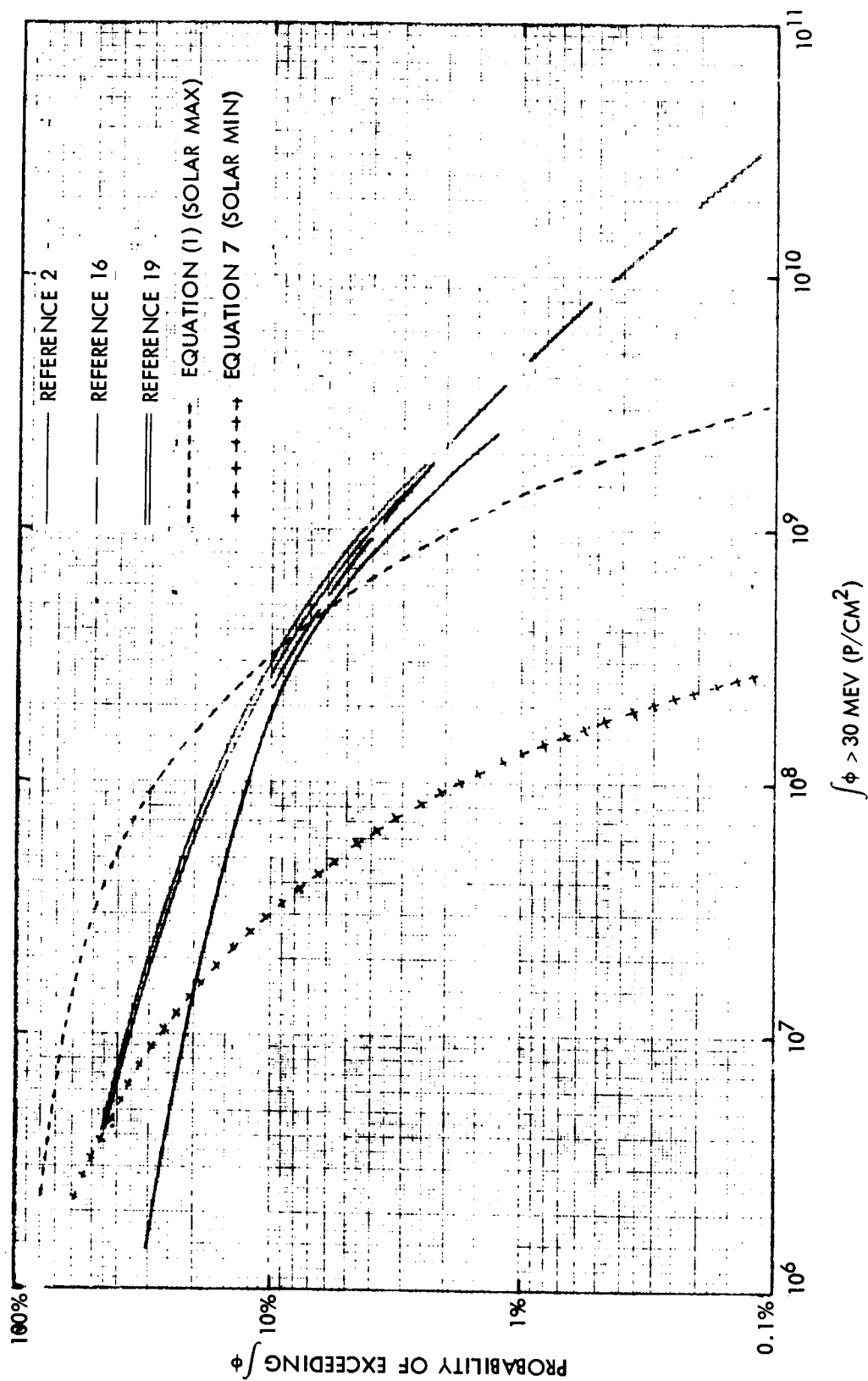


Figure 14. Comparison of Solar Flare Proton Probabilities for a Four-Week Mission at 1 AU, $t = 4$ Weeks

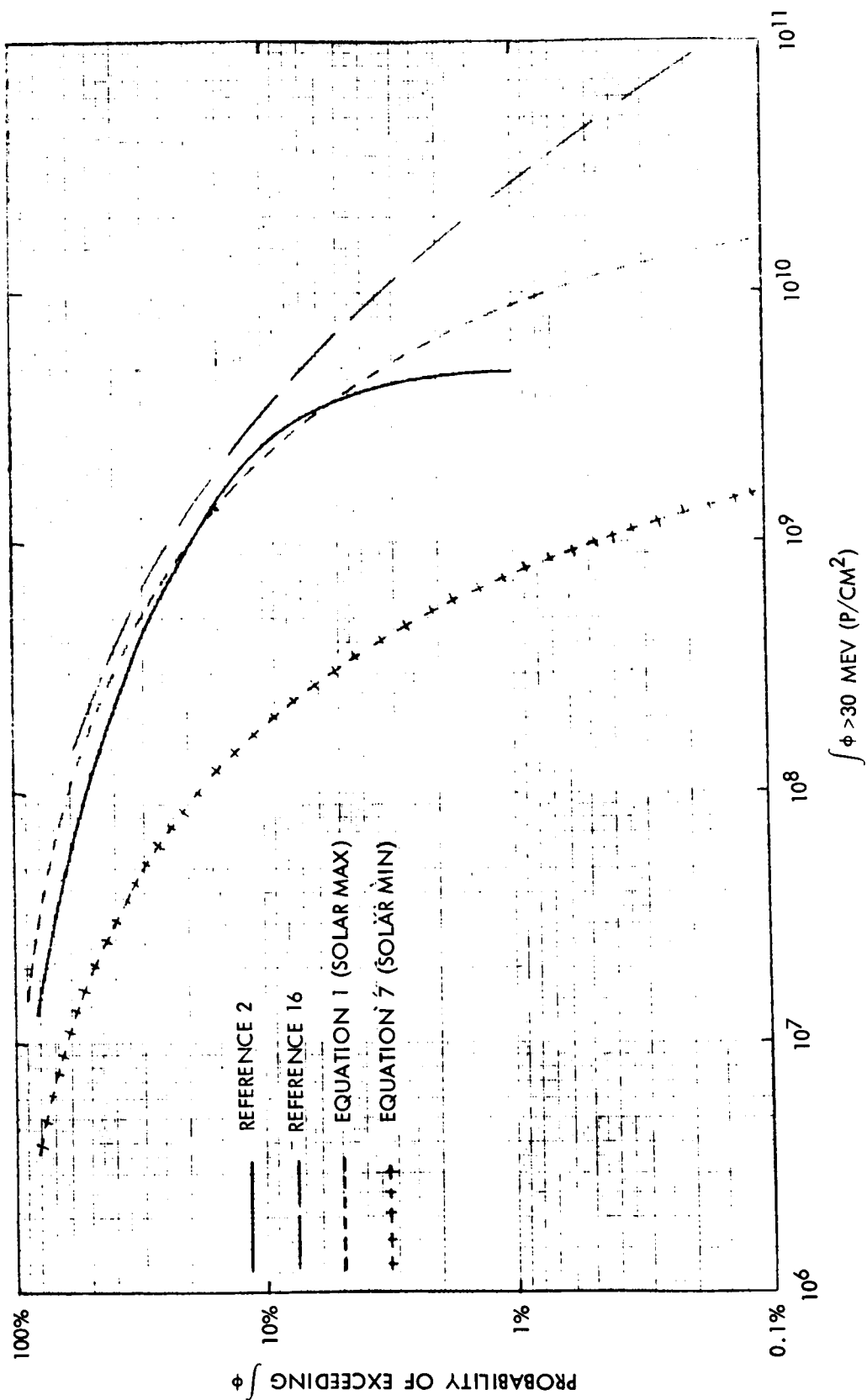


Figure 15. Comparison of Solar Flare Proton Probabilities for a 26-Week Mission at 1 AU, $t = 26$ Weeks

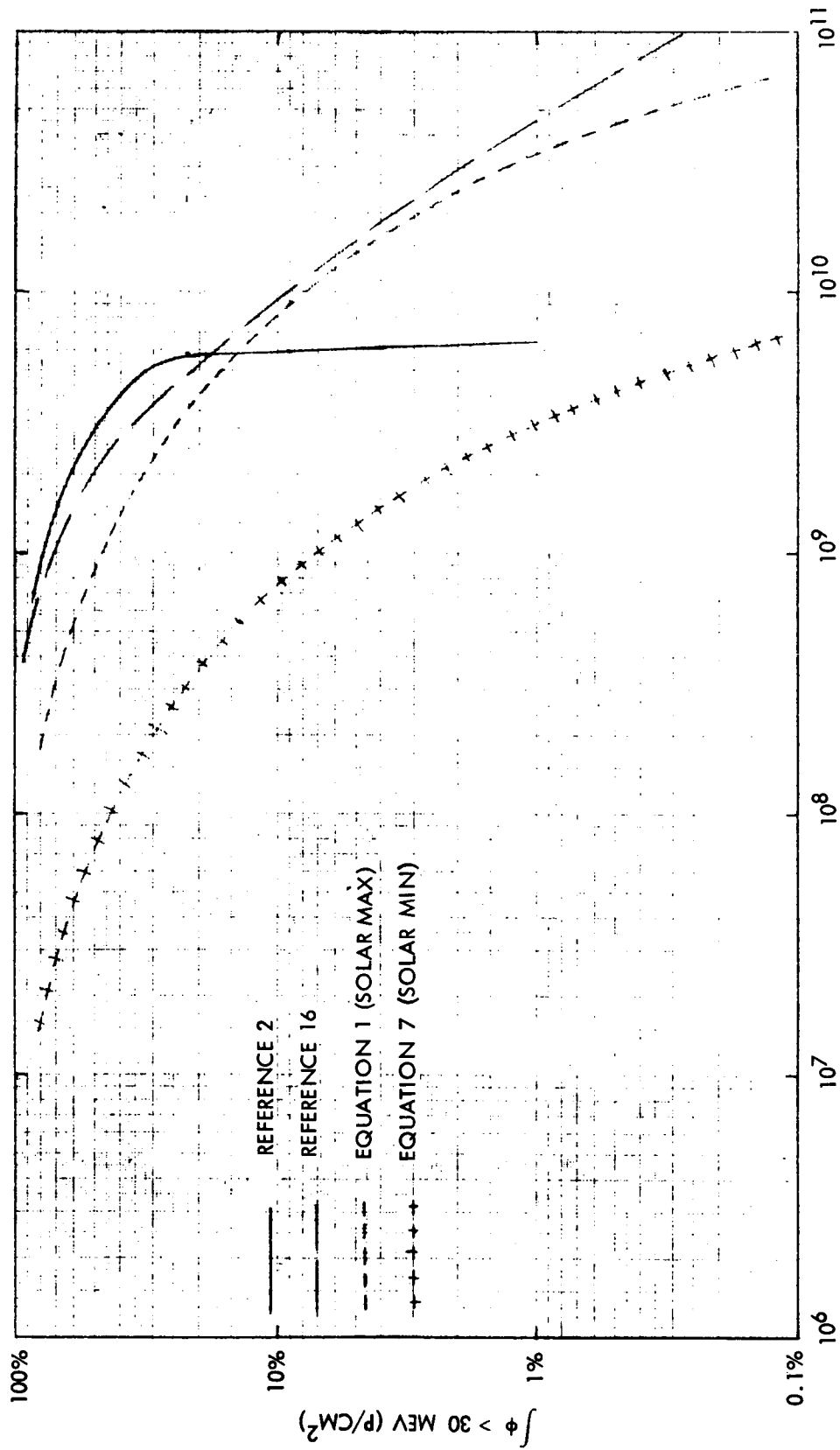


Figure 16. Comparison of Solar Flare Proton Probabilities for a 104-Week Mission at 1 AU, $t = 104$ Weeks

The approximate 11-year solar cycle has a major effect upon the nuclear space radiation environment. There have been three published studies specifically concerned with the solar flare radiation activity at solar minimum. Webber (Reference 3) obtained the relationship

$$\int \phi > 10 \text{ Mev (p/cm}^2 \text{ - year)} = 10^{7 + 0.02 \text{ Ry}} \quad (2)$$

where Ry is the annual smoothed sunspot number.¹ Based upon this formula, since the average of sunspot numbers at solar maximum is approximately 100, the average of $\int \phi_y > 10 \text{ Mev}$ should be $10^9 \text{ protons/centimeter}^2 \text{ - year}$. At solar minimum, which has an average sunspot number of 10, the average of $\int \phi_y > 10 \text{ Mev}$ should be about $1.6 \times 10^7 \text{ protons/centimeter}^2 \text{ - year}$. Therefore, a ratio of approximately 62.5 between the 10-Mev flux at solar maximum and solar minimum is expected.

A second analysis was carried out by Weddell and Haffner (Reference 19), who obtained the relationship

$$\int \phi_y > 10 \text{ Mev (P/cm}^2 \text{ - year)} \approx 10^{8.9 + 0.004 \text{ Ry}} \quad (3)$$

Based upon this relationship, the average ratio of $\int \phi_y > 10 \text{ Mev}$ at solar maximum to that at solar minimum is approximately 2.5. This ratio is appreciably less than that obtained by Webber, probably due to the influence of the 23 February 1956 solar event.

A third relationship, developed by Haffner (Reference 6-19) is

$$\int \phi_y > 10 \text{ Mev (P/cm}^2 \text{ - year)} = 5.5 \times 10^5 (R_{y-1})^2 \quad (4)$$

Based on this formula, the proton flux ratio at solar maximum to that at solar minimum is approximately 100. While this ratio agrees fairly well with that of Webber, this formula essentially omits the anomalous event of 23 February 1956.

¹The sunspot number (R) is defined as (Reference 16):

$$R = k(f + 10g)$$

where g is the number of disturbed regions on the Sun (single sunspots or groups of sunspots); f is the total number of individual sunspots; and k is a factor assigned to a particular observer. Records of sunspots have been kept for over two centuries and the resultant smoothed sunspot number are shown in Figure 1-1 of Reference 80.

Therefore, a factor of 10 between $\int \phi > 10 \text{ Mev p/cm}^2 - \text{year}$ at solar maximum to that at solar minimum represents a conservative estimate. Use of such a ratio has a high probability of overestimating the solar flare radiation in quiet years and a low probability of underestimating it at any time. However, mission shielding requirements are relatively small (less than $5 \text{ gm/centimeter}^2$), except for missions undertaken during years when the sun is active.

To account for the effects of the solar cycle, it is necessary to modify β in Equation 1. Based upon a factor of 10 in annual proton flux between solar maximum and solar minimum, it is necessary to increase β to approximately 8.5×10^{-4} ($2.5 \times 10^{-4} \times \sqrt{10}$) at solar minimum. Thus, for the same probabilities, the mission proton fluxes will be a factor of 10 lower. In addition, it is required that β vary approximately sinusoidally between these limits. This can be accomplished if:

$$\beta = \frac{5.5 + 3 \cos \left[\frac{2\pi}{11} (\text{year} - 1965) \right]}{10^4} \quad (5)$$

where 1965 was the year of the most recent solar minimum. Substituting Equation 5 in Equation 1 yields

$$P(t) = \exp \left[- \left\{ \frac{5.5 + 3 \cos \left[\frac{2\pi}{11} (\text{Year} - 1965) \right]}{10^4} \right\} \sqrt{\frac{\int \phi}{t}} \right] \quad (6)$$

At solar minimum, this becomes

$$P(t) = e^{-8.5 \times 10^{-4} \sqrt{\frac{\int \phi}{t}}} \quad (7)$$

This equation is also plotted in Figures 14 through 16.

These expressions were obtained from the data for the past solar cycle (Cycle 19). Therefore, they can be applied to future solar cycles only if it is assumed that future solar cycles will be like the last one. Several analyses (References 4 and 19) of the peak sunspot number expected on the next solar cycle have been reported. These analyses all yield peak sunspot numbers in the 80 to 140 region, as contrasted with the 189.5 recorded on the last cycle. (Since the last cycle was the most active ever observed, the use of the above equations is believed to be conservative when applied to future solar cycles.)

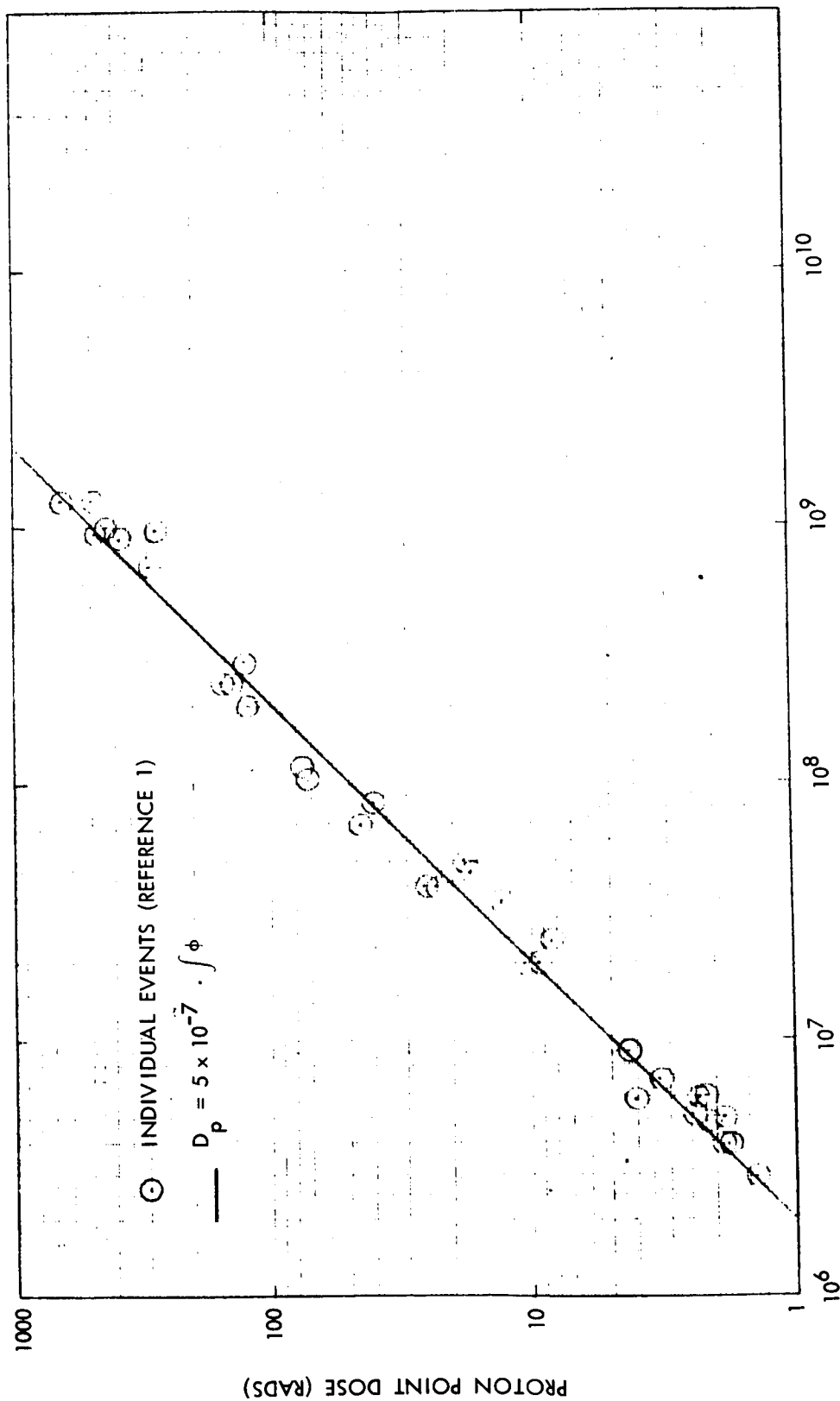


Figure 17. Relationship Between Flux and Rad Dose for Solar Flare Proton Events

There is a simple relationship between solar flare proton flux and the corresponding point dose. The point dose is essentially a linear function of the flux above the shield cutoff energy (Figure 17). For the case shown, the proton flux above 30 Mev is proportional to the point dose behind 1 gm/centimeter² of aluminum. The relationship (Reference 21) is

$$D_p \text{ (rads)} = 5 \times 10^{-7} \int \phi_p > 30 \text{ Mev (p/cm}^2) \quad (8)$$

The scatter of dose points about this straight line is due to individual differences in the proton spectral shapes. However, the majority of the proton dose is contributed by protons whose ranges just exceed the shield thickness. This is a consequence of the fact that they are much more numerous than the higher-energy protons and that their dose effectiveness is also higher because of their high linear-energy transfer (LET). Similar relationships hold for shields of other thicknesses.

In dealing with solar-flare radiation doses, the effects of both the protons and the alpha particles should be considered. Alpha-particle energy spectra have been measured for many of the larger events since 1958. For only those events for which both proton and alpha particle spectra have been measured, the aggregate spectra on an energy-per-particle basis are quite similar (Figure 18). The ratio of incident protons to alpha particles is about 1.2 on this basis. However, two effects must be considered as contributing to the dose. The first is that the alpha particles have shorter ranges than protons of the same energy. Therefore, the ratio of protons to alpha particles increases as shield thickness increases. However, due to their higher LET, each penetrating alpha particle has four times the rad dose effectiveness and about twenty times the rem dose effectiveness as the corresponding penetrating protons. The results of calculations are multiplicative correction factors which must be applied to solar-flare proton-dose calculations (Reference 21 and Figure 19).

The solar flare dose versus shield thickness relationships can be obtained for an isotropic flux with an integral proton energy spectrum of the form (Reference 21)

$$\int \phi(E > E_o) = \frac{A}{E_o^{1.55}} \text{ (protons/centimeter}^2 \text{ - event)} \quad (9)$$

where E_o is the proton energy (Mev) and A is a normalization constant.

If the proton range-energy relationship is represented by the simple equation

$$R = \delta E^n \quad (10)$$

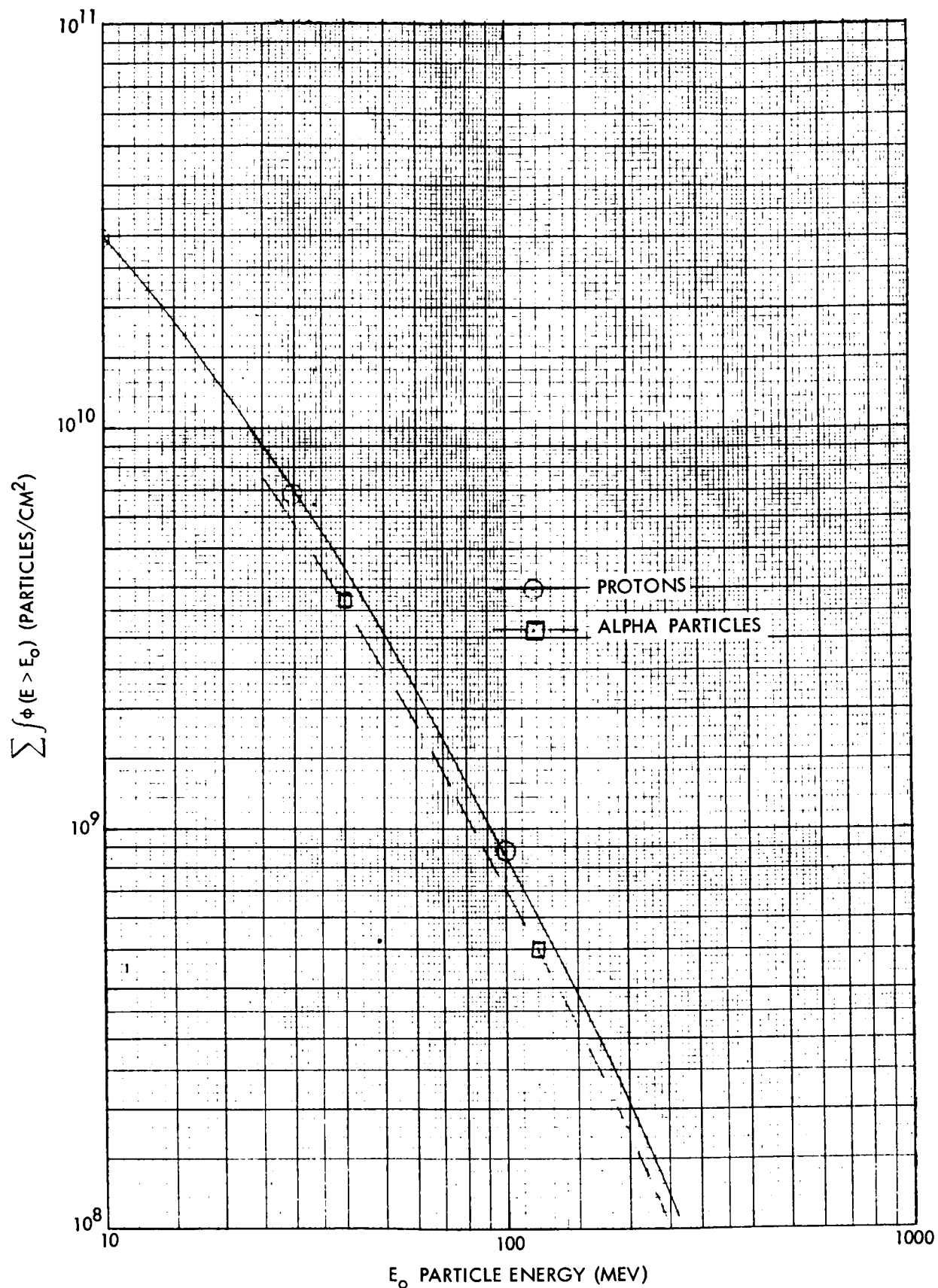


Figure 18. Comparison of Solar Flare Proton and Alpha Particle Integral Energy Spectra (Summed Over Events for Which Both Spectra Were Available)

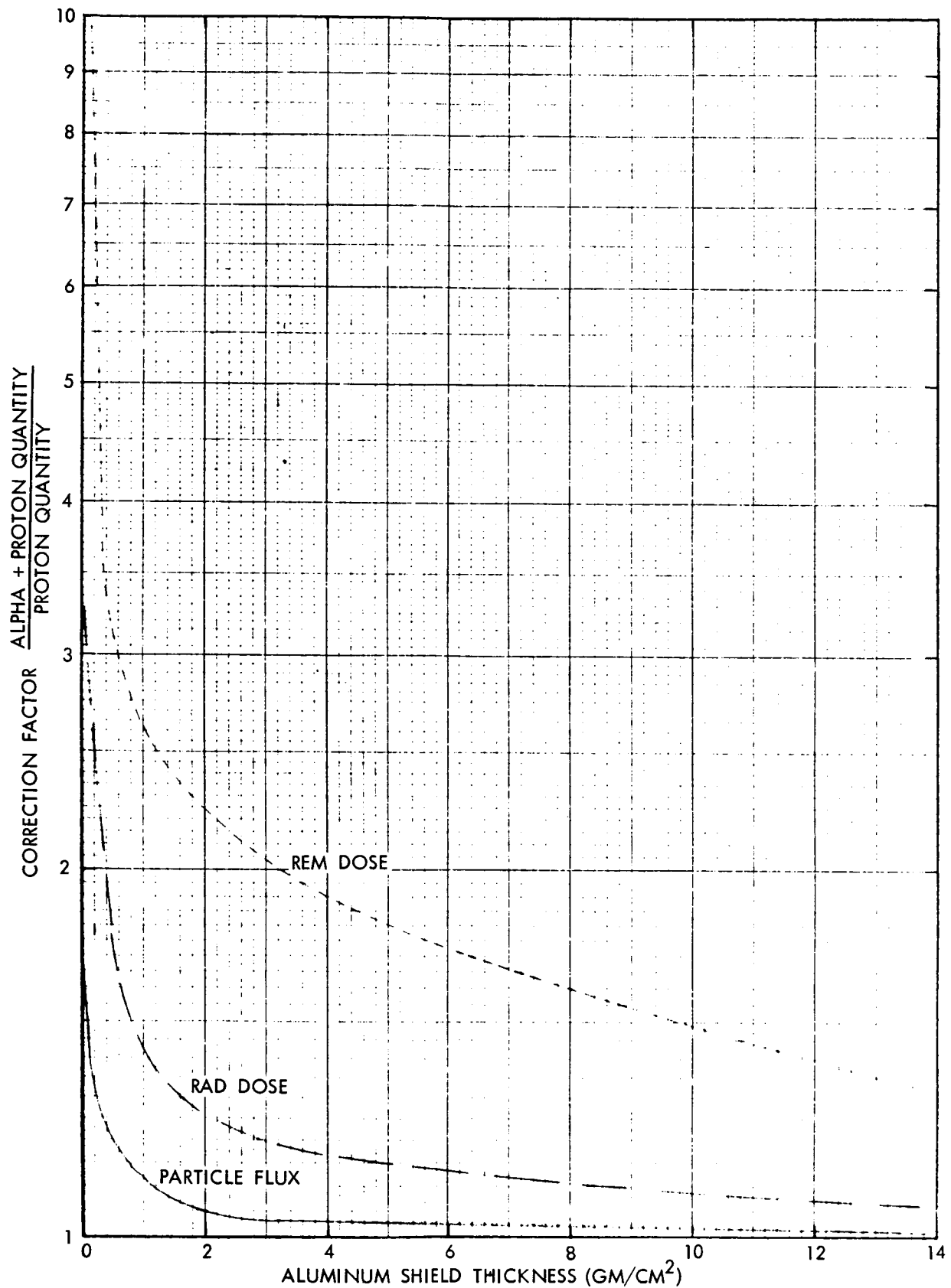


Figure 19. Calculated Multiplicative Correction Factors for Solar Flare Protons to Include Effects of Solar Flare Alpha Particles

a proton of incident energy E_0 will emerge with an energy E' after penetrating a thickness X (gm/centimeter²) of shielding where

$$E' = \left[E_0^\eta - \frac{X}{\delta} \right]^{1/\eta} \quad (11)$$

where

R is the proton range (gm/cm²)

δ and η are constants

$$\left. \begin{array}{l} \delta = 3.47 \times 10^{-3} \\ \eta = 1.73 \end{array} \right\} \text{ for aluminum}$$

Therefore, the integral energy spectrum of solar flare protons after penetrating a shield thickness X is

$$\int \phi(E > E_0) = \frac{A}{\left[E_0^\eta + \frac{X}{\delta} \right]^{\frac{1.55}{\eta}}} \quad (12)$$

The corresponding differential energy spectrum is

$$\phi(E, X) dE = \frac{1.55 A E^{\eta-1} dE}{\left[E^\eta + \frac{X}{\delta} \right]^{\frac{1.55}{\eta} + 1}} \quad (13)$$

The Gibson flux (Reference 22) to rad dose conversion function $C(E)$ can be fit by an expression

$$C(E) = B_1 E^{-C_1} + B_2 E^{C_2} \quad (14)$$

where

$$\left. \begin{array}{l} B_1 = 4 \times 10^{-6} \\ B_2 = 6 \times 10^{-10} \\ C_1 = 0.8 \\ C_2 = 0.85 \end{array} \right\} \text{ constants for tissue.}$$

The proton rad dose is the integral

$$D(X) = \int_0^{\infty} \phi(E, X) C(E) dE \quad (15)$$

where $\phi(E, X)$ and $C(E)$ are the functions defined above. Unfortunately, this dose integral cannot be evaluated in closed form, so calculations were carried out graphically. The results are shown in the bottom curve of Figure 20.

The other curves of Figure 20 were obtained from the proton rad dose calculations described first and the alpha particle dose correction factors shown in Figure 19. It will be noted that these calculations neglect secondary radiations produced by nuclear interactions initiated by the solar flare protons and alpha particles. These secondaries are negligible for shield thicknesses less than 10 gm/centimeter², and do not become important until thicknesses on the order of 30 gm/centimeter² are reached.

It is possible to approximate the curves of Figure 20 by straight-line expressions of the form

$$D_p^x \text{ (rad)} = \frac{D_p^1}{X^{1.2}} \text{ (rad)} \quad (16)$$

$$D_{p+\alpha}^x \text{ (rad)} = \frac{D_{p+\alpha}^1}{X^{1.3}} \text{ (rad)} = \frac{1.4 D_p^1}{X^{1.3}} \text{ (rad)} \quad (17)$$

$$D_{p+\alpha}^x \text{ (rem)} = \frac{D_{p+\alpha}^1}{X^{1.6}} \text{ (rem)} = \frac{4D_p^1}{X^{1.6}} \text{ (rad)} \quad (18)$$

These expressions have an error of somewhat less than 20 percent over the thickness range of 0.5 to 20 gm/centimeter².

The sun-to-spacecraft distance (r) is an important parameter in the analysis of the expected mission space-radiation dose. The small amount of experimental data available indicates an r^{-k} dependence, where k apparently lies between 1 and 2. The various theoretical treatments of solar flare radiation either assume or derive expressions of approximately r^{-2} (Reference 19). Since the probability of receiving the solar-flare radiation must decrease as some function of distance, an r^{-2} dependence is a reasonable assumption. The present analysis assumes that the event probabilities are independent of r , but that the particle fluxes decrease as r^{-2} .

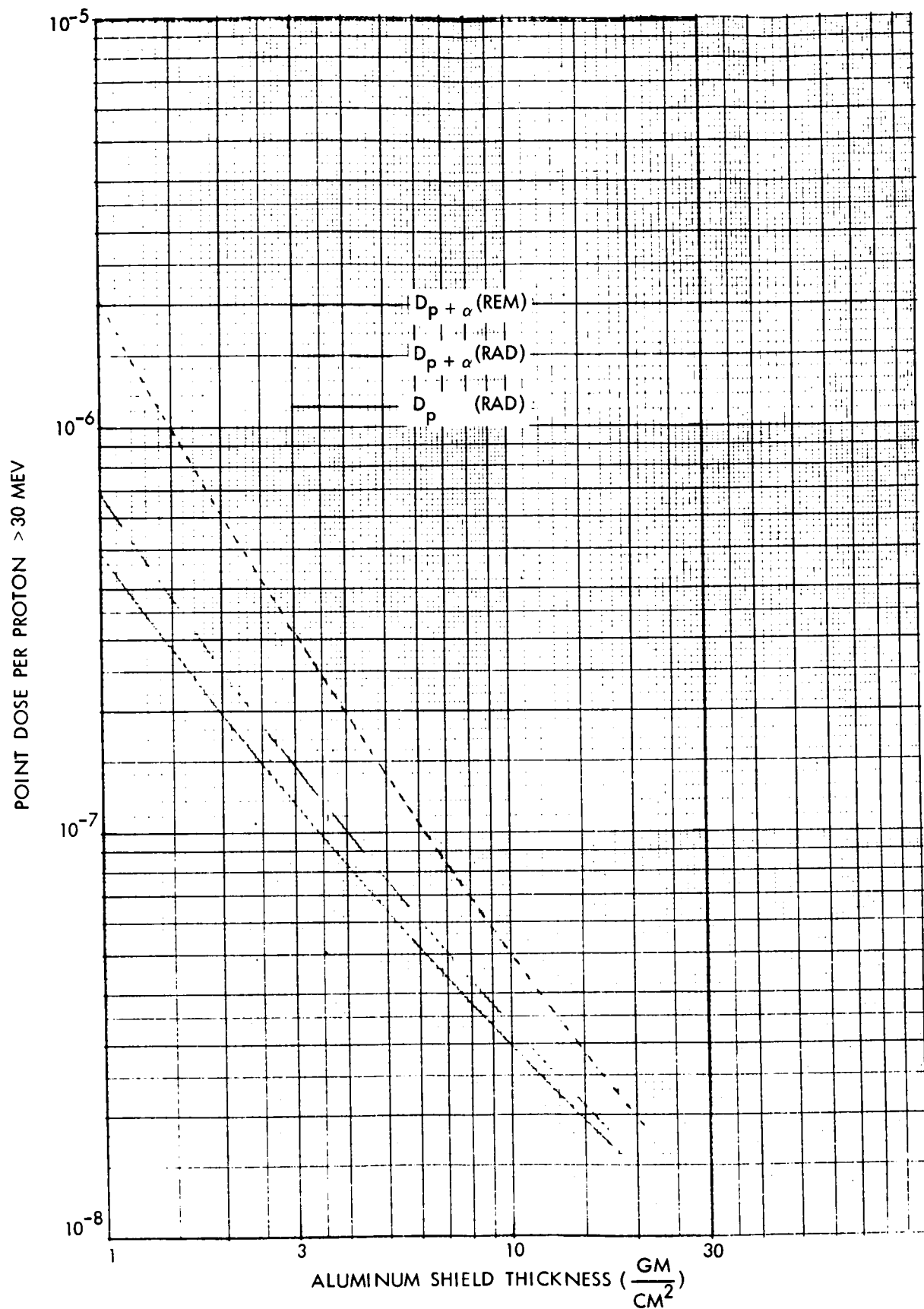


Figure 20. Point Dose Per Solar Flare Proton Above 30 Mev as a Function of Aluminum Shield Thickness

The average value of r^{-2} for a given mission leg is

$$\left(\overline{\frac{1}{r^2}}\right) = \frac{1}{\Delta t} \int_{t_1}^{t_2} \left(\frac{1}{r^2}\right) dt \quad (19)$$

where

Δt = transfer time

r = heliocentric radius of the spacecraft

and

t_1 = mission time

However,

$$\left(\frac{1}{r^2}\right) dt = \left(\frac{1}{h}\right) dv \quad (20)$$

from which

$$\left(\overline{\frac{1}{r^2}}\right) = \frac{1}{\Delta t} \int_{v_1}^{v_2} \frac{1}{h} dv \quad (21)$$

or

$$\left(\overline{\frac{1}{r^2}}\right) = \frac{\Delta v}{h \Delta t}^* \quad (22)$$

*Note that, as can be inferred from Equation (10) in the previous section, if the dosage varies as r^{-1} then $\left(\frac{1}{r}\right) = \frac{a \sqrt{1 - e^2} (\Delta E)}{h \Delta t}$

where

Δv = change in true anomaly of the heliocentric conic

h = angular momentum of the heliocentric conic

The above expression can be extended to include any number of mission legs, i. e.,

$$\left(\frac{1}{r^2}\right) = \frac{1}{t} \left(\frac{\Delta v_1}{h_1} + \frac{\Delta v_2}{h_2} + \frac{\Delta v_3}{h_3} + \dots + \frac{\Delta v_n}{h_n} \right) \quad (23)$$

where t is the mission duration. For the planetary parking orbit phase of the mission, the planetary heliocentric orbital elements are used to define Δv and h .

Thus, the basic equations are

$$P(t) = e^{-\left(\beta \sqrt{\frac{\int \phi}{t}}\right)} \quad (1)$$

where

$$\beta = \frac{5.5 + 3 \cos \left[\frac{2\pi}{11} (\text{Year} - 1965) \right]}{10^4} \quad (5)$$

$$D_p^1 (\text{rad}) = \frac{5 \times 10^{-7} \int \phi}{r^2} \quad (8)$$

$$D_p^1 (\text{rad}) = 0.72 \times 10^{1.3} D_{p+a}^X (\text{rad}) \quad (17)$$

$$D_p^1 (\text{rad}) = 0.25 \times 10^{1.6} D_{p+a}^X (\text{rem}) \quad (18)$$

$$\left(\frac{1}{r^2}\right) = \frac{1}{t} \left(\frac{\Delta v_1}{h_1} + \frac{\Delta v_2}{h_2} + \frac{\Delta v_3}{h_3} + \dots + \frac{\Delta v_n}{h_n} \right) \quad (23)$$

It is a relatively straightforward matter to combine these equations to yield

$$X \left(\frac{\text{gm}}{\text{cm}^2} \right) = 26 \left[\left(\frac{t}{D_{p+a}^X (\text{rad})} \right) \left(\frac{\bar{I}}{r^2} \right) \right]^{0.77} \left[\frac{-\ln P(t)}{10^4 \beta} \right]^{1.54} \quad (24)$$

$$X \left(\frac{\text{gm}}{\text{cm}^2} \right) = 59 \left[\left(\frac{t}{D_{p+a}^X (\text{rem})} \right) \left(\frac{\bar{I}}{r^2} \right) \right]^{0.625} \left[\frac{-\ln P(t)}{10^4 \beta} \right]^{1.25} \quad (25)$$

In these and subsequent equations, t is in weeks and $\left(\frac{\bar{I}}{r^2} \right)$ is in AU^{-2} .

These equations yield the aluminum equivalent shield thickness X required on a deep space mission to protect a point dosimeter from exceeding a solar flare radiation dose D_{p+a}^X with a probability P . The other inputs required are the year in which the mission largely falls, the mission duration time and the maximum and minimum sun-to-spacecraft distances.

The formula given in Equations 24 and 25 requires further modification to incorporate the galactic and Van Allen radiations. It is also necessary to investigate the analysis of missions whose durations are not short compared with the 11-year solar cycle. These matters are considered in the following sections.

Van Allen Radiation

The space, time, temporal, and energy distributions of the geomagnetically trapped radiation (Van Allen Belts) have been investigated and reported by dozens of researchers (References 11 through 14). As a result it is possible to calculate rather accurately the particle (electron and proton) fluxes and doses expected along any desired trajectory. Several computer programs (References 24 and 25) have been written which yield these quantities directly once the trajectory is known.

For deep space missions, it is possible to make simplifying assumptions with little effect on the radiation shielding required. Presumably, any passage through the geomagnetically trapped radiation will be done by high-thrust vehicles. For a chemical rocket travelling radially through the radiation in the plane of the geomagnetic equator, the point rad dose is fairly small, unless the shield thickness is less than $1 \text{ gm/centimeter}^2$ (Figure 21). For deep space missions undertaken at solar maximum, the trapped radiation contributes less than 3 percent of the mission dose, often less than 1 percent (Reference 21). For missions at solar minimum, these

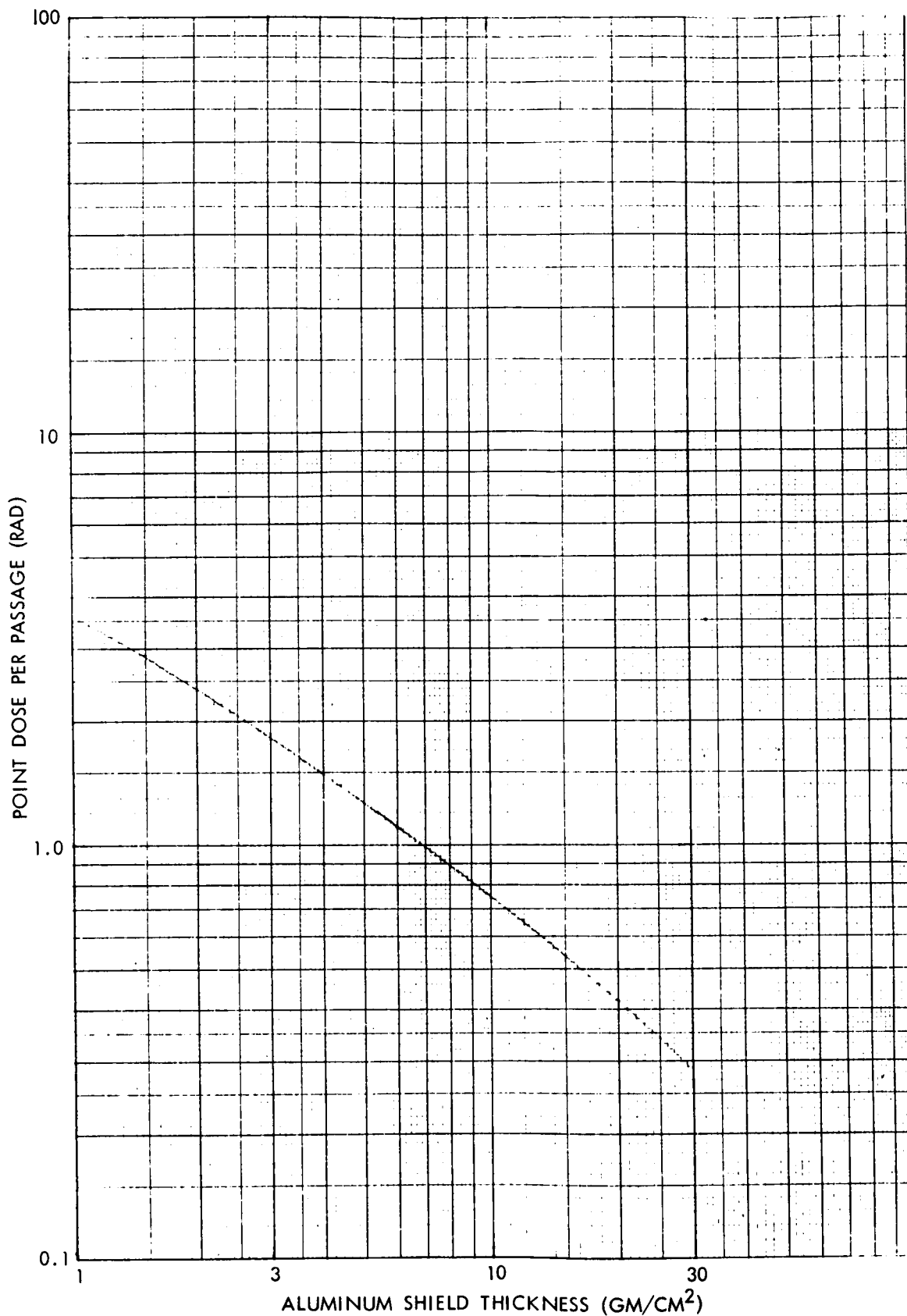


Figure 21. Point Rad Dose Per High-Thrust Passage Through the Geomagnetically Trapped Radiation Belts

numbers may increase to approximately 5 percent, with 3 percent being far more common. For this study, it was assumed that the geomagnetically trapped radiation dose amounted to 3 percent of the solar radiation dose for all missions.

This assumption is conservative except for shorter missions (less than six months) undertaken when the sun is quiet. It is equivalent to the assumption that the geomagnetically trapped radiation is attenuated like the solar-flare radiation. A comparison of Figures 20 and 21 shows that this is not true. However, as the shield thickness required for solar flare radiation increases, the ratio of the geomagnetically trapped radiation dose to the solar flare radiation dose decreases. Thus, the hardness of the trapped radiation energy spectrum tends to balance the variation in the ratio of their doses, so neglecting both introduces relatively little error. Uncertainties in the future solar flare radiation environment mitigate against further refinements in accounting for the geomagnetically trapped radiation.

Galactic (Cosmic) Radiation

In spite of the fact that the characteristics of the galactic radiation have been studied for approximately 50 years, there is much which is not well known (Reference 15). The temporal behavior near the earth has been measured, but the spatial dependence throughout our solar system has not been investigated to any appreciable extent. The perturbing influences of the sun and planets having magnetic fields (e. g. , Jupiter, Saturn) on the time, space, composition, and energy distributions are not known except in the vicinity of the earth.

Near the earth, flux and dose measurements have been made which extrapolate to a deep space value of approximately 50 millirads per day (quiet sun). Since any perturbing influences will decrease this deep space value, a conservative assumption is to use a time and space constant value of 0.35 rad/week (Reference 21). The very high energies of the galactic particles make this value essentially independent of shield thickness as well (up to a thickness of approximately 30 gm/centimeter²). The very low LET of the radiation yields an RBE of unity, so the point rem dose rate may be taken as 0.35 per week as well.

SUMMARY AND EXAMPLE

It is now possible to incorporate the effects of the geomagnetically trapped radiation and the galactic radiation into Equation 24. The result is

$$X \left(\frac{\text{gm}}{\text{cm}^2} \right) = 26 \left[\left(\frac{1.03 t}{D - 0.35 t} \right) \left(\frac{1}{r^2} \right) \right]^{0.77} \left\{ \frac{-\ell n P}{5.3 + 3 \cos \left[\frac{2\pi}{11} (\text{Year} - 1965) \right]} \right\}^{1.54} \quad (26)$$

where

D = mission point dose limit (rad)

P = acceptable probability of exceeding D

Year = year the mission takes place

The corresponding equation for a dose limit D' in rem is

$$X \left(\frac{\text{gm}}{\text{cm}^2} \right) = 59 \left[\left(\frac{1.03 t}{D' - 0.35 t} \right) \left(\frac{1}{r^2} \right) \right]^{0.625} \left\{ \frac{-\ell n P}{5.5 + 3 \cos \left[\frac{2\pi}{11} (\text{Year} - 1965) \right]} \right\}^{1.25} \quad (27)$$

All other quantities are as defined above. As stated previously, these equations are based upon the assumption that the future solar cycles are as severe as the last one (Cycle 19). This is almost certainly a conservative assumption.

Mission-dose limits are usually specified for one or more of the human critical organs (eyes, skin, bone marrow, central nervous system, reproductive organs). In the absence of given values, the following dose limits may be taken as representative (References 26, 27, and 28).

Organ	Dose Limit (rem)
Skin	600-1000
Bone marrow	150-200

The other critical organs are more localized and can be protected by special shielding without much of a weight penalty.

Skin and bone marrow doses (for solar and geomagnetically trapped radiation) are related to point doses by the following equations.

$$\text{Skin Dose (X)} = 0.5 \text{ Point Dose (X)} \quad (28)$$

$$\text{Bone Marrow Dose (X)} = 0.5 \text{ Point Dose (X + 5)} \quad (29)$$

For shield thickness (X) less than approximately 5 gm/centimeter², the skin dose is usually the determining factor, while if X is greater than approximately 5 gm/centimeter², the bone marrow dose becomes dominant. The Equations 26 and 27 thus become:

$$\left. \begin{aligned} X &= 26 \left[\left(\frac{1.03t}{2D_{\text{skin}} - 0.35t} \right) \left(\frac{\bar{I}}{r^2} \right) \right]^{0.77} \left\{ A \right\}^{1.54} \\ X + 5 &= 26 \left[\left(\frac{1.03t}{2D_{\text{marrow}} - 0.35t} \right) \left(\frac{\bar{I}}{r^2} \right) \right]^{0.77} \left\{ A \right\}^{1.54} \end{aligned} \right\} \begin{array}{l} \text{If rad} \\ \text{dose} \\ \text{limits} \end{array} \quad (30)$$

$$\left. \begin{aligned} X &= 59 \left[\left(\frac{1.03t}{2D_{\text{skin}} - 0.35t} \right) \left(\frac{\bar{I}}{r^2} \right) \right]^{0.625} \left\{ A \right\}^{1.25} \\ X + 5 &= 59 \left[\left(\frac{1.03t}{2D_{\text{marrow}} - 0.35t} \right) \left(\frac{\bar{I}}{r^2} \right) \right]^{0.625} \left\{ A \right\}^{1.25} \end{aligned} \right\} \begin{array}{l} \text{If rem} \\ \text{dose} \\ \text{limits} \end{array} \quad (31)$$

$$\left. \begin{aligned} X &= 59 \left[\left(\frac{1.03t}{2D_{\text{skin}} - 0.35t} \right) \left(\frac{\bar{I}}{r^2} \right) \right]^{0.625} \left\{ A \right\}^{1.25} \\ X + 5 &= 59 \left[\left(\frac{1.03t}{2D_{\text{marrow}} - 0.35t} \right) \left(\frac{\bar{I}}{r^2} \right) \right]^{0.625} \left\{ A \right\}^{1.25} \end{aligned} \right\} \begin{array}{l} \text{If rem} \\ \text{dose} \\ \text{limits} \end{array} \quad (32)$$

$$\left. \begin{aligned} X &= 59 \left[\left(\frac{1.03t}{2D_{\text{skin}} - 0.35t} \right) \left(\frac{\bar{I}}{r^2} \right) \right]^{0.625} \left\{ A \right\}^{1.25} \\ X + 5 &= 59 \left[\left(\frac{1.03t}{2D_{\text{marrow}} - 0.35t} \right) \left(\frac{\bar{I}}{r^2} \right) \right]^{0.625} \left\{ A \right\}^{1.25} \end{aligned} \right\} \begin{array}{l} \text{If rem} \\ \text{dose} \\ \text{limits} \end{array} \quad (33)$$

where

$$A = \left\{ \frac{-\ln P(t)}{5.5 + 3 \cos \left[\frac{2\pi}{11} (\text{Year} - 1965) \right]} \right\}$$

As derived, these formulae assume that the mission takes place within a period of time (e. g., one year) short compared with the 11-year solar cycle. The radiation dose is considered to be recieved uniformly throughout the duration of the mission. While the assumption of a uniform radiation environment

is reasonable (so long as dose rate constraints are not a problem), the durations of missions considered in this study are generally in excess of one year. For these situations, it is necessary to use an averaging technique.

While β varies sinusoidally with time, the probability of exceeding a given solar flare proton flux on a mission of a given duration does not (Figure 22). However, the shielding thickness (X) required does vary approximately sinusoidally. Therefore, if an effective year is known, the equations can be applied for missions of any duration (assuming, of course, all solar cycles are identical to Cycle 19). The effective year is one which will yield the same value of

$$10^4 \beta(t) = 5.5 + 3 \cos \left[\frac{2\pi}{11} (\text{Year} - 1965) \right] \quad (34)$$

as would be obtained by averaging this function over the mission duration. If the mission begins in year Y_1 and is completed in year Y_2 , the average of the above function $\beta(t)$ is

$$10^4 \overline{\beta(t)} = \frac{1}{Y_2 - Y_1} \int_{Y_1}^{Y_2} \left\{ 5.5 + 3 \cos \left[\frac{2\pi}{11} (Y - 1965) \right] \right\} dY \quad (35)$$

$$= 5.5 + \frac{33}{2\pi} \left\{ \frac{\sin \left[\frac{2\pi}{11} (Y_2 - 1965) \right] - \sin \left[\frac{2\pi}{11} (Y_1 - 1965) \right]}{Y_2 - Y_1} \right\} \quad (36)$$

This can be substituted into the expression for A, yielding

$$B = \frac{-\ln P}{5.5 + \frac{33}{2\pi} \left[\frac{\sin \left[\frac{2\pi}{11} (Y_2 - 1965) \right] - \sin \left[\frac{2\pi}{11} (Y_1 - 1965) \right]}{Y_2 - Y_1} \right]} \quad (37)$$

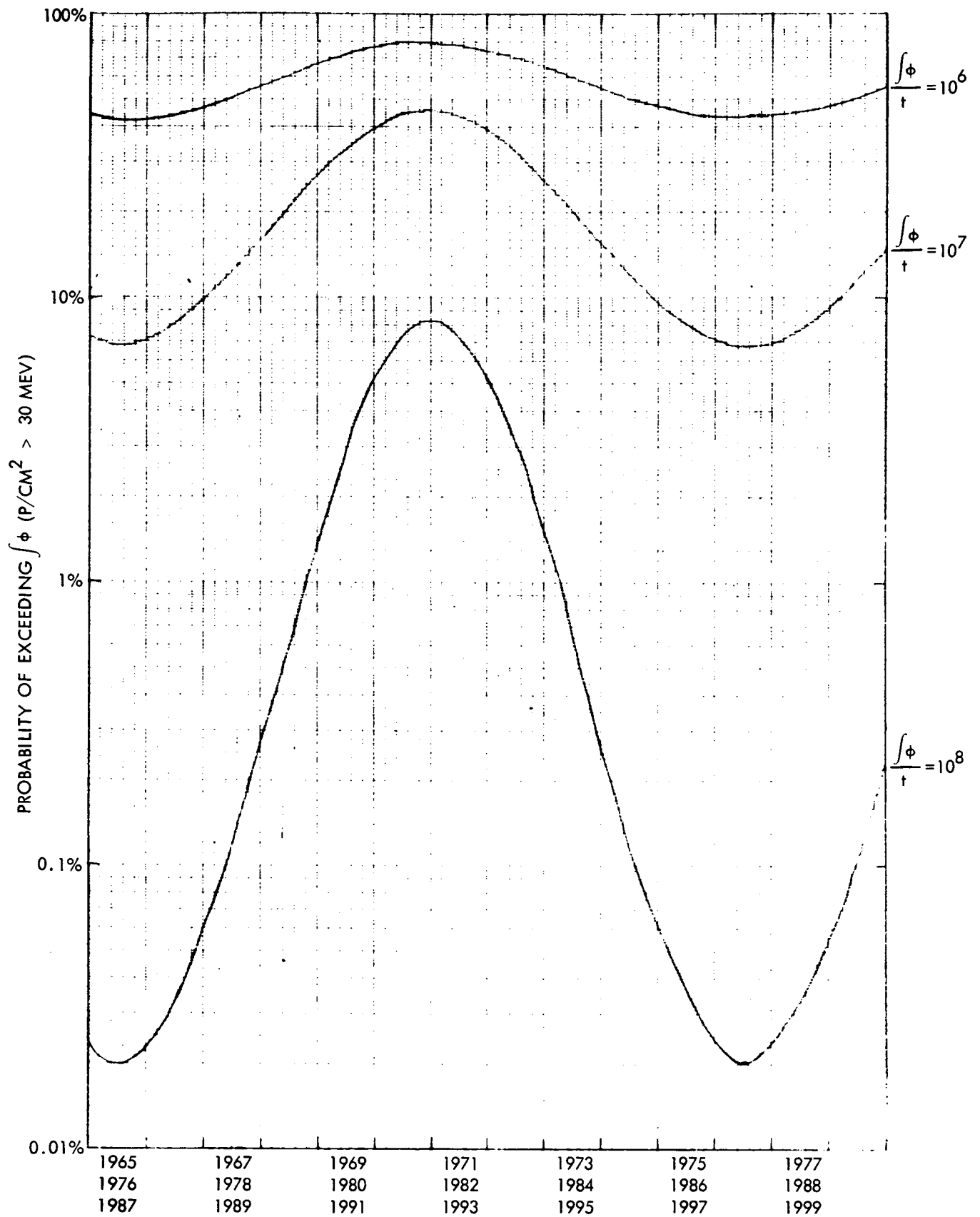


Figure 22 .. Theoretical Probability of Exceeding a Solar Flare Proton Flux of $\int \phi \text{ (p/cm}^2 > 30 \text{ MeV)}$ on a Mission of Duration t (Weeks)

The final formulae obtained are, thus:

$$X = 26 \left[\left(\frac{1.03t}{2D_{\text{skin}} - 0.35t} \right) \left(\frac{1}{r^2} \right) \right]^{0.77} \left\{ B \right\}^{1.54} \quad (38)$$

$$X + 5 = 26 \left[\left(\frac{1.03t}{2D_{\text{marrow}} - 0.35t} \right) \left(\frac{1}{r^2} \right) \right]^{0.77} \left\{ B \right\}^{1.54} \quad (39)$$

$$X = 59 \left[\left(\frac{1.03t}{2D_{\text{skin}} - 0.35t} \right) \left(\frac{1}{r^2} \right) \right]^{0.625} \left\{ B \right\}^{1.25} \quad (40)$$

$$X + 5 = 59 \left[\left(\frac{1.03t}{2D_{\text{marrow}} - 0.35t} \right) \left(\frac{1}{r^2} \right) \right]^{0.625} \left\{ B \right\}^{1.25} \quad (41)$$

D in
rad

D in
rem

where

$$B = \frac{-\ell n P}{5.5 + \frac{33}{2\pi} \left[\frac{\sin \left[\frac{2\pi}{11} (Y_2 - 1965) \right] - \sin \left[\frac{2\pi}{11} (Y_1 - 1965) \right]}{Y_2 - Y_1} \right]} \quad (42)$$

As stated previously, the required inputs are

t = mission duration (weeks)

D = mission dose limit (rad or rem, skin or marrow)

$\left(\frac{1}{r^2} \right)$ = time average value of r^{-2} (AU^{-2})

Y_1 = year mission started (to nearest tenth of the year)

Y_2 = year mission completed (to nearest tenth of the year)

P = probability of exceeding the dose limits

The output is X (gm/centimeter^2 aluminum equivalent) required for that particular mission if the probability of not exceeding the dose D is P.

To summarize, the assumptions inherent in these equations are:

Solar particle fluxes decreases as r^{-2} .

Future solar cycles will produce the same annual particle fluxes as the past one (Cycle 19).

The probabilities of receiving a given solar particle flux at solar minimum is 0.1 the corresponding probabilities at solar maximum, with an approximate sinusoidal behavior in between.

The mission dose due to the passage through the geomagnetically trapped radiation is 3 percent that due to solar flare radiations.

The galactic dose rate is 50 millirads per day (50 millirem per day) independent of all variables including distance from the sun, the solar cycle, and spacecraft shielding.

Secondary radiations are neglected, thus effectively limiting the region of validity to values of X (shield thickness) to 1 to 20 gm/centimeter². Outside these limits the formula underpredicts the shielding required.

As an example, consider a 1982.0 - 1983.9 low energy Mars flyby mission (675-day duration). The assumed mission dose limits are 200 rem to the blood-forming organs (bone marrow) and 800 rem to the skin. It is desired to calculate the shielding required if the probabilities of exceeding these dose limits are 50 percent, 10 percent, and 1 percent. Straightforward substitution in Equations 40 and 41 yields the following results (gm²/centimeter).

Organ	50-Percent Probability	10-Percent Probability	1-Percent Probability
Skin (Equation 40)	0.8 (1.7)	3.6	8.7 (5.8)
Marrow (Equation 41)	~ 0 (1.1)	4.0	16.6 (9.5)

The shield thicknesses obtained by detailed analyses are listed in the parentheses. It will be noted that the formulae developed in this report yield greater shield thicknesses for low probabilities, and thinner thicknesses for high probabilities. This is a consequence of the conservatism employed in the development.

A reasonable use of the equation might be to carry out calculations for a 10-percent probable environment. For such situations, the results will agree well with those obtained by a more exact analysis, while retaining such factors as biological recovery (via the ERD concept), short-term warning mechanisms, and the inherent conservatism of the approach as insurance.

Equations 38 through 42 were incorporated in the Weight Synthesis computer program and were used in the determination of the radiation shielding requirements during the mission/system analyses (Appendix D). The required shielding requirements were determined and compared with the inherent spacecraft shielding. If additional shielding was required, it was added to a solar flare "storm cellar" which was assumed to be contained within the mission module.

The total shielding requirements are shown in Figure 23 as a function of the year the mission is initiated for missions to Mercury, Venus, Mars, and Jupiter. The data are based on a 10 percent probability of exceeding mission dose limits of 200 rem to the blood-forming organs and 800 rem to the skin. Since the inherent spacecraft shielding is on the order of 3 to 5 gm/cm², additional shielding will be required only for missions that occur during periods of maximum solar activity.

The shielding requirements are given in thickness of equivalent aluminum since aluminum is often used as a spacecraft material. As long as the spacecraft shielding is less than approximately 20 gm/cm² the attenuation of space radiation is largely determined by low energy protons and alpha particles ($E \leq 300$ Mev nuclear). For these particles the range-energy relationship is a good approximation. A common form of the range-energy relationship is

$$R = \delta E^n \quad (43)$$

where

R = particle range (gm/cm²)

E = particle energy (Mev)

$\left. \begin{matrix} \delta \\ n \end{matrix} \right\} = \text{constants depending on the particle type and shielding material.}$

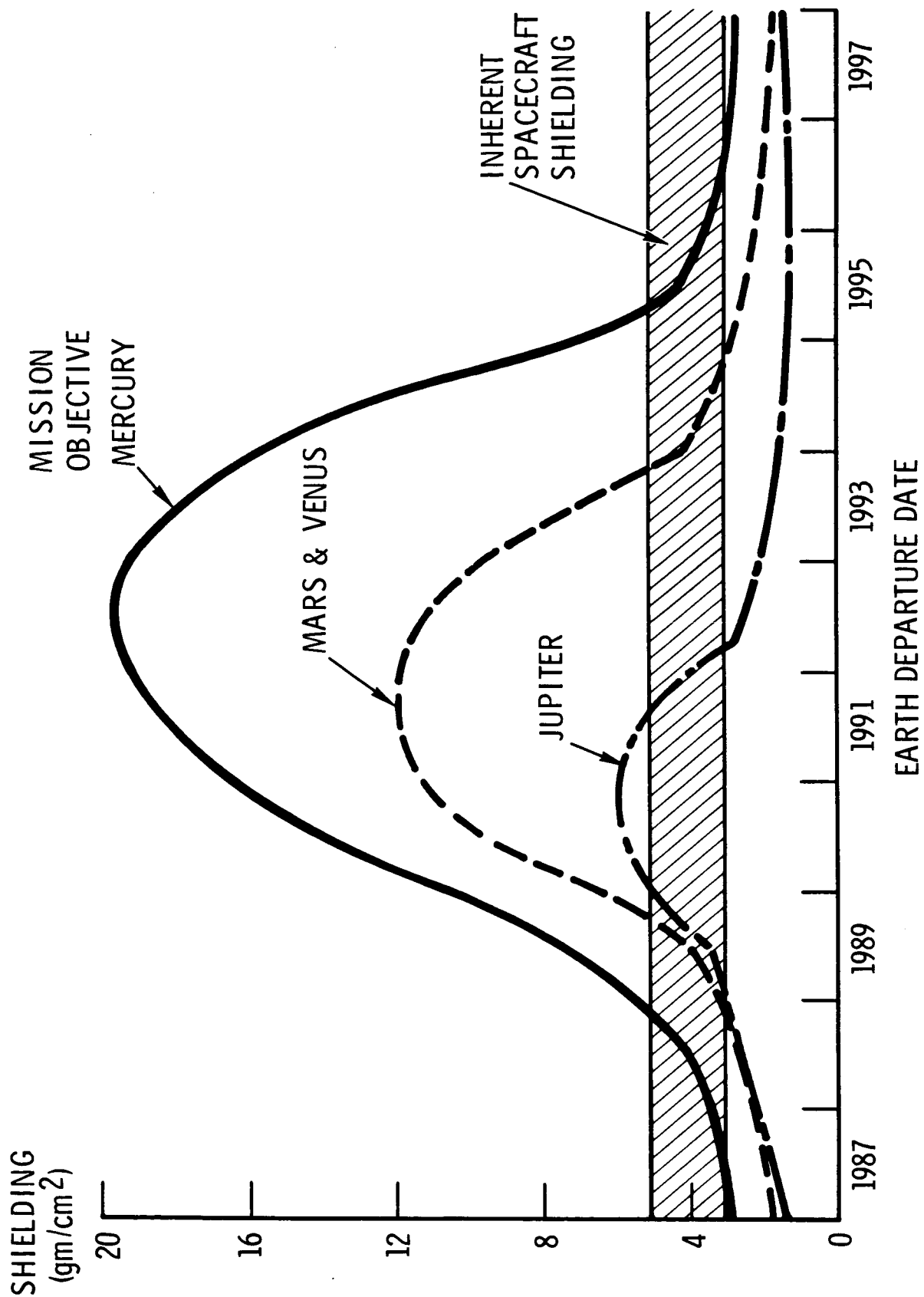


Figure 23. Mission Module Space Radiation Shielding

If two shields of different materials are equivalent, they both have the same cutoff energy. Therefore,

$$E_1 = E_2 \quad (44)$$

$$\left(\frac{X_1}{\delta_1}\right)^{1/n_1} = \left(\frac{X_2}{\delta_2}\right)^{1/n_2} \quad (45)$$

or

$$X_2 = \delta_2 \left(\frac{X_1}{\delta_1}\right)^{n_2/n_1} \quad (46)$$

Thus, a thickness X_2 of material 2 is equivalent to a thickness X_1 of material 1. Values of n and δ for some materials are listed in Table 14.

It will be noted that the relative effectiveness of two materials depends slightly on the thickness considered. For example, 1 gm/cm² aluminum is equivalent to 0.895 gm/cm² Teflon but 10 gm/cm² aluminum is equivalent to 9.8 gm/cm² Teflon. This is due to the fact that the constant n is slightly dependent upon the material. However, due to the fact that the constant n is independent of particle type (for proton and alpha particles) the relative contributions of protons and alpha particles are independent of material type (so long as the equivalent thickness remains unchanged). Thus, the equivalent thickness obtained for two materials are independent of whether proton or alpha particle constants (n and δ) are used in Equation 46.

Table 14. Range-Energy Constants

Material	Protons		Alpha Particles	
	n	δ	n	δ
Hydrogen	1.817	8.21×10^{-4}	1.817	6.62×10^{-5}
Beryllium	1.788	2.35×10^{-3}	1.788	1.98×10^{-4}
Carbon	1.787	2.22×10^{-3}	1.787	1.86×10^{-4}
Aluminum	1.730	347×10^{-3}	1.730	3.15×10^{-4}
Copper	1.728	4.07×10^{-3}	1.728	3.71×10^{-4}
Cadmium	1.708	4.97×10^{-3}	1.708	4.70×10^{-4}
Lead	1.680	7.18×10^{-3}	1.680	7.00×10^{-4}
Air	1.777	2.39×10^{-3}	1.777	2.0×10^{-4}
Water	1.793	1.95×10^{-3}	1.793	1.62×10^{-4}
Tissue	1.783	2.17×10^{-3}	1.783	1.83×10^{-4}
Teflon	1.800	2.47×10^{-3}	1.800	2.17×10^{-4}

JUPITER TRAPPED RADIATION ANALYSIS

Directly observed information relating to trapped radiation belts around Jupiter consists of nonthermal energy from the vicinity of that planet. This nonthermal radiation lies in the decameter and decimeter wavelength regions, and the characteristics of each are discussed here.

In 1954 Burke and Franklin (Reference 29) discovered the existence of bursts of decametric radiation originating from the direction of Jupiter. Since the source of the bursts moved with the planet, it was concluded that they originated from Jupiter or adjacent regions. Subsequent observations (References 30 through 36) have established the following characteristics of these bursts:

1. Burst durations are usually on the order of seconds to minutes, although shorter (<1 second) and longer (>1 hour) bursts have been observed.
2. Bursts are usually observed in the frequency region of 5 to 40 megahertz. During the burst, the frequency will usually experience a unidirectional drift of ~ 50 percent (References 37 and 38).
3. The burst intensities vary, ranging up to about 10^{-20} watts/m² Hz at earth.
4. The spatial distribution of the burst source extends to about 3 Jupiter radii.
5. The burst radiation exhibits elliptical polarization, especially in the frequency range of 20 to 30 megahertz (References 39 through 42).
6. Occurrences of the bursts directly correlate with the periods of Jupiter's inner satellites, especially Io. There appears to be negative correlation between burst activity and the 11-year solar cycle, but there may be a positive correlation with individual solar events (flares). (See References 43 through 49.)

In 1956, Mayer, McCullough, and Sloanaker (Reference 50) detected 3-cm radiation from Jupiter. This radiation exhibited relatively small fluctuations (on the order of a few percent of the steady-state intensity). The following characteristics have been established:

1. The radiation intensity is $\sim 10^{-25}$ w/m² Hz from 3 centimeters to 100 centimeters.
2. The spatial distribution extends to about 3 Jupiter radii in the equatorial plane to ~ 1 Jupiter radius in the polar directions (References 51 through 54).
3. The radiation exhibits some (~ 30 percent) linear polarization in the direction of Jupiter's equator and almost no (≤ 5 percent) elliptical polarization (References 55 and 56).
4. The time fluctuations correlate with the rotation of Jupiter. An accurate measurement of the planet's rotation was made possible by observation of this microwave radiation.

These characteristics of the decameter and decimeter radiations from Jupiter are discussed in more detail in several review articles (References 57 through 63).

Theories

Various theories have been offered to account for the nonthermal radiation associated with Jupiter. While approaches based upon electrical discharges in the atmosphere (lightning), disturbances in the planet (earthquakes, gravitational contraction, etc.), and ionospheric phenomena have been proposed, by far the most probable explanations are based upon the assumption of trapped radiation around the planet (References 64 through 68). The spatial distributions of the sources of the nonthermal radiation and the earth's Van Allen belts' radiation of radio-frequency (RF) energy are powerful arguments in this direction.

The decimetric radiation is the easier to explain. If an electron is placed in a static or slowly varying magnetic field (B), it will rotate about a line of flux according to the relationship

$$Bev_{\perp}^2 = \frac{m v_{\perp}^2}{r} \quad (47)$$

where m is the electron mass, e the electron charge, v_{\perp}^2 the component of the electron velocity perpendicular to the direction of B, and r the gyroradius

of the electron's rotation. The frequency of the radiation that the electron will emit depends upon the field strength (B) and the electron velocity relative to that field (v_{\perp}). If the electron is nonrelativistic, the radiation (cyclotron) frequency is

$$\Omega = \frac{v_{\perp}}{r} = \frac{Be}{m_0} \quad (48)$$

where m_0 is the rest mass of the electron. In this approximation, the radiation frequency depends only upon the strength of the magnetic field; however, if the electron is relativistic, the radiated (synchrotron) energy exhibits a series of frequencies given by the relationship

$$\Omega_n = \frac{Be n}{m_0 \gamma}; \gamma = \frac{1}{\sqrt{1 - (v_{\perp}/c)^2}} \quad (49)$$

where $n = 1, 2, 3$, etc. The frequency of this radiation (sometimes called magnetic bremsstrahlung) depends not only upon the magnetic field strength, but also upon the electron energy (References 70 and 71).

Calculations have been carried out to determine the magnetic field strengths necessary to account for the frequencies of the decimetric radiation ($3 \times 10^8 - 10^{10}$ Hz). (See References 57 and 64 through 69.) If the radiating electrons are nonrelativistic, a magnetic field of 20 to 600 gauss is required independent of electron energy. On the other hand, if the radiating electrons are relativistic, the required fields are ~ 0.1 gauss (10-100 Mev electrons) to ~ 10 gauss (1-10 Mev electrons). It will be noted that these are the field strengths at the electrons. (The strengths at the surface of the planet will be ~ 30 times as high.) Since it is easier to explain a surface magnetic field of ~ 3 to 300 gauss than one of ~ 600 to 18,000 gauss, synchrotron radiation from relativistic trapped electrons is the most probable source of Jupiter's decimetric radiation.

The origin of the decametric radiation is less clear. The burst occurrences' correlating with the orbit periods of Jupiter's large satellites suggests that it may be bremsstrahlung emitted when the electrons hit these satellites (References 72 through 74). Such bremsstrahlung is directional at high energies, so its detection at earth would be possible only when the emission cone was pointed toward earth. The fact that the orbit periods of Io, Europa, and probably Ganymede correlate with the occurrences of these decametric bursts strongly suggests that the trapped radiation extends past their orbits.

Magnetic Field Calculations

If it is assumed that the decimetric radiation received from Jupiter is due to synchrotron radiation from relativistic electrons in a dipole magnetic field, it is possible to calculate various parameters of the Jovian Van Allen belts. The equatorial magnetic field (B_0) is basic to these calculations, and, therefore, it is necessary to establish probable values of this field in order to proceed.

For any equatorial magnetic field strength, there are two limiting electron populations: the number of electrons necessary to account for the intensity of the decimetric radiation received from Jupiter, which number varies inversely with B_0 , and the number of electrons the magnetic field can stably contain, which number varies directly with the square of B_0 . The minimum possible equatorial field (B_0) is that in which these two electron populations are equal.

The intensity (power per unit solid angle) radiated by a single electron in a magnetic field is (References 70 and 71).

$$I_n = \frac{e^2 \Omega^2 m^2}{2 \pi c \lambda^2} \left\{ (\tan \theta - \beta_{\parallel} \sec \theta) J_n^2 \left(\frac{n \Omega}{\Omega_e} \right) \beta_{\perp} \cos \theta + \beta_{\perp} \left(J_n^1 \right)^2 \left(\frac{n \Omega}{\Omega_e} \right) \beta_{\perp} \cos \theta \right\} \quad (50)$$

$$\beta = v/c$$

$$\gamma = 1 / \sqrt{1 - (v/c)^2}$$

e = electron charge

B = magnetic field intensity

v = electron velocity

c = velocity of light

n = harmonic number (1, 2, 3, etc.)

$$\lambda = (1 - \beta_{\parallel}) \cdot \sin \theta$$

θ = angle of observation relative to direction of B

V_{\perp} and v_{\parallel} are velocity components perpendicular and parallel to B , respectively. Calculation of the radiation intensity for an assembly of electrons is difficult but has been done through one or more approximations by various authors (Reference 71). The important aspect here is that the intensity per electron varies directly with B , so that the number of electrons required to achieve any given radiation intensity varies inversely with B . For electrons in Jupiter's magnetic field, the relationship is (Reference 57)

$$N \cdot B \sim 10^{28} \text{ electrons gauss} \quad (51)$$

where B is the magnetic field intensity at the heart of the electron belt. For the earth's Van Allen belt, the intensity of the electrons is a maximum at about 3.5 R_E . Since dipole fields drop off as r^{-3} , the intensity at 3.5 R_E is 0.023 that at the equator. As a first approximation, it is assumed that the ratio of magnetic field strength at the heart of Jupiter's electron belt to that at the equator is 0.033. This corresponds to a peak at 3.1 R_J , measured from the center of the dipole.

The number of electrons that can be stably contained in a magnetic dipole field has been calculated by Kennel and Petschek (Reference 75). They were able to show that as the particle density increases an unstable condition is reached in which plasma waves exchange energy with the gyro-rotation of the particle, leading to particles being "shaken out" into the planetary atmosphere. In addition, an asymmetric pitch angle distribution makes the particles particularly susceptible to whistler mode instabilities. By calculating the electron and ion densities at which these perturbations will propagate without attenuation, Kennel and Petschek were able to estimate an upper limit to the fluxes of stably trapped particles in a dipole field. Electron fluxes calculated this way agree well with measurements in the earth's Van Allen belts.

The basic formula developed by Kennel and Petschek is

$$\phi(>E_R) \approx \frac{\left(1 - \frac{\omega}{\Omega}\right) \left(\frac{c}{\pi^2 e R}\right)}{A - \frac{1}{\Omega/\omega - 1}} \cdot \frac{B \ln G}{\ell} \quad (52)$$

where $\phi(>E_R)$ is the omnidirectional electron flux (electrons/cm²-sec) above the resonant energy, E_R

ω is the plasma frequency (sec⁻¹) = $\sqrt{4\pi N e^2/m}$

N is the electron density (cm⁻³)

m is the electron mass (gm)

e is the electron charge (esu)

A is the anisotropy in diffusion equilibrium (typically 1/6)

Ω is the cyclotron frequency (sec^{-1})

$$\Omega = \frac{e B}{m c}$$

B is the magnetic field strength (gauss)

G is the wave gain in one traversal of the active regions of a magnetic tube of force ($\ln G \sim 3$)

ℓ is the effective length of a line of magnetic flux in units of planetary radii

Under most conditions, $\Omega \gg \omega$ (i. e., the cyclotron frequency is appreciably greater than the plasma frequency). For a dipole field, $\ell \sim L$ (the McIlwain parameter).

The resonant energy (E_R) for magnetically trapped electrons is given by the formula

$$E_R \approx E_c \left(\frac{\omega}{\Omega} \right) \left(1 - \frac{\Omega}{\omega} \right)^3 \quad (53)$$

where $E_c = \frac{B^2}{8 \pi N}$ = the magnetic energy per particle.

Since $B \propto r^{-3}$ for a dipole, the formulae shows an $\sim r^{-4}$ dependence for the particle fluxes above E_R . The total number of trapped particles based upon the assumption of spherical symmetry is

$$\int N = \frac{\hat{\phi}}{c} \int_{r_{\min}}^{r_{\max}} \frac{4 \pi r^2}{\left(\frac{r}{R} \right)^4} \cdot dr = \frac{4 \pi \hat{\phi} R^4}{c} \left(\frac{1}{r_{\min}} - \frac{1}{r_{\max}} \right) \sim \frac{4 \pi \hat{\phi} R^3}{3c} \quad (54)$$

where R is the radius of the planet

r_{\max} is the radius of the magnetosphere

ϕ is the electron flux at r_{\min}

The radius of the magnetosphere is obtained by equating the energy densities of the solar wind, $W(\phi_w)$, and of the planetary magnetic field, $W(B)$. The relevant equations are

$$B(r, \theta) = \frac{B_0 \cos \theta}{\left(\frac{r}{R}\right)^3} \quad (55)$$

$$W(B) = \frac{B^2}{2\mu_0} \quad (56)$$

$$W(\phi_w) = N \cdot 1/2 M_0 v^2 \quad (57)$$

where B_0 is the equatorial magnetic field strength

$$\mu_0 = 4\pi \times 10^{-7}$$

N = proton density in the solar wind at 5.2 AU

M_0 = rest mass of a proton

v = directed velocity of the solar wind at 5.2 AU

While N and v are somewhat uncertain at 5.2 AU, to a first approximation $W(\phi_w)$ probably decreases as r^{-1} to r^{-2} . At 1 AU, $W(\phi_w)$ is $\sim 2 \times 10^{-10}$ joules/m³, so at 5.2 AU a reasonable value is $\sim 4 \times 10^{-11}$ joules/m³. Therefore, the equatorial ($\theta = 0$) value of r for the magnetosphere in terms of B is

$$r_{\max} \sim R \cdot \sqrt[3]{10^4 B} \quad (58)$$

It is seen that $r_{\max} \gg r_{\min}$, so that

$$\int N \sim \frac{\pi \hat{\phi} R^3}{c} \quad (59)$$

The minimum Jovian magnetic field can be calculated from the preceding. In Table 15, various values of B_0 (the equatorial magnetic field strength) and the corresponding values of the field strength at $\sim 3 R_J$ (where the electron flux is presumably a maximum) are listed. For each value of B_0 , the radius of the magnetosphere (r_{\max}) is determined. The required number of electrons (to account for the observed intensity of the decimetric radiation) and the required effective energy of these electrons (to account

Table 15. Trapped Electron Populations as a Function of Jovian Equatorial Field, B_0

Equatorial Field $\rightarrow B_0$ (gauss)	Field at 3.1 R_J (gauss)	Magnetosphere Radius (R_J)	$N_{\max > 40 \text{ Kev}}$ (electrons)	E_e Required (Mev)	$\int N > E_e$ Required (electrons)	$\int N > E_e$ Available (electrons)
300	10	140	10^{36}	1.0	10^{27}	4×10^{34}
100	3	100	10^{35}	1.8	3×10^{27}	2.2×10^{33}
30	1	66	10^{34}	3	10^{28}	1.4×10^{32}
15	0.5	52	2×10^{33}	4.5	2×10^{28}	3×10^{31}
10	0.3	45	10^{33}	5.5	3×10^{28}	7.5×10^{30}
5	0.17	36	2.5×10^{32}	8.0	6×10^{28}	1.5×10^{30}
3	0.1	30	10^{32}	10	10^{29}	4×10^{29}
2	0.067	26	4×10^{31}	13	1.5×10^{29}	1.5×10^{29}
1	0.03	20	10^{31}	18	3×10^{29}	2.2×10^{28}
0.3	0.01	14	10^{30}	30	10^{30}	1.4×10^{27}
0.1	0.003	10	10^{29}	55	3×10^{30}	7.5×10^{25}

for the observed frequency of the decimetric radiation) were calculated from Equations (51) and (49), respectively. The maximum number of electrons with energies >40 Kev that could be stably contained in each field was calculated from Equations (52) and (54). To bridge the difference in energies (40 Kev to E_e) it was necessary to assume a spectral shape. In the earth's Van Allen belts, the slope of the electron energy spectrum decreases as the magnetic field strength increases, reaching $\sim E^{-2.5}$ at $r = 1.5 R_e$. Various authors (References 57 and 63) have concluded that the Jovian trapped electrons probably have a spectral shape of $\sim E^{-1}$ close to the planet. Such an assumption is not incompatible with the spectral-slope-magnetic-field-strength relationship observed in the earth's Van Allen belts (so long as the Jovian equatorial field strength is at least a few gauss). Therefore, an E^{-1} integral spectral shape was assumed to hold for the region >40 Kev at the heart of the Jovian electron belts. This made possible the direct comparison of the two electron populations: the number of electrons that can be stably contained and the number of electrons that are required to account for the observed intensity of the decimetric radiation. The last two columns of Table 19 show that an equatorial field (B_0) of at least 2 gauss is required. (It should be noted, however, that if the peak flux occurs at less than $3.1 R_J$, B_0 can be less than 2 gauss.) A weaker dipole field will not be able to hold all the electrons it needs to account for the decimetric radiation. It is quite probable that the field is stronger than this. A number of researchers have concluded that B_0 may be as large as 15 gauss. To obtain a feel for the range of fluxes and dose rates in the Jovian trapped radiation belts, three cases were considered:

Low case $B_0 = 2$ gauss

Probable case $B_0 = 5$ gauss

High case $B_0 = 15$ gauss

Dose Rate Calculations

The electron fluxes as a function of position in the equatorial plane were calculated for the three values of B_0 . An L^{-4} distribution was assumed, based upon the work of Kennel and Petschek (Reference 75). To normalize this distribution, two different approaches were used. One approach was to calculate the peak flux, ϕ , from Equation (8) for $r \sim 3 R_J$. The second approach was to assume that if a magnetic field of $\sim 7 \times 10^{-3}$ gauss (the value of the geomagnetic field at $3.5 R_e$) could hold $\sim 10^9$ electrons/cm²-sec >40 Kev (the approximate value of the peak electron flux) in the earth's Van Allen belts, a similar field could hold a similar flux at Jupiter. The peak fluxes (electrons/cm²-sec >40 Kev) calculated this way agreed with each other to within a factor of 5. The values selected for $3 R_J$ were the averages of these two. The peak locations, however, were taken to be at 0.1 the radius

of the magnetosphere, which reduced these peak fluxes somewhat. This was done because of the possible off-center location of the Jovian dipole and to bring the proportions of the spatial distribution of the trapped radiation more in agreement with those of the earth's Van Allen belts. The influence upon the fluxes at Io was < a factor of 2 and was negligible at the other satellite (Figure 24).

The calculation of the electron dose rates on each of the four large Jovian satellites was based on the integrals of the form

$$DR(x) = \int_0^{\infty} \phi(E', x) C(E') dE' \quad (60)$$

where $DR(x)$ is the electron dose rate as a function of the shield thickness

$\phi(E', x)$ is the emergent electron energy spectrum as a function of shield thickness

$C(E')$ is the flux-to-dose conversion function

E' is the electron energy after penetrating the shield

Evaluation of these integrals was aided by the fact that $C(E')$ has the approximately constant value of 3×10^{-8} rad-cm²/electron (Reference 76). Thus, it was only necessary to calculate the electron flux above the shield cutoff energy and multiply by 3×10^{-8} to obtain the rad dose rate. The shield cutoff energies were read from range-energy tables for electrons (Reference 77).

To obtain the electron flux above the cutoff energy for any shield, it was necessary to make some assumptions concerning the shape of the electron energy spectrum. As pointed out, this spectral shape is a function of the magnetic field strength. At 3.5 Re in the earth's Van Allen belts, the integral electron energy spectrum is approximately E^{-3} (Figure 25 and Reference 78). The magnetic field strength at 3.5 Re is $\sim 7 \times 10^{-3}$ gauss. At Ganymede (the satellite of primary interest in this study) the magnetic field strength is calculated to lie in the range 6×10^{-4} gauss to 4×10^{-3} gauss. This is sufficiently close to 7×10^{-3} gauss that the Jovian electron integral energy spectrum at Ganymede can be taken as E^{-3} (approximately equal to that shown in Figure 25). It will be noted that the assumption of an E^{-1} integral energy spectrum was made at ~ 3 R_J, where the magnetic field is on the order of 0.1-0.5 gauss.

The electron dose rates at Ganymede as functions of aluminum shield thickness are shown in Figure 26. These values were obtained by evaluating

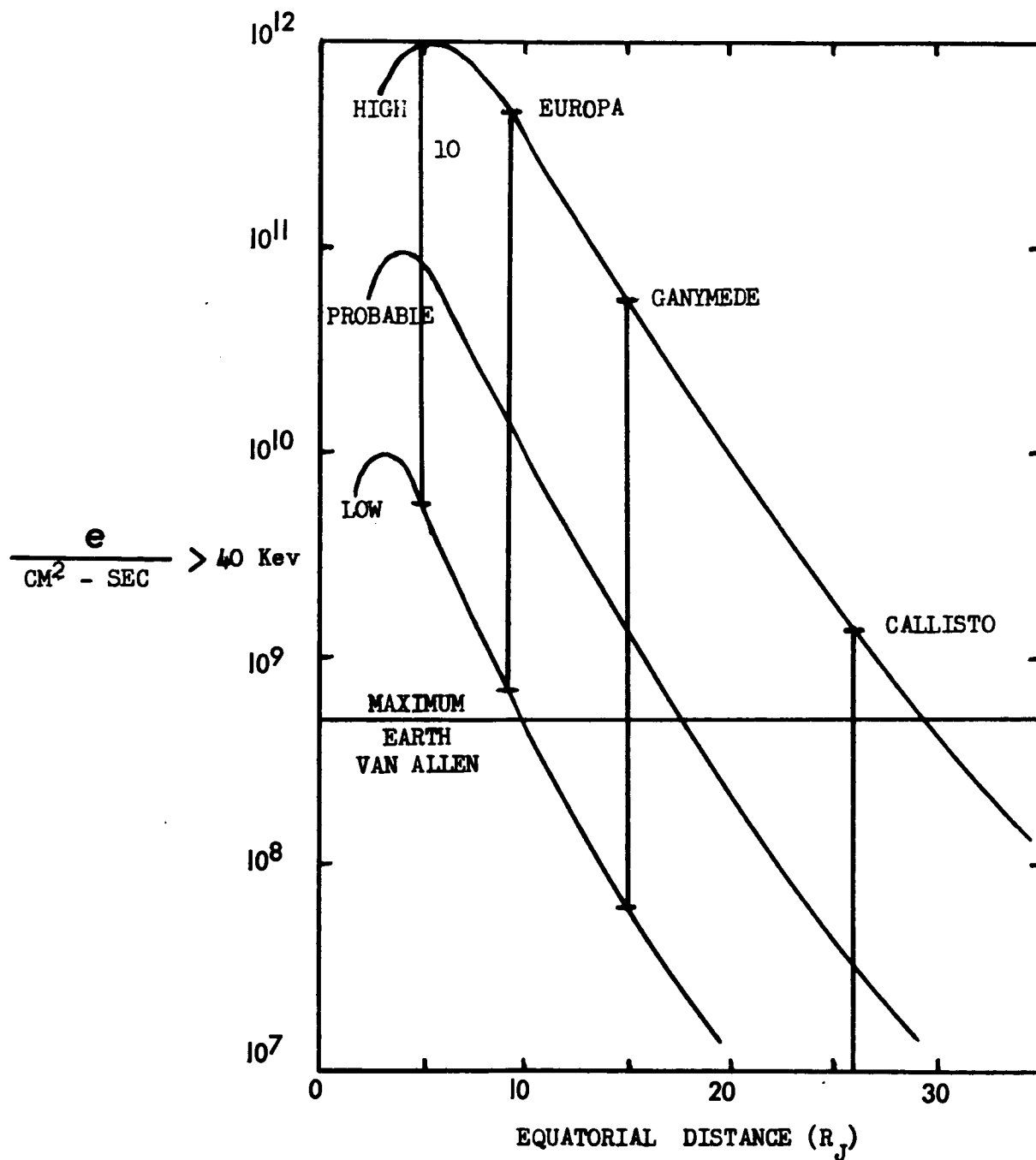


Figure 24. Electron Flux

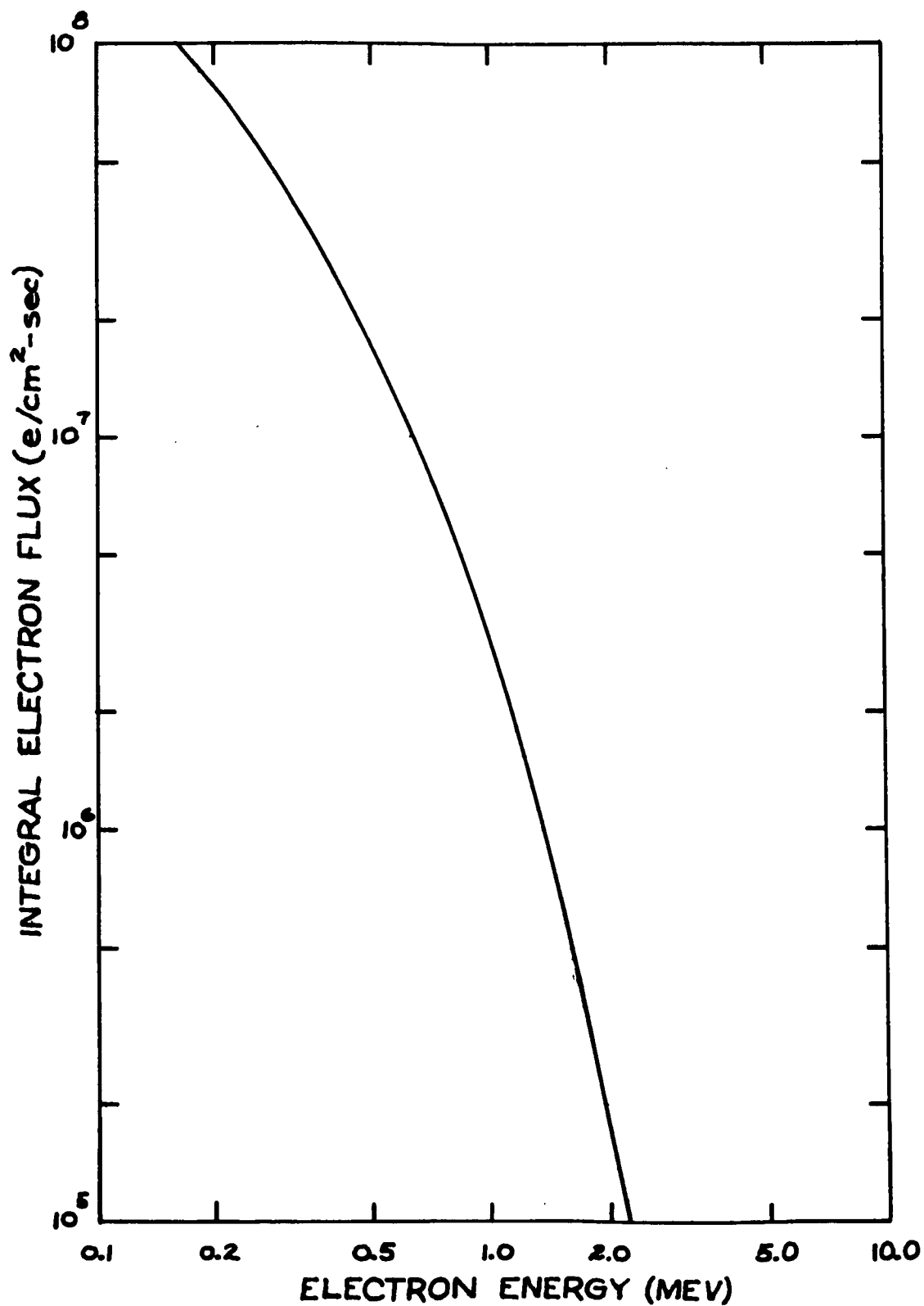


Figure 25. Measured Electron Integral Energy Spectrum at 3.5 R_E (Earth Van Allen Belts)

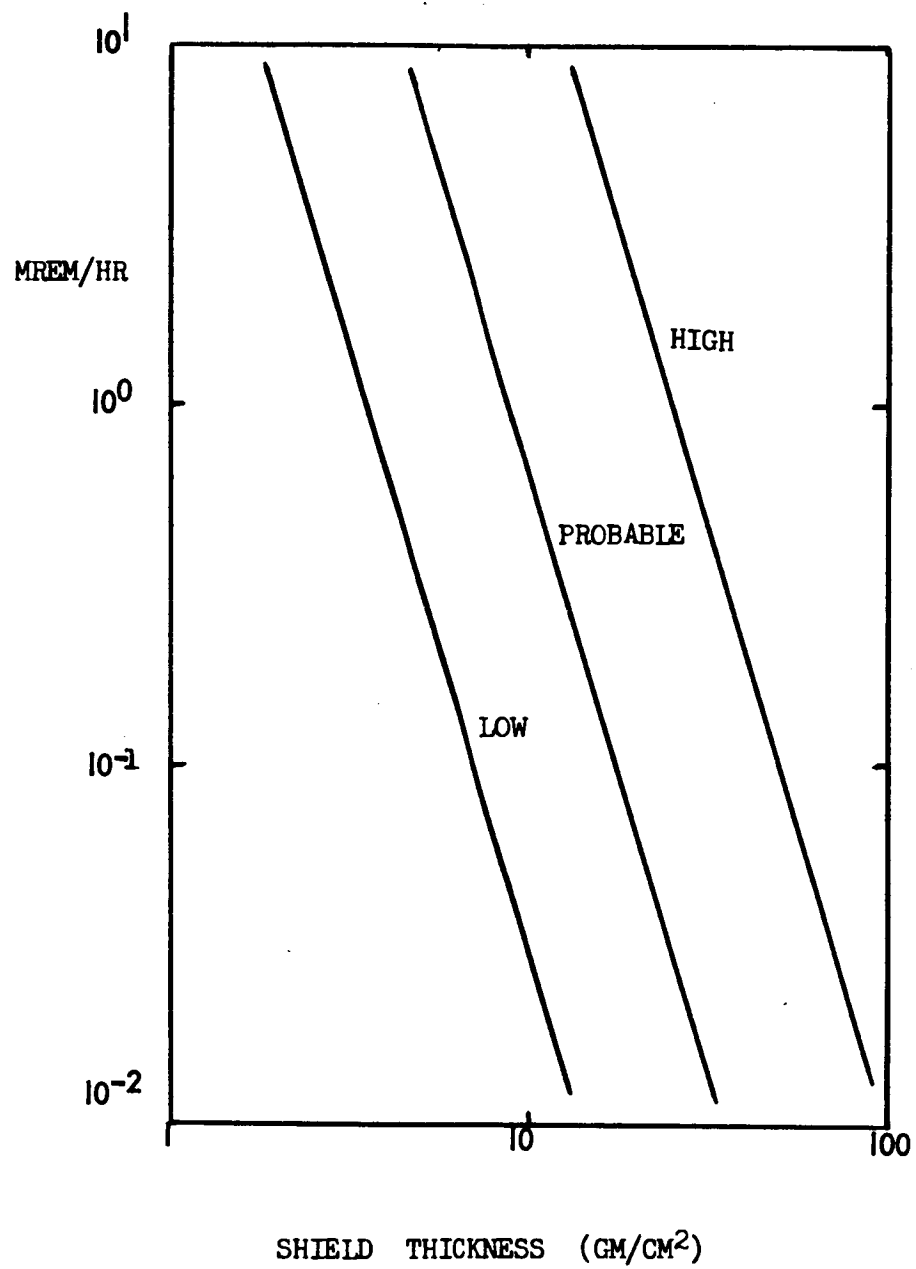


Figure 26. Electron Dose Rate at Ganymede

Equation (60) as discussed. It is apparent at this stage that the uncertainties in the Jovian magnetic field strength are at least as important as the shield present in determining the electron dose rates.

It is recognized that there may be trapped protons in the Jovian belts. Electron bremsstrahlung has been neglected here as also contributing less than the uncertainties in the Jovian field strength to the spread in values. Some compensation is provided by neglecting the 2π solid angle shielding afforded by the satellite at its surface. Another factor of 2 for the self-shielding of the human body has been omitted for the same reason. Thus, the dose rates shown in Figure 26 may be taken as skin dose rates.

Ganymede Dose and Stay Time Calculations

To assess the operational significance of these dose rates, three round-trips from earth to Jupiter were considered. These 200-week missions had starting dates of 1985.3, 1987.5, and 1990.8. The shielding required for each of these missions, in the absence of the Jovian radiation belts, was calculated using Equations (40) and (41).

Shield thicknesses were calculated for probabilities of 50 percent, 10 percent, and 1 percent for each of the three missions based upon dose limits of 800 rem (skin) and 200 rem (blood-forming organs). Results are listed in Table 16. For comparison, the same calculations were carried out using an alternative approach (Reference 19) based upon sunspot number and solar flare radiation correlations. Results of these detailed calculations are listed in Table 16, also in parentheses. The comparisons show that the use of Equations (40) and (41) lead to somewhat greater shield thicknesses for severe solar radiation environments than the detailed analysis. The agreement in most cases is good, however.

For each mission and each probability, it was necessary to select a shield thickness as a standard. The philosophy here was to select a shield thickness that equaled or exceeded that required for skin and for blood-forming organ protection for at least one of the calculational approaches. Thus, at least three of the four numbers for each mission and probability of Table 16 were exceeded. The thickness selected are also shown in Table 16, boxed in the middle of the four numbers used in their selection. These shield thicknesses represent the standards used for subsequent analysis.

To land upon Ganymede during any of these missions, it is necessary to increase the shield thickness above the standards discussed. If the mission dose limits are fixed, it is necessary to save some dose tolerance for the Jovian radiation belt fluxes present at Ganymede. The relationship between added shielding and Ganymede stay time obviously depends upon the mission considered and the radiation belt model used. The procedure

Table 16. Spacecraft Shielding Required Without the Presence of Jupiter Radiation Belts*

Probability of Exceeding Dose Limits	May 1987 Mission		July 1989 Mission		October 1990 Mission	
	Shielding (gm/cm ²)		Shielding (gm/cm ²)		Shielding (gm/cm ²)	
	Skin	BFO	Skin	BFO	Skin	BFO
50%	0.3	0	0.4	0	0.95	0
	[0.5] (0.6)	(0)	[0.7] (0.8)	(0)	[1.5] (1.5)	(0.5)
10%	1.3	0	1.8	0	4.2	6.5
	[1.2] (1.2)	(0)	[1.7] (1.5)	(0.2)	[5.0] (3.0)	(4.5)
1%	3.0	3.0	4.3	6.3	10	16.8
	[3.0] (2.5)	(2.7)	[5.0] (3.1)	(3.2)	[12] (8.0)	(12)
Mission dose limits		200 rem - blood-forming organs (BFO) 800 rem - skin				

**Top numbers calculated using analytical formula; bottom numbers based upon detailed analysis

used was to select a shield thickness in excess of the standard. This reduces the solar and earth's Van Allen mission radiation doses (but not the galactic radiation dose) to values less than the mission dose limits (Figure 27). The remaining dose was available for the stay on Ganymede. The shield thickness selected corresponds to an electron dose rate due to the Jovian trapped radiation. The stay time is simply the ratio of the remaining dose to the electron dose rate.

The stay times calculated this way are shown in Figures 28 through 30. It is seen that the greater the standard shield thickness (that required if no encounter occurs with the Jovian trapped radiation) the greater the stay time per unit added shielding. This is due to the electron dose rates being a steep function of shield thickness; however, the curves tend to converge for large amounts of added shielding because the electron dose approaches the mission dose regardless of the solar radiation environment.

It is possible to treat this problem analytically. The dose (D') available for a stay on Ganymede is

$$D' = (D_0 - 0.35 t) \cdot \left[1 - \left(\frac{x + y}{x} \right)^{-1.6} \right] \quad (61)$$

where

D_0 is the mission dose limit (rem)

t is the mission duration exclusive of a stay on Ganymede (rem)

x is the standard shield thickness (gm/cm^2) required to meet the mission dose limit D_0

y is the added shield thickness (gm/cm^2)

Thus, if $y = 0$, $D' = 0$, with D' increasing to a maximum of $D_0 - 0.35 t$. The $0.35 t$ represents the galactic radiation dose rate that is considered to be independent of shield thickness up to $\sim 30 \text{ gm}/\text{cm}^2$.

The electron dose rate on Ganymede ($D' R$) may be represented analytically by an expression of the form

$$D' R = 3.3 \cdot \frac{B_0^{3.3}}{(x + y)^3} \quad (62)$$

where B_0 is the equatorial magnetic field strength in gauss. The stay time (τ) in hours is

$$\tau = \frac{(D_0 - 0.35 t) \cdot \left[1 - \left(\frac{x + y}{x} \right)^{-1.6} \right]}{\frac{3.3 B_0^{3.3}}{(x + y)^3}} ; \tau \ll t \quad (63)$$

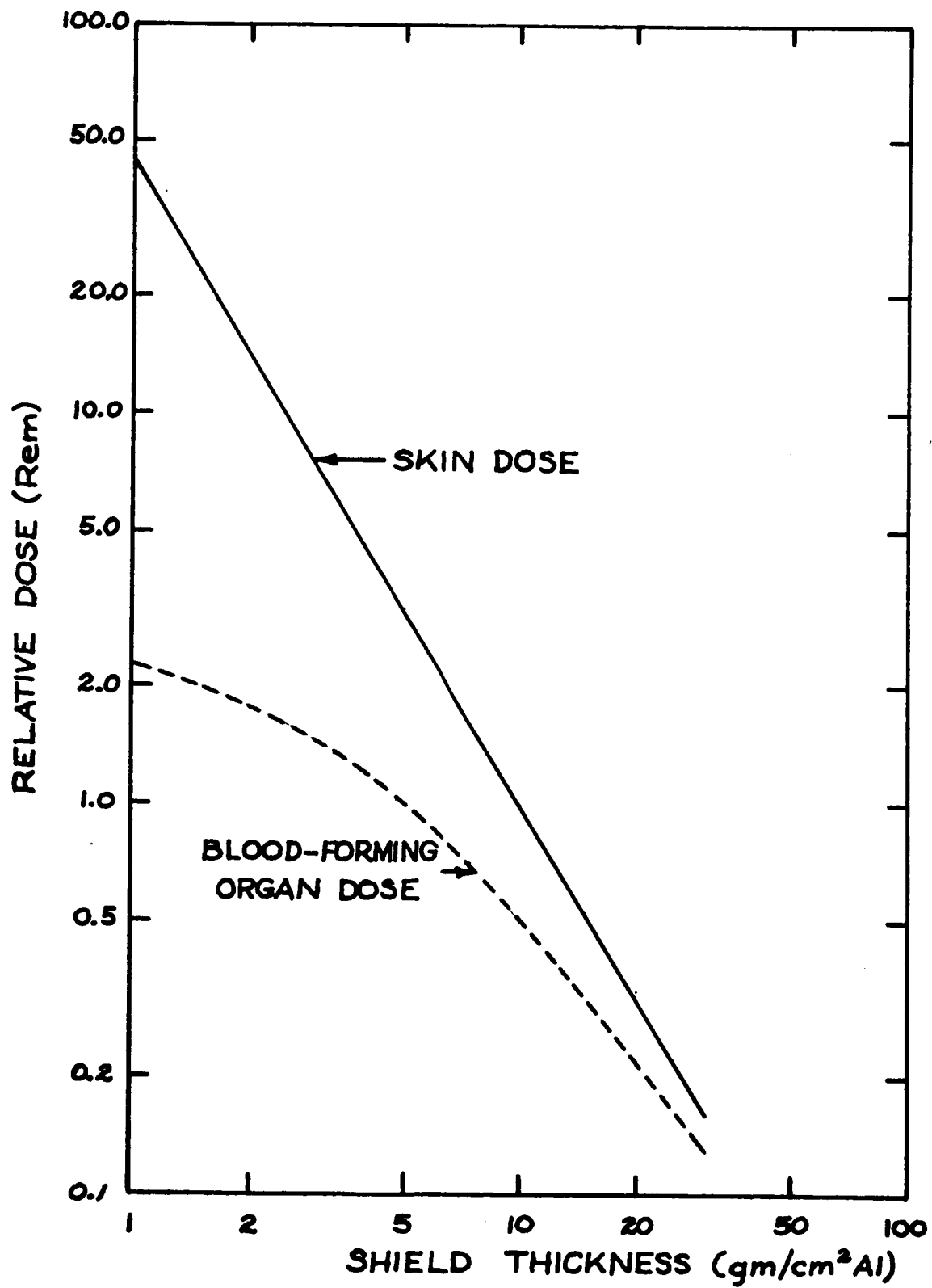


Figure 27. Effect of Shield Thickness

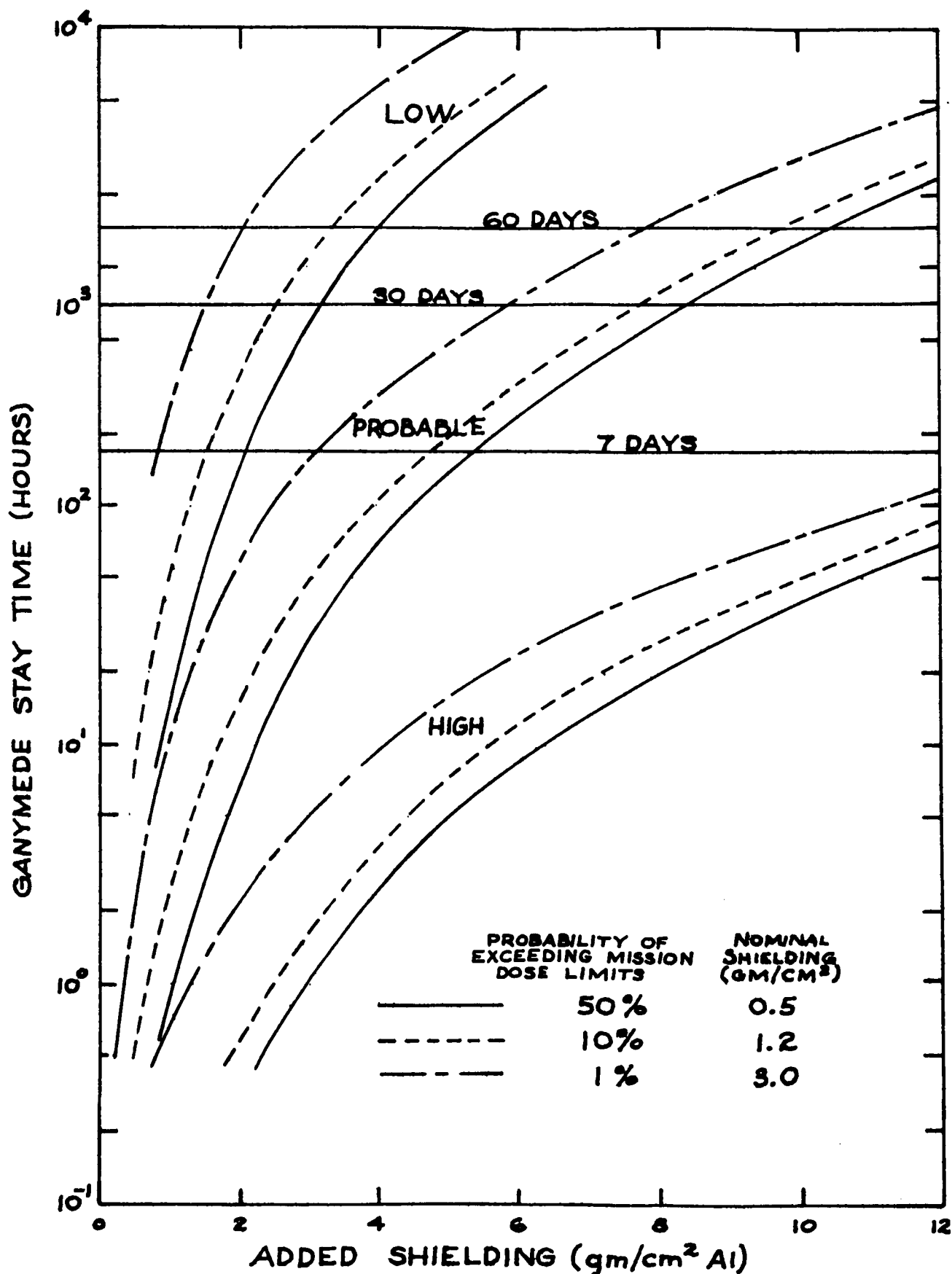


Figure 28. Added Shielding (1985-1989 Mission)

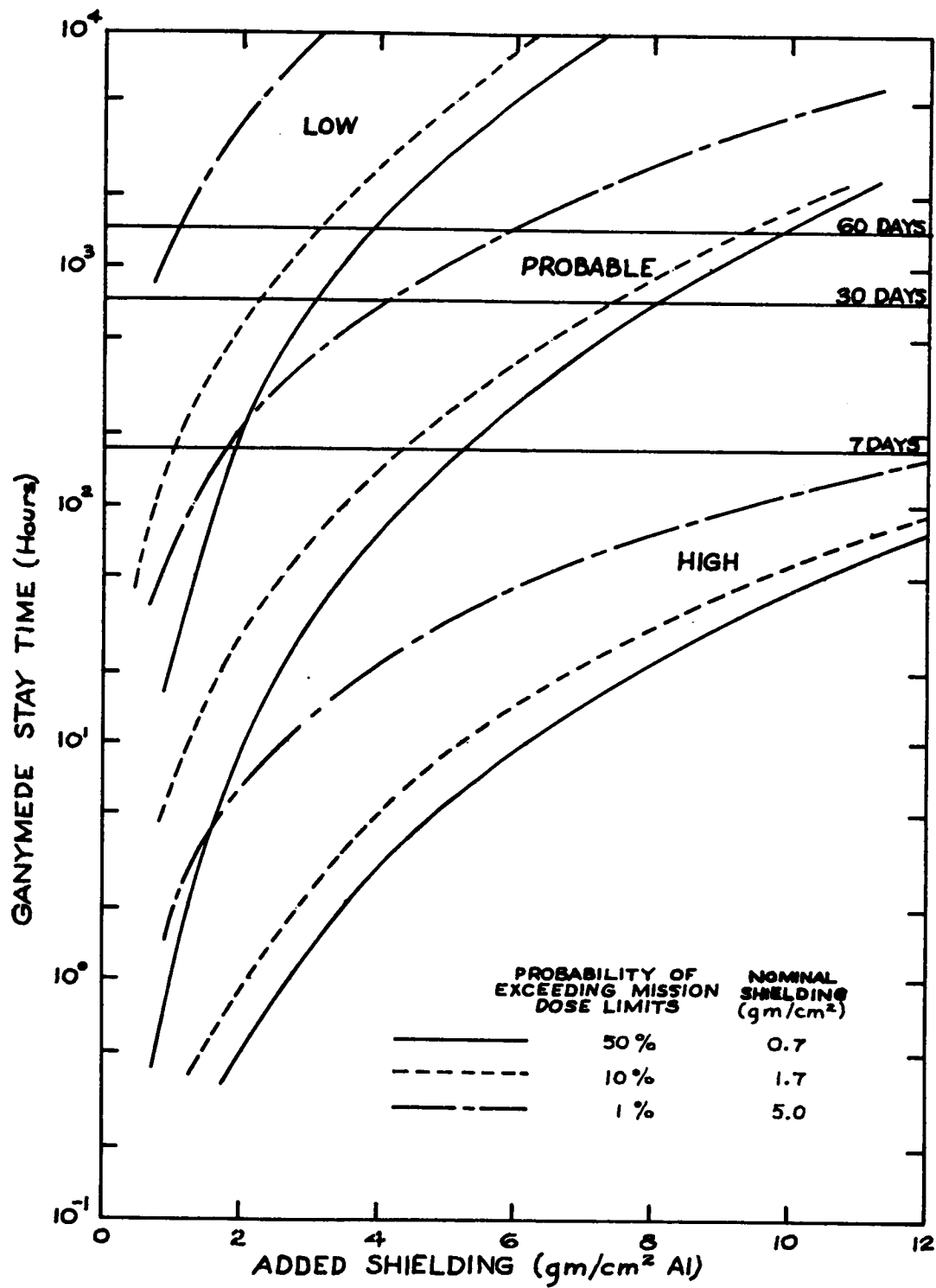


Figure 29. Added Shielding (1987-1991 Mission)

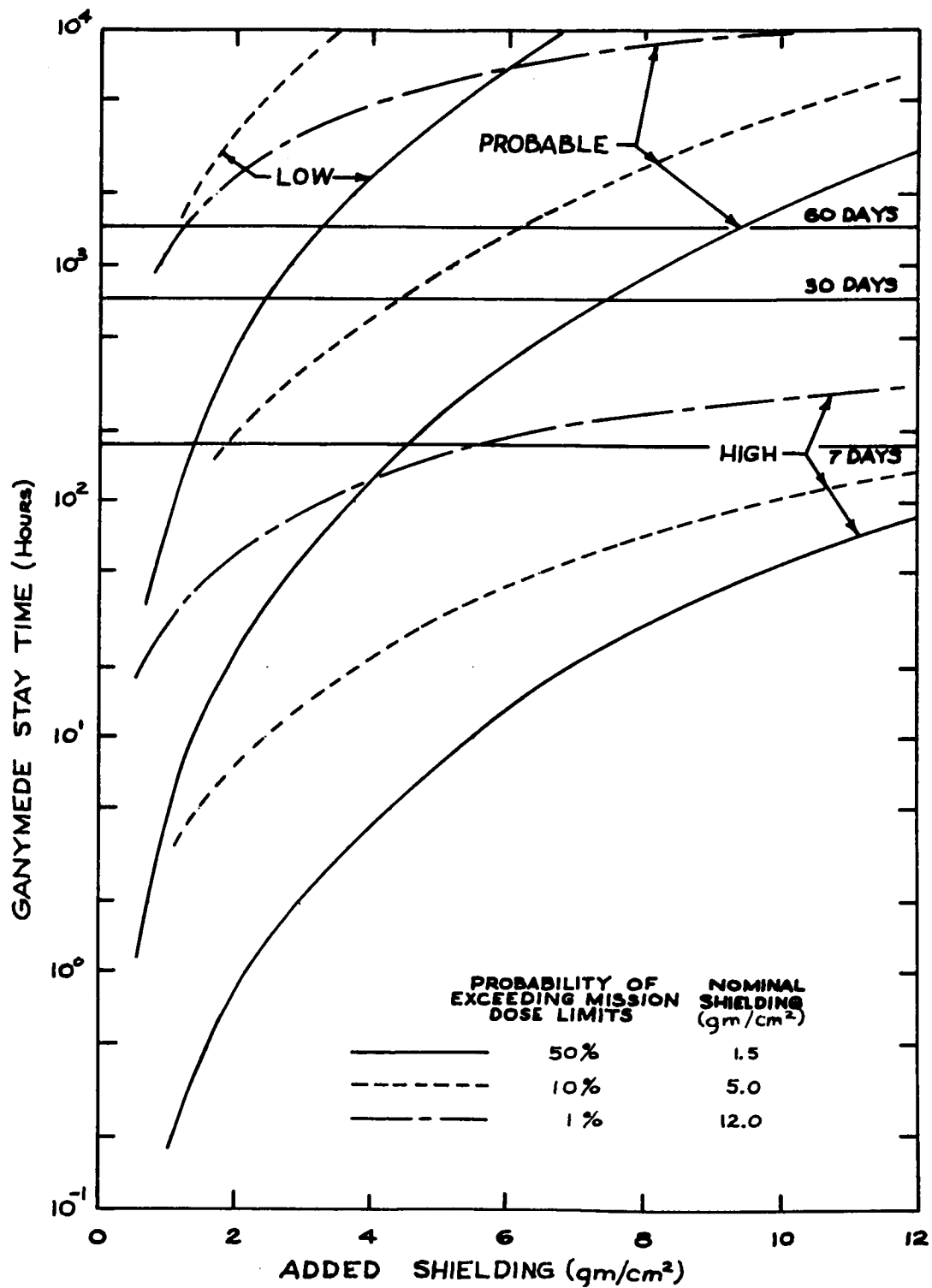


Figure 30. Added Shielding (1990-1994 Mission)

Corresponding expressions can be developed for Io, Europa, and Callisto. The numerators will be identical to that of Equation (63), but the numbers in the denominator will be different. It will also be noted that the value of x in Equation (63) can be obtained analytically from Equations (40) and (41); the larger of the two values of x is appropriate.

Among the assumptions of Equation (63) is that the skin dose will be the limiting factor. If x is ≤ 3 gm/cm², this is true; but if $x \geq 3$ gm/cm², the blood-forming dose will be the limiting factor for small values of y . As y increases, however, the skin dose will again become the limiting factor due to the steepness of the curves shown in Figure 26. If x is selected so both the skin and blood-forming organ dose limits are satisfied, the use of Equation (63) will lead to conservative values of τ .

Conclusions

There are order-of-magnitude uncertainties associated with the trapped radiation about Jupiter. The decimetric and decametric radiation make possible approximate calculations of the flux and spatial extent of trapped electrons; the corresponding quantities for any trapped protons are matters for conjecture. Until the source mechanisms for the earth's Van Allen belts' protons are better understood, it is not possible to estimate parameters associated with protons in the Jovian trapped radiation.

It is probable that the calculations carried out here bracket the actual situation on Jupiter. The values calculated for an equatorial field (B_0) of 2 gauss represent a lower limit, which will most probably be exceeded. On the other hand, the values calculated for $B_0 = 15$ gauss are probably too high. Therefore, for planning purposes, the values associated with $B_0 = 5$ gauss are recommended.

The fluxes and dose rates associated with $B_0 = 5$ gauss are such that a landing on Ganymede appears possible, but is not clearly a desirable part (from a radiation-shielding standpoint) of a manned mission to Jupiter. For missions undertaken during the active portion of the solar cycle, a small amount of extra shielding (≤ 3 gm/cm²) will most probably suffice for 60 days on Ganymede, while for missions undertaken when the sun is quiet ≥ 6 gm/cm², extra shielding will be required. Total shield thicknesses of ≥ 10 gm/cm² appear necessary in any event if a 60-day stay on Ganymede is contemplated. Reducing the stay time to 30 days only decreases this ~ 2 gm/cm² at the most.

As an alternative, Callisto could be considered for manned landings since the shield thickness required will be approximately a factor of two less.

PRECEDING PAGE BLANK NOT FILMED.

REFERENCES

1. Interplanetary Meteoroid Shielding Requirements. Memorandum, Technical Assistant, Mission Analysis Division to Distribution Mission Analysis Division (15 August 1966).
2. Webber, W. R. , An Evaluation of the Radiation Hazard due to Solar Particle Events, Report D2-90469, The Boeing Company (1963).
3. Webber, W. R. , An Evaluation of Solar Cosmic Ray Events During Solar Minimum, Report D2-84274-1, The Boeing Company (1966).
4. Saylor, W. P. , et al, Space Radiation Guide, Report AMRL-TDR-62-86, U. S. Air Force Medical Research Laboratories (1962).
5. Lewis, L. R. , et al, Solar Flare Radiation Survey, Report RTD-TDR-63-3044, U. S. Air Force Weapons Laboratory (1963).
6. McDonald, F. B. , editor, Solar Proton Manual, NASA Technical Report TR-R-169 (1963).
7. Webber, W. R. and H. H. Malitson, A Summary of Solar Cosmic Ray Events, NASA Report X-611-62-122 (1963).
8. Hess, W. N. , editor, AAS-NASA Symposium on the Physics of Solar Flares, NASA Report SP-50 (1964).
9. Anderson, K. A. , Energetic Solar Particles, Chapter 16 of Space Physics, D. P. LeGalley and A. Rosen, editors, John Wiley and Sons (1964).
10. Roberts, W. T. , The Solar Flare Environment, NASA Technical Memo TM-X-53216 (1965).
11. Kistler, V. E. , A Discussion and Bibliography of Current Literature Concerning VanAllen Belts for Use in SNAP Space Environment Studies, NAA Report SR-7849 (1962).
12. O'Brien, B. J. , The Trapped Radiation Zones, "Chapter 14 of Space Physics," D. P. LaGalley and A. Rosen, editors, John Wiley and Sons (1964).

13. Vette, J. I., Models of the Trapped Radiation Environment, Vols, I and II, NASA Report SP-3024 (1966).
14. McCormac, B. M., editor, Radiation Trapped in the Earth's Magnetic Field, Reidel Publishing Company (1966).
15. Rosen, A., and J. L. Vogl, "Cosmic Rays in Space," Chapter 17 of Space Physics, D. P. LeGally and A. Rosen, editors, John Wiley and Sons (1964).
16. Modisette, J. L., T. M. Vinson, and A. C. Hardy, Model Solar Proton Environments for Manned Spacecraft Design, NASA Technical Note D-2746 (1965).
17. Dye, D. L., and M. Wilkinson, "Radiation Hazards in Space," *Science* 147, 19 (1965).
18. Haffner, J. W., "Mission Dose Probabilities Due to Solar Proton Events," *Transactions of the American Nuclear Society* 9, 334 (1966)
19. Weddell, J. B., and J. W. Haffner, Statistical Evaluation of Proton Radiation from Solar Flares, JPL Contract 951293, NAA S&ID, SID 66-421 (1966).
20. McRae, W. V., et al., Manned Planetary Flyby Missions Based on Saturn/Apollo Systems, NAA S&ID, SID 66-1676-1 (1966).
21. Haffner, J. W., A Study of Space Radiation Shielding, NAA S&ID, SID 64-2037 (1964).
22. Gibson, W. A., Energy Removed from Primary Proton and Neutron Beams by Tissue, Report ORNL 3260, Oak Ridge National Laboratory (1962).
23. Savin, R. C., J. M. Deerwester, and A. C. Masey, "Sensitivity of Manned Planetary Spacecraft to Radiation Uncertainties," Paper Presented at 11th Annual Meeting of the Health Physics Society, Houston, Texas (1966).
24. McGarrigle, K. S. and B. W. Mars, Computer Codes for the Evaluation of Space Radiation Hazards, Report D2-90418, The Boeing Company (1963).
25. Hill, C. W. et al, Computer Programs for Shielding Problems in Manned Space Vehicles, Report ER-6643, Lockheed-Georgia Company (1964).

26. Edgerly, R. H., "Radiation Shielding Limitations," Section 3.1.2 of Manned Mars Landing and Return Mission Study, A. L. Jones and W. V. McRae, editors, NAA S&ID, SID 64-619-3 (1964).
27. Billingham, J., "Apollo Dose Limits," Second Symposium on Protection Against Radiations in Space, NASA SP-71, pp. 139 (1964).
28. Kelton, A. A., Radiation Guidelines for Manned Space Vehicles - a Review with Recommendations, Report SM-47749, Douglas Aircraft Company (1964).
29. Burke, B. F., and K. L. Franklin. "Observations of a Variable Radio Source Associated With the Planet Jupiter," Nature (London) 175, 1074 (1955) also Journal of Geophysical Research 60, 213 (1955).
30. Warwick, J. W., and W. T. Kreiss. Observations of Jupiter's Sporadic Radio Emission in the Range 7.5-41 Mc/Sec for the Years 1960-1963. IGY Solar Activity Report Series No. 28 (November 1964).
31. Warwick, J. W., and G. A. Dulk: Observation of Jupiter's Sporadic Radio Emission in the Range 7.6-41 Mc/Sec - January 1964 Through May 1965. IGY Solar Activity Report Series No. 32 (August 1965).
32. Gledhill, J. A., G. M. Gruber, and M. C. Bosch. "Radio Observations of Jupiter During 1962," Nature 197, 474 (1963).
33. Alexander, J. K., and R. G. Stone. "Low-Level Decameter Emissions for Jupiter," Astronomical Journal 69, 1 (1964).
34. Smith, A. G., G. R. Lebo, N. F. Six, and J. D. Carr. "Decameter Wavelength Observations of Jupiter-The Apparitions of 1961 and 1962," Astrophysical Journal 141, 457 (1965).
35. Slee, O. B., and C. S. Higgins. "Long Baseline Interferometry of Jovian Decametric Radio Bursts," Nature 197, 781 (1963).
36. Warwick, J. W., and G. A. Dulk. "Faraday Rotation on Decametric Radio Emissions From Jupiter," Science 145, 380 (1964).
37. Carr, T. D., G. W. Brown, A. G. Smith, C. S. Higgins, H. Bollhagen, J. May, and J. Levy. "Spectral Distribution of the Decametric Radiation From Jupiter in 1961," Astrophysical Journal 140, 778. (1964).
38. Riihimaa, J. J. "High Resolution Spectral Observation of Jupiter's Decametric Radio Emission," Nature 202, 476 (1964).

39. Dowden, R. L. "Polarization Measurements of Jupiter Radio Bursts at 10.1 Mc/Sec," Australian Journal of Physics 16, 398 (1963).
40. Barrow, C. H. "Polarization Observations of Jupiter at Decameter Wavelengths," Icarus 3, 66 (1964).
41. Sherrill, W. M. "Polarization of Jovian Emission at Decameter Wavelengths," Nature 205, 270 (1965).
42. Sherrill, W. M. "Polarization Measurements of Decameter Radiation From Jupiter," Astrophysical Journal 142, 1171 (1965).
43. Douglas, J. N., and H. J. Smith. "Change in Rotation Period of Jupiter's Decameter Radio Sources," Nature 199, 1080 (1963).
44. Bigg, E. K. "Influence of the Satellite Io on Jupiter's Decametric Emission," Nature 203, 1008 (1964).
45. Lebo, G. R., A. G. Smith, and T. D. Carr. "Jupiter's Decametric Emission Correlated With the Longitudes of the First 3 Galilean Satellites," Science 148, 1724 (1965).
46. Dulk, G. A. "Io-Related Radio Emission From Jupiter," Science 148, 1585 (1965).
47. Duncan, R. A. "Modulation of Jupiter Decametric Emission by the Satellite Io," Planetary and Space Science 13, 997 (1965).
48. Bigg, E. K. "Periodicities in Jupiter's Decametric Radiation," Planetary and Space Science 14, 741 (1966).
49. Holmes, J. R. Periodicities in the Jovian Decametric Radio Emission. Technical Note R-206, Brown Engineering Co., Huntsville, Alabama (1966).
50. Mayer, C. H., T. P. McCulbough, and R. M. Sloavaker. "Observations of Mars and Jupiter at a Wavelength of 3.15 cm," Astrophysical Journal 127, 11 (1958).
51. Gower, J. F. R. "Radiation From Jupiter at 178 Mc/Sec," Nature 199, 1273 (1963).
52. Roberts, M. S., and G. R. Huguenin. "The Radiation Belt of Jupiter," Proceedings of the Eleventh International Astrophysical Symposium, Liege, Belgium (July 1962) p. 569.

53. Roberts, J. A. , and R. D. Ekers. "The Position of Jupiter's Van Allen Belt," Icarus 5, 149 (1966).
54. McAdam, W. B. "The Extent of the Emission Region on Jupiter at 408 Mc/Sec." Planetary and Space Science 14, 1041 (1966).
55. Morris, D. , and J. F. Bartlett. "Polarization of the 2840 Mc/Sec Radiation From Jupiter," Proceedings of the Eleventh International Astrophysical Symposium, Liege, Belgium (July 1962) p. 564.
56. Roberts, J. A. , and M. M. Komesaroff. "Observations of Jupiter's Radio Spectrum and Polarization in the Range From 6 cm to 100 cm," Icarus 4, 127 (1965).
57. Roberts, J. A. "Radio Emission From the Planets," Planetary and Space Science 11, 221 (1963).
58. Ellis, G. R. A. , and P. M. McCulloch. "The Decametric Radio Emissions of Jupiter," Australian Journal of Physics 16, 380 (1963).
59. Hirshfield, J. L. , and G. Bekefi. "Decameter Radiation From Jupiter," Nature 198, 20 (1963).
60. Barrow, C. H. "38 Mc/Sec Radiation From Jupiter," Nature 197, 580 (1963).
61. Wildt, R. , H. J. Smith, E. E. Salpeter, and A. G. W. Cameron. "The Planet Jupiter," Physics Today 16 (5), 19 (1963).
62. Douglas, J. N. "Decametric Radiation From Jupiter," IEEE Transactions on Antennas and Propagation AP-12 (7), 839 (1964).
63. Warwick, J. W. "Radio Emission From Jupiter," Annual Reviews of Astronomy and Astrophysics 2, 1 (1964).
64. Ellis, G. R. A. "Cyclotron Radiation From Jupiter," Australian Journal of Physics 15, 344 (1962).
65. Douglas, J. N. , and H. J. Smith. "Observations Bearing on the Mechanism of Jovian Decametric Emission," Proceedings of the Eleventh International Astrophysical Symposium, Liege, Belgium (July 1962) p. 551.
66. Chang, D. B. , and L. Davis. "Synchrotron Radiation as the Source of the Polarized Decameter Radiation From Jupiter," Astrophysical Journal 136, 567 (1962).

67. Korchak, A. A. "The Polarization of Synchrotron Radiation in a Dipole Field," Geomagnetism of Aeronomiya 3, 394 (1962).
68. Thorne, K. S. "The Theory of Synchrotron Radiation From Stars With Dipole Magnetic Fields," Supplement to Astrophysical Journal 8, 1 (1963).
69. Nakada, M. P. "Synchrotron Radiation Calculations for the Artificial Radiation Belt," Journal of Geophysical Research 68, 4079 (1963).
70. Linhart, J. G. Plasma Physics. North Holland: Amsterdam (1961).
71. Montgomery, D. C., and D. A. Tidman. Plasma Kinetic Theory. McGraw Hill; New York (1964).
72. Smith, A. G., N. F. Six, T. D. Carr, and G. W. Brown. "Occultation Theory of Jovian Radio Outbursts," Nature 199, 267 (1963).
73. Warwick, J. W. Mechanism of Decameter Radiation. Report AFCRL-66-774, Cambridge Research Laboratories (Sept. 1964).
74. Duncan, R. A. "Factors Controlling Jovian Decametric Emission," Planetary and Space Science 14, 1291 (1966).
75. Kennel, C. F., and H. E. Petschek. "Limit on Stably Trapped Particle Fluxes," Journal of Geophysical Research 71, 1 (1966).
76. Crawford, G. W. "Space Dosimetry," Chapter 18 of Space Physics, LeGalley, D. P., and A. Rosen eds., Wiley: New York (1964).
77. Berges, M. J., and S. M. Seltzer. Tables of Energy Losses and Ranges of Electrons and Positrons. NASA Report SP-3012 (1964).
78. Vette, J. I. Models of the Trapped Radiation Environment. NASA Report SP-3024 (1966).
79. Haffner, J. W. "Radiation Protection," Section I of Manned Planetary Flyby Missions Based on Saturn-Apollo Systems. McRae, W. V. ed. NAA Space Division, SID 66-1676-1 (1966).
80. Haffner, James W. Radiation and Shielding in Space. New York and London: Academic Press, 1967.